2016

# Two-Stage Psa System For CO2 Removal And Concentration During Closed-Loop Human Space Exploration Missions

Hanife Erden
*University of South Carolina*

# TWO-STAGE PSA SYSTEM FOR $CO_2$ REMOVAL AND CONCENTRATION DURING CLOSED-LOOP HUMAN SPACE EXPLORATION MISSIONS

by

Hanife Erden

Bachelor of Science
Ege University, Turkey, 2005

Master of Science
Mugla University, Turkey, 2009

---

Submitted in Partial Fulfillment of the Requirements

For the Degree of Doctor of Philosophy in

Chemical Engineering

College of Engineering and Computing

University of South Carolina

2016

Accepted by:

James A. Ritter, Major Professor

Armin D. Ebner, Committee Member

John Monnier, Committee Member

Jamil Khan, Committee Member

John Weidner, Committee Member

Cheryl L. Addy, Vice Provost and Dean of the Graduate School

# DEDICATION

To my brilliant, beloved, miracle son Levent Ege Erden.

# ACKNOWLEDGEMENTS

I want to express my deepest appreciation to my advisor Dr. James A. Ritter, for being a tremendous mentor for me. Without his guidance and encouragement this dissertation would have not been possible. I would particularly like to thank my second advisor Dr. Armin D. Ebner for his insightful comments and suggestions and teaching me the art of problem solving. Many thanks to my committee members, John Monnier, Jamil Khan, John Weidner for their time, and guidance.

I am grateful to Dr. Marjorie Nicholson and Charles E. Holland for all their help in carrying out my experiments. I would also like to express my thanks to all my previous and present research group mates, Dr. Shubhra Bhadra, Dr. Fan Wu, Dr Mohammad Iftekhar Hossain, Dr. Anahita Abdollahi Govar, Dr. Atikur Rahman, Nima Mohammadi, Hind Shabbani.

I would like to offer my special thanks to my husband Lutfi Erden for his unconditional love and endless support. I owe much gratitude to my hard working parents Mehmet Kurt and Murvet Kurt for all the sacrifices they made, their love and care. Special thanks also to my sisters Meltem Kacan and Havva Kurt for their endless support and always believing in me.

Finally, I would like to thank to National Education Ministry of Turkey for the economic support as a scholarship I was gathered during my doctorate education in USA.

# ABSTRACT

A novel two-stage pressure swing adsorption (PSA) system has been developed to remove metabolic $CO_2$ removal from the spacecraft cabin air of the International Space Station (ISS). This PSA system enriches and recovers the $CO_2$ to make it suitable for use in a Sabatier reactor ($CO_2$ reduction). This two-stage PSA process utilizes Stage 1 to concentrate metabolic $CO_2$ from about 0.2667 vol% to about 40 to 60 vol% and Stage 2 to further enrich the $CO_2$ product from Stage 1 up to > 97 vol% $CO_2$, while recovering at least 95% of it, which corresponds to removing 4.0 kg/day of $CO_2$. Each stage of this PSA system utilizes a combination of equalization, cocurrent depressurization, heavy and light reflux cycle steps to facilitate significant heavy component enrichment and recovery (i.e., $CO_2$) from a dilute feed stream. The first generation of this two-stage PSA process utilizes beaded commercial adsorbent, i.e., 13X zeolite, in both stages. These two PSA systems were designed via simulation using the Dynamic Adsorption Process Simulator (DAPS). The DAPS results were validated using an experimental multi-bed PSA system. DAPS was then used to scale up Stage 1 and scale down stage 2 to size the full scale two-stage PSA system that might someday be used on the ISS. The modeling results from Stage 1 revealed that longer heavy and light reflux step times played an important role in concentrating the $CO_2$ in the heavy product and modeling results from Stage 2 showed that a heavy reflux step was essential to achieving the desired performance. Implications from these modeling and experimental results began to hint at the possibility of significantly concentrating $CO_2$

from ambient air up to around 10 to 15 vol% at relatively high recovery using a simple PSA cycle.

The Environmental Control and Life Support System (ECLSS) for the Space Station performs several functions such as $O_2$ and $N_2$ supply and control, $CO_2$ removal and reduction, potable water supply, comfortable cabin temperature and humidity levels and total cabin pressure, and .adequate nutrition. An atmosphere revitalization system (ARS) includes oxygen and nitrogen supply and control, carbon dioxide removal and reduction, trace contaminant removal. For a closed loop system for future long term duration spaceflights, $CO_2$ removal system has an important role on not only cabin atmosphere quality but also water recovery, via $CO_2$ reduction, and $O_2$ recovery, via water electrolysis.

Detailed information about $CO_2$ capture from flue gas, $CO_2$ capture from atmospheric air, International Space Station (ISS), Environmental Control and Life Support System (ECLSS) and its subsystems such as Humidity and Temperature Control, Atmosphere Control and Supply, Waste Management, Food Management, Fire Detection and Suppression, and Atmosphere Revitalization: Oxygen Generation, Nitrogen Supply, Trace Contaminant Removal and Monitoring, mostly Carbon Dioxide Removal subsystem, Carbon Dioxide Reduction, Water Recovery and Management and lastly about Pressure Swing Adsorption (PSA) were given in Chapter 1.

Chapter 2 is about model description of a FORTRAN based in house dynamic adsorption process simulator (DAPS) that simulations of all PSA cycles in this thesis were carried out.

In Chapter 3, simulations of a 3-bed 9-step pressure swing adsorption (PSA) cycles were carried out to study the enrichment and recovery trace amount of $CO_2$ from a $CO_2$-air mixture using 13X zeolite using dynamic adsorption process simulator DAPS. Extensive parametric studies were investigated in order to determine how process performances are affected by process parameters such as HR/LR step time (thus cycle time), light reflux ratio, co-current and counter-current depressurization pressures, and light reflux pressure.

In Chapter 4, initial simulations using the full scale flow rates in search of the bed size, light reflux ratio, cycle time and vacuum pressure that lead to the desired performance with a 3-bed 8-step pressure swing adsorption (PSA) cycles (0.4% $CO_2$ from a $CO_2$-$N_2$ mixture) were carried out by using 13X zeolite as an adsorbent using dynamic adsorption process simulator DAPS. The initial DAPS results were then used to determine the 3-bed experimental conditions. Experimental runs have been done by using a 4-bed PSA apparatus. Model validation was carried out via running simulations with no adjustable parameters against experimental results.

In Chapter 5, a novel two-stage pressure swing adsorption (PSA) system has been developed to remove metabolic $CO_2$ removal from the spacecraft cabin air of the International Space Station (ISS). These two PSA systems were designed via simulation using the Dynamic Adsorption Process Simulator (DAPS). The DAPS results were validated using an experimental multi-bed PSA system. DAPS was then used to scale up Stage-1 and scale down Stage-2 to size the full scale two-stage PSA system.

Overall this study showed that target process performance for NASA has been achieved with two-stage PSA system. Two-stage PSA process performances are 98.10% $CO_2$ purity with 97.46% $CO_2$ recovery, (4.13kg $CO_2$ removal / day) from 0.2667 vol. % $CO_2$ concentration in feed stream.

# TABLE OF CONTENTS

# LIST OF TABLES

# LIST OF FIGURES

# LIST OF SYMBOLS

| | |
|---|---|
| $A$ | Cross sectional area, $m^2$ |
| $B_{j,i}$ | heat of adsorption for component i on site j, K |
| $b_{j,i}$ | Affinity parameter for site j in TPL isotherm for component i, $kPa^{-1}$ |
| $b^0_{j,i}$ | pre-exponential constant for temperature dependence, $kPa^{-1}$ |
| $Cp_{a,j}$ | the molar heat capacity of species *i* in the adsorbed phase, kJ/mol/K |
| $Cp_{g,i}$ | the molar heat capacity of species *i* in the gas, kJ/mol/K |
| $Cp_g$ | gas phase heat capacity, kJ/mol/K |
| $Cp_p$ | the heat capacity of the pellet, kJ/mol/K |
| $C_T(t)$ | total molar conc. at the downstream of the bed at time t, mol/m3 |
| $C_T$ | total molar concentration, mol/m3 |
| Cv | valve coefficient |
| $c_v$ | the valve coefficient |
| $E$ | Energy, J |
| $F_{feed}$ | Feed flow rate, slpm |
| $h_w$ | the heat transfer coefficient at the wall of the bed |
| $k_m$ | micropore mass transfer coefficient |
| $k_{M,i}^*$ | overall effective macropore mass transfer coeff. of component *i*, $s^{-1}$ |
| $k_{M,i}$ | Macropore mass transfer parameter of component *i*, $s^{-1}$ |
| L | length of the column, m |
| m | Number of the species |
| $M_g$ | average molecular weight of the gas phase |
| $m_{step}(t)$ | the molar flow leaving the bed at time t, mol/s |
| N | number of components |
| $P$ | Power, W |
| $P_o$ | the pressure outside the valve |
| $P_{step}(t)$ | the pressure at the downstream of the bed at time t, kPa |

| | |
|---|---|
| $q_i$ | adsorbed phase conc. of component *i* in the solid phase, mol/kg |
| $q^{s}{}_{j,i}$ | maximum possible adsorbed amount of component i on site j, mol/kg |
| $q_i^*$ | equilibrium adsorbed amount of component *i*, mol/kg |
| $\mu_g$ | the viscosity of the gas phase |
| R | Universal Gas Constant, 8.314Pa.m$^3$/mol/K |
| $r_i$ | the internal radius of the bed |
| $r_p$ | the effective radius of the pellet |
| $RR_{LPP}$ | Light product pressurization reflux ratio |
| *s* | the number of energy consuming steps |
| $S_g$ | the specific gravity of the gas relative to air at 1 atm and 21.45 $^o$C |
| Subscript f | Denotes end of the step (in Table2) |
| T (t) | the temperature at the downstream of the bed at time t, K |
| *T* | temperature of both gas and solid phases, K |
| $t_{cycle}$ | the total cycle time, s |
| $t_{feed}$ | the feed step time, s |
| $t_{step}$ | the total time of a specific step which the energy is calculated for, s |
| *v* | interstitial velocity, m/s |
| $v_{step}$ *(t)* | the velocity at the downstream of the bed at time t, m/s |
| $yCO_2$ *(t)* | the $CO_2$ gas phase conc. at the downstream of the bed at time t |
| $\bar{y}CO_{2,\,cum}$ | Cumulative $CO_2$ gas phase concentration |
| $yCO_{2,f}$ | $CO_2$ concentration in feed |
| $y_i$ | molar fraction of species i in the gas phase |
| $y_i^f$ | Feed stream concentration of component i (i 1-3) |
| $\gamma$ | the ratio of heat capacities (1.4 in all energy calculations in this work**)** |
| $\Delta H_i$ | heat of adsorption of component *i*, kJ/mol |
| $\varepsilon_b$ | bed porosity |
| $\varepsilon_p$ | pellet porosity |
| $\rho_g$ | the density of the gas phase |
| $\rho_p$ | density of the particle, kg/m$^3$ |
| $\eta$ | the efficiency |

# LIST OF ABBREVIATIONS

| | |
|---|---|
| 4BMS | 4-bed molecular sieve |
| AES | Advanced exploration systems |
| ARS | Air revitalization system |
| C | Carbon |
| C.M.B. | Component mass balances |
| $C_2H_4$ | Ethylene |
| $C_6H_6$ | Benzene |
| CCS | Carbon capture and sequestration |
| CDRA | Carbon dioxide removal assembly |
| $CH_4$ | Methane |
| CnD | Counter-current depressurization |
| CO | Carbon monoxide |
| $CO_2$ | Carbon dioxide |
| CoD | Co-current depressurization |
| DAC | Direct air capture |
| DAPS | Dynamic adsorption process simulator |
| E | Equalization down |
| E* | Equalization up |
| E.B. | Energy balance |
| ECLSS | Environmental control and life support system |
| EVA | Extra vehicular activity |
| F | Feed |
| $H_2$ | Hydrogen |
| $H_2O$ | Water |
| HR | Heavy reflux |
| I | Idle |

| | |
|---|---|
| IPCC | The intergovernmental panel on climate change |
| ISS | International space station |
| KOH | Potassium Hydroxide |
| LDF | Linear driving force |
| LPP | Light product pressurization |
| LR | Light reflux |
| M.B. | Momentum balance |
| MCA | Major Constituent Analyzer |
| MEMS | Micro-electromechanical |
| $N_2$ | Nitrogen |
| NASA | The National Aeronautics and Space Administration |
| $NH_3$ | Ammonia |
| $NO_X$ | Nitric oxides |
| O.M.B. | Overall mass balance |
| $O_2$ | Oxygen |
| PSA | Pressure swing adsorption |
| STEL | Short-term exposure limit |
| TCCS | Trace contaminant control system |
| TPL | Triple process langmuir isotherm |
| TSA | Temperature swing adsorption |
| UPA | Urine processor assembly |
| V.E. | Valve equation |
| VCD | Vapor compression distillation |
| WPS | Water processor assembly |
| WRS | Water recovery system |

# CHAPTER 1

# INTRODUCTION

Widespread research and development focused on slowing or reducing carbon dioxide ($CO_2$) emissions have been motivated by the growing understanding that the atmosphere is not an infinite sink thus the rising atmospheric $CO_2$ concentration and its impact on climate (Ebner and Ritter 2009; Ebner et al. 2011). The Intergovernmental Panel on Climate Change (IPCC) has also stated that $CO_2$ is the greenhouse gas contributing the largest portion of the increase in global warming (Zeman and Lackner 2004). The general agreement is to reduce $CO_2$ emissions in order to avoid negative consequences such as global warming, the spread of diseases, the destruction of ecosystems, and sea level rise (Satyapal et al. 1999; Jones 2011; Satyapal et al. 2000).

In addition to greenhouse gas capture, technology for removing $CO_2$ from air has been practiced for decades to maintain safe levels of $CO_2$ in submarines (Carey, Gomezplata, and Sarich 1983) and spaceships (DallBauman and Finn 1999). Another words, such systems for efficient removal of $CO_2$ at low concentration are also a key for the proper operation of submarines and space crafts (Satyapal et al. 2001; Ernsting 1999), mining and diving (Moore 2007), and also medical applications (Dosch 2006), where $CO_2$ concentrations are typically below 5000 ppm (J. C. Knox 2000; Mulloth and Finn 1998; Satyapal et al. 2001).

### 1.1 $CO_2$ capture from flue gas

The most frequently targeted point sources for $CO_2$ emission are fossil-fuel power plants; they are responsible for more than 40% of $CO_2$ emission. More development of carbon capture and sequestration (CCS) technologies will be required for a reduction of $CO_2$ emissions (K. S. Lackner et al. 2012). In this process $CO_2$ is captured before its emission to atmosphere. $CO_2$ capture in CCS process can be done in three ways: pre-combustion capture, post-combustion capture (more applicable, energy is produced by direct combustion of coal) and oxy-combustion. In terms of $CO_2$ capture from flue gas, several CCS technologies are under development such as absorption (both chemical and physical), adsorption, membranes, and cryogenic processes (Ebner and Ritter 2009; Satyapal et al. 1999). None of these technologies is economically feasible because of power requirements, energy integration, $CO_2$ compression, and $O_2$ supply for pre-combustion and oxy-combustion capture. Among these technologies, pressure swing adsorption (PSA) does not need heat or steam for regeneration and it can easily be modified for more improvements (Ebner et al. 2011). Even after eliminating all emissions from power plants with the commercial technologies for $CO_2$ capture, the remaining would still be released to the atmosphere, so atmospheric $CO_2$ will still require stabilizing.

### 1.2 $CO_2$ capture from atmospheric air

Besides capturing $CO_2$ with conventional CCS from coal fired and other fossil fuel based power plants, concentrated industrial sources, it is physically possible to capture $CO_2$ directly from air as a plausible alternate approach, which is called direct air capture (DAC). $CO_2$ capture from air, unlike conventional CCS, could address all other sources of

anthropogenic carbon such as cars, buses, and planes (Jones 2011; K. S. Lackner et al. 2012). A significant challenge for air capture is that separating and concentrating a gas from ultra-dilute conditions is more difficult than from a moderately dilute conditions (Jones 2011). The idea of $CO_2$ removal from atmospheric air first was introduced by Lackner and colleagues in 1999 (K. Lackner, Ziock, and Grimes 1999; K. Lackner, Grimes, and Ziock 1999). Both conventional CCS and DAC approaches have three steps; separation and concentration, compression and pipelining of $CO_2$, and pumping and storage. The only difference is separation and concentration techniques for the two approaches (Jones 2011). Air capture operates at lower temperatures (at ambient conditions); while CCS processes typically operate at higher temperatures because of these different techniques. The main approaches for the separation and concentration techniques in air capture are to use metal hydroxides or oxides to capture $CO_2$ from air and convert it to metal carbonates to concentrate $CO_2$, and then the concentrated $CO_2$ stream is released via a calcination step by heating to high temperature, around 900$^{o}$C (Baciocchi et al., 2006; Zeman and Lackner, 2004). Baciocchi and coworkers' air capture process was based on a sodium/calcium cycle in 2006, while Zeman and Lackner's process was based on absorption of $CO_2$ in aqueous sodium hydroxide solutions in 2004. Thereafter, Sodium Hydroxide Spray tower instead of a packed column cotactor has been reported to capture $CO_2$ from air to reduce the costs (Stolaroff and Keith 2008), but the overall cost of the process was expected to be quite large. However, the main disadvantage of these approaches is being energy intensive processes. Another state-of-the-art adsorption technology for air capture relies on adsorption-based approaches with the solid adsorbents such as zeolites, activated carbon, solid amine, and alumina. In 2008, a sodium-based and calcium-based $CO_2$ adsorption

cycle has been done by Steinfeld and coworkers. A technical challenge was the slow carbonation rate of the solids that leads slow adsorption rates and inefficient use of the sorbents. Sodium or calcium hydroxides as the reacting species in solid forms or in solution require substantial heat input to regenerate the sorbent or solution; leading significant energy costs (Nikulshina, Ayesa, and Steinfeld 2008). Another adsorption based DAC has been done by using weakly basic, quaternary ammonium ion-exchange resins between the bicarbonate and carbonate forms and exposed water. The main disadvantage is that having low $CO_2$ adsorption capacity causes large masses of adsorbent (Klaus S Lackner and Brennan 2009). Therefore, a follow-up adsorption-desorption process was based on adsorption on dry resin (K S Lackner 2009). The process operates with multiple filters; one in adsorption mode and the others in various stages of regeneration. In the regeneration stages, either water vapor or liquid water has been used for inducing desorption. However, the presence of water vapor will adversely affect the selectivity and adsorption capacity for $CO_2$ (Belmabkhout, Serna-Guerrero, and Sayari 2010). Adsorption based studies given so far has been at elevated temperatures those studied in high-temperature CCS processes. Some other groups are also studied novel air capture materials and processes that are based on adsorption at ambient temperatures. Those air capture materials are oxide-supported amine materials and silica-supported amines as adsorbents for the extraction of $CO_2$ from ambient air (Choi et al. 2009; Belmabkhout, Serna-Guerrero, and Sayari 2010). It can be said that supported amine adsorbents are promising materials for use in potential air capture processes because of being regenerable with low-cost. So far, there is no detailed scale-up design reported in the literature for air capture. Overall, technologies for the removal of $CO_2$ from ambient air on a larger scale are still in their infancy, they have gained increased

attention recently (Jones, 2011; Wang et al., 2015) because DAC presents an even greater challenge because of the extremely dilute $CO_2$ concentrations in ambient air. If air capture economically practical, it can actually reduce the global $CO_2$ concentration in the atmosphere.

In addition to greenhouse gas capture from flue gas and ambient air, technology for removing $CO_2$ from air has been practiced for decades to maintain safe levels of $CO_2$ in submarines (Carey, Gomezplata, and Sarich 1983) and spaceships (DallBauman and Finn 1999).

### 1.3 International Space Station (ISS), Environmental Control and Life Support System (ECLSS)

The National Aeronautics and Space Administration (NASA) is responsible in civilian space program as well as advancement of aeronautics and space science and involved developing the life support technology required to support current and future long-duration manned space flight; extensive research and development is being continuing on individual life support subsystems (L. and C. 1970; Pearson A.O. 1971; Rudolph, Hebestreit, and Harzer 2000; NASA Facts 2004).

In the International Space Station (ISS), basic life support needs $O_2$ supply, $CO_2$ removal, comfortable temperature and humidity range, pure water supply, adequate nutrition that the crew can live and work. Physical storage of the necessary quantities of food, water, oxygen, absorbents leads increasingly weight penalties, especially when missions of several months or more are considered. For such missions, regenerative systems will be required (Bowman and Lawrence 1971). Environmental Control and Life

Support System (ECLSS) is the responsible with all these needs. Another word, ECLSS functions are oxygen supply for metabolic consumption, potable water supply for consumption, food preparation and hygiene uses, carbon dioxide removal from the cabin air, particulates and microorganisms filter from the cabin air, removal of volatile organic trace gases from the cabin air, cabin pressure control, cabin atmosphere composition and purity control, monitoring and controlling cabin environment partial pressures of nitrogen, oxygen, carbon dioxide, methane, hydrogen and water vapor, temperature and humidity control, cabin ventilation, collect, stabilize, store, and dispose of wastes (waste management), and fire detection and suppression for all mission and recycle water and oxygen for long mission (NASA Facts 2004; DallBauman and Finn 1999; Daues 2006; Ewert, Barta, and Mcquillan 2009; Wieland 1994; R. Carrasquillo 2013). The functions and sub-functions of ECLSS are given in Table 1.1. ECLSS modes of operation are open loop for current short term missions and closed loop for future long term missions. In open-loop ECLSS uses resources being brought from the Earth, continuous input and output, while in closed-loop flow diagram life support system recovers other sources with processing possibilities of non-useful waste. The current and future long-duration manned space flight flow diagrams of ECLSS are given in Figure 1.1 and Figure 1.2 respectively.

### 1.3.1 Humidity/Temperature Control

Temperature and Humidity Control system of ECLSS is responsible for temperature control, humidity control, ventilation, equipment cooling, shown in Figure.1.3 Firstly, To keep the temperature even, the station is insulated with a highly-reflective blanket called Multi-Layer Insulation because the temperature range of outside of the Space Station is 250 to minus 250 $^{o}$F (Sun-facing side and the dark side) without thermal

controls (NASA 2001). Temperature Humidity Control subsystem maintains a habitable environment and monitors the temperature inside the Space Station by removing heat and humidity, and circulating the cool dry air. Circulating cool, dry air minimizes the temperature variations, keeps the humidity low and supports smoke detection (NASA Facts, 2008). Cabin temperature nominal range is 65 to 80˚F (NASA 2001). Heat exchangers have been used on all crewed spacecraft to date to control temperature and to condense moisture from the atmosphere (R. L. Carrasquillo 2008; Council 1997; Wieland 1994). Sources of heat include electronics, lighting, and solar heating of the habitat as well as metabolic sources. Excess heat is removed via ventilation. Ventilation is the primary method of removing heat (Wieland 1994).

Cabin humidity is usually maintained at about 60% relative humidity because high humidity can promote the growth of microbes and fungi and low humidity can cause drying of the eyes and skin and the decreasing protection against respiratory infections (NASA 2001; Wieland 1994). In addition to effects on human health, low humidity leads the generation of sparks, very serious fires on a space station when being mixed with oxygen, hydrogen, and other flammable gases, caused by a buildup of static electricity ((NASA, n.d.). A rotary liquid centrifugal separator, mechanical device has been used to remove condensate from the air stream in a microgravity environment (Council 1997). Currently ISS uses condensing heat exchangers with anti-microbial hydrophilic coatings requiring periodic dry out, which is a disadvantage (Gatens and Ruff 2013). Using membranes instead of mechanical separators have been investigating in order to simplify the system design for future long-duration spaceflights (Council 1997; R. L. Carrasquillo 2008).

### 1.3.2 Atmosphere Control and Supply

The cabin atmosphere in the ISS is maintained at the Earth-normal conditions at sea level for reasons including safety and easier testing of equipment, with a partial pressure of oxygen sufficient to sustain human life. The Atmosphere Control and Supply subsystem especially monitors the amount of nitrogen and oxygen in the space station's air. The subsystem consists of pressure sensors and regulators, shutoff valves, check valves, relief valves, distribution lines and tanks, and valves and controls to provide the proper concentrations of oxygen and nitrogen (Council 1997; Wieland 1994; R. L. Carrasquillo 2008). The total pressure for an extravehicular activity (EVA) or spacewalks is regulated to 70.3 kPa (10.2 psia) to ease the transition to the space suit pressure. A simplified schematic of an atmosphere control and supply system is shown in Figure 1.4 (Wieland 1994). After monitoring major constituents ($N_2$, $O_2$, $CO_2$, and humidity) by having separate analyzers for each gas such as a solid-state laser diode absorption system for $O_2$, a solid-state infrared absorption system for $CO_2$, and a solid-state, thin film capacitance detection system for relative humidity, reports are sent to the Major Constituent Analyzer (J. L. Perry et al. 2015). The pressure control panel monitors total pressure and the $O_2$ partial pressure of the space station's cabin to determine $N_2$ and $O_2$ amounts (NASA, n.d.; Wieland 1994; J. L. Perry et al. 2015). High pressure tanks and cryogenic storage of liquefied gases have been used for storage of the atmosphere constituent gases, $N_2$ and $O_2$, (NASA, n.d.; Wieland 1994). The Major Constituent Analyzer (MCA) on ISS is based on mass spectrometry.

### 1.3.3 Atmosphere Revitalization

National Aeronautics and Space Administration's (NASA) Advanced Exploration Systems (AES) Program has been studying and developing candidate atmosphere revitalization System (ARS) equipment technologies for deep space exploration missions (J. C. Knox et al. 2012; J. Perry et al. 2012; Howard, D., Perry, J., and Roman, M. 2014). Therefore, the ISS AR subsystem has served as the starting basis to economically advance environmental control and life support (ECLSS) technology for developing the AR subsystem of the future long-duration space exploration missions (J. L. Perry et al. 2015; Hodgson et al. 2012). Fundamentals of air revitalization system (ARS) are oxygen and nitrogen supply and control, carbon dioxide removal, carbon dioxide reduction for oxygen recovery and trace contaminant removal, shown in Figure 1.5 (Murdock 2010; Ewert, Barta, and Mcquillan 2009; J. L. Perry et al. 2015). These processes also interact with the water recovery system to re-form water by carbon dioxide reduction assembly for water electrolysis to produce oxygen with the hydrogen by-product which is utilized by the carbon dioxide reduction assembly along with the waste carbon dioxide (Murdock 2010). Carbon dioxide reduction step is a necessary step for closed-loop that minimizes the resupply needed for crew support for long duration mission (Murdock 2010).

#### 1.3.3.1 Oxygen Generation

The concentration of $O_2$ must be maintained near the sea-level $O_2$ partial pressure to avoid physiological effects such as decreased night vision, impaired memory and coordination, unconsciousness, death of nerve tissue (Anoxia) and hypoxia (lack of $O_2$) at lower partial pressures of $O_2$ and lung irritation at higher partial pressures of $O_2$. It is extremely vital to maintain an adequate $O_2$ supply because of these physiological effects

(Wieland 1994; NASA, n.d.). In the space crafts, oxygen is consumed by the crew, experimental animals, and lost through leakage (Council 1997). Oxygen can be provided by resupply and storage. On all U.S-crewed missions to date, the $O_2$ has been supplied from stored gaseous or cryogenic oxygen (Council 1997; NASA, n.d.; Daues 2006). For longer duration missions, mass penalty of these open-loop technologies is excessive, thus recovery of $O_2$ is required. Electrolysis of recovered waste water to supply $O_2$ is the technology chosen by the ISS for future long-duration missions (Wieland 1994; Council 1997; J. L. Perry et al. 2015; R. L. Carrasquillo 2008; NASA, n.d.; Murdock 2010). The machine that produces oxygen using electrolysis is called "Elektron" which is powered by the solar panels and batteries (NASA, n.d.). Electrolysis process dissociates water ($H_2O$) into oxygen and hydrogen gas ($O_2$ and $H_2$) by an electric current (R. L. Carrasquillo 2008). Hydrogen goes to the negative electric pole while oxygen goes to the positive electric pole. By-product of electrolysis, $H_2$, is currently sending to space, overboard venting, but it would be used in $CO_2$ reduction processes for future long duration mission (Wieland 1994; Council 1997; R. L. Carrasquillo 2008). The technologies for water electrolysis are static feed water electrolysis with KOH electrolyte, solid polymer water electrolysis with a per-fluorinated sulfonic acid polymer, which has been used in the ISS, and circulating KOH electrolysis (Council 1997; Wieland 1994). Only in emergencies, perchlorate candle produces oxygen through chemical reactions. A Portable Breathing Apparatus or gas mask can also be used in critical situations (NASA, n.d.).

#### 1.3.3.2 Nitrogen Supply

Nitrogen is needed to maintain the total atmospheric pressure of cabin. Nitrogen is safely stored onboard spacecraft because of being inert gas then it is generally resupplied

from stored gaseous or cryogenic tanks in the ISS (Council 1997). The nitrogen replacement system consists of pressurized tanks of nitrogen with electrically and manually controlled valves (NASA, n.d.). $N_2$ might also be provided by the catalytic dissociation of hydrazine ($N_2H_4$) or ammonia ($NH_3$) for future mission because of having a lower mass penalty than storing $N_2$, but hydrazine is highly toxic (Council 1997; Wieland 1994). The recovery of nitrogen from metabolic waste products has also being investigated.

#### 1.3.3.3 Trace Contaminant Removal and Monitoring

In a space habitat, even a small amount of a contaminant may result in the crew discomfort or sickness because the atmosphere of a space habitat does not have the volume of the Earth's atmosphere, as a result, does not dilute contaminants (Wieland 1994; Council 1997). Therefore, it is essential to monitor even the trace amounts of contaminants in the closed environment of a space habitat atmosphere. The crewmembers receive the proper air make-up. Trace Contaminant Control and removal system must protect crew for metabolic and chemical contaminants and particles, and deal with sources of trace contaminants. The sources of trace contaminants include off-gassing of materials, contaminants produced by humans (feces, urine, perspiration, etc.), food preparation, housekeeping cleaners, and experimental activity (Council 1997; Wieland 1994). Some contaminants are common to all missions such as the products of human metabolism while others will vary from mission to mission and time duration of mission (Council 1997). There might be as many as trace contaminants. The main contaminants are carbon monoxide (CO) from machine off-gassing and in their urine and their breath, ammonia ($NH_3$) from cleaning supplies and the breakdown of urea in sweat, nitric oxides ($NO_X$), ethylene ($C_2H_4$), benzene ($C_6H_6$), methane ($CH_4$), is produced in the intestines, and

particulates (NASA, n.d.). On the Earth these contaminants are not a big problem because of existing as small amounts but on the ISS, air is constantly reused and the chemicals will accumulate if the air is not cleaned properly. To protect crew members, Trace Contaminant Control and removal system must detect hazardous trace gases, control contaminants below the maximum allowable concentrations in space, and keep them an acceptable range. Therefore, the level of the trace-contaminant should be monitored at all time. The method of trace contaminant monitoring used on the ISS is a second miniature mass spectrometer integrated with a micro-electromechanical (MEMS) gas chromatograph (J. L. Perry et al. 2015; Wieland 1994; Council 1997). The ISS Trace Contaminant Control System (TCCS) has four contaminant removal components: particulate filters, activated charcoal adsorption bed and thermal catalytic oxidizer with post-sorbent bed (R. L. Carrasquillo 2008; Council 1997). The method to remove dust particles, aerosols, and airborne microbes is a high efficiency particulate atmosphere filters in the ventilation system (Wieland 1994; Council 1997). Activated charcoal adsorption bed removes compounds with high molecular weights compounds. Thermal catalytic oxidizer oxidizes compounds at high temperature (400oC). Chemisorbant beds are used to remove nitrogen and sulfur compounds, halogens, and metal hybrids (Council 1997; Wieland 1994). Advanced Trace Contaminant Control (ATCC) systems such as photo catalytic oxidation, thermal catalytic oxidation and regenerable adsorbent process are being investigated (Ewert, Barta, and Mcquillan 2009).

#### 1.3.3.4 Carbon Dioxide Removal

Environmental air normally contains ca. 0.03 vol. % $CO_2$ with 4 vol. % $CO_2$ in air exhaled by humans. According to the United States Occupational Safety and Health

Administration, the threshold limit value (TLV) of $CO_2$ is 0.5% with 3% for short-term exposure limit (STEL) during 15 minutes. The danger of suffocation in closed rooms is the displacement of oxygen by $CO_2$-accumulation (Knox, J.C. and Howard 2007; Mattox and Bardot 2011). Therefore, if the exhaled gas is to be recycled, it is necessary to remove the carbon dioxide in the breathing loop considering human health (Dosch 2006). Because spacecrafts are completely closed environment, produced carbon dioxide by the crew's normal metabolic respiration, other living organisms, and chemical processes must be removed from the atmosphere, therefore the concentration of $CO_2$ must maintain at a very low level (0.4 kPa or below) in order to avoid adverse physiological effects n crew members (Council 1997; Wieland 1994). One crew member generates $CO_2$ during normal metabolic respiration is at an average rate of 1kg (2.2 lb) per day and that must be removed at a nominal rate of 1kg per day per person. The methods considered for use on space habitat to remove $CO_2$ from cabin air are rely on absorption (chemical or electrochemical reaction with a sorbent material) such as electrochemical depolarization concentration and air polarized concentrator, adsorption (physical attraction to a sorbent material) such as metal oxide, solid phase amine, lithium hydroxide, and molecular sieves, membrane separation (osmotic membranes, amine-functional membranes), and scrubbing $CO_2$, such as permeable membranes, liquid amine, adsorbents, and absorbents (Wieland 1994; Sherif et al. 2005; Tsai et al. 2003).

The primary method to remove $CO_2$ in space life support systems has been used on most U.S. space habitats until early 1990s was absorption by lithium hydroxide (LiOH); granular lithium hydroxide (LiOH) canisters (Ewert, Barta, and Mcquillan 2009; Council 1997; Wieland 1994; DallBauman and Finn 1999; NASA, n.d.; Hwang et al. 2008;

Satyapal et al. 2001; scott R. Johnson, Garrad, and Mitchell 1993; S. R. Johnson 1992; Satyapal et al. 1999). Although the storage capacity of LiOH is high (30 wt %), the material cannot be practically regenerated because of having nonreversible chemical reaction. In this process chemisorption of $CO_2$ on LiOH is a nonreversible chemical reaction which means that the LiOH must be periodically replaced with fresh LiOH material (Wieland 1994). In addition, the required LiOH amount to remove generated $CO_2$ from one person per day is 2kg and this mass is increasing linearly with the duration of mission and the crew size (DallBauman and Finn 1999). This works well for short duration missions, but for future long duration missions, additional storage of fresh LiOH canisters will be required which is prohibitive because of weight penalty of spacecrafts for long duration. Therefore, non-regenerable lithium hydroxide canisters are nor useful for long duration missions (Wieland 1994; Council 1997). Later on, a regenerable amine based system has been demonstrated for carbon dioxide removal and partial humidity control; regeneration has been done via a vacuum swing process (Ewert, Barta, and Mcquillan 2009). This system functions on two adjacent sorbent beds; one bed is for removing $CO_2$ and water vapor by exposing to the ventilation loop flow, while the other is regenerated by vacuum exposure or inert gas (Filburn, Dean, and Thomas 1998).

Currently the International Space Station uses the Carbon Dioxide Removal Assembly (CDRA) to remove carbon dioxide from the cabin atmosphere. This assembly is a 4-Bed molecular sieve (4BMS); the first two regenerative desiccant beds are packed with silica gel and zeolite 13X to remove water and the other two regenerative beds are packed with zeolite 5A to remove carbon dioxide or to maintain $CO_2$ within tolerable limits (generally below 7.6 mm Hg) with the temperature swing adsorption (TSA) technology,

which utilizes an adiabatic thermal cycling process that involves the adsorption and regeneration of $CO_2$ using an adsorbent (Mattox and Bardot 2011; James C Knox et al. 2005; J. Perry et al. 2012; J. L. Perry et al. 2015; J. C. Knox et al. 2012; J. C. Knox et al. 2013; J. C. Knox et al. 2014; R. L. Carrasquillo 2008; Ewert, Barta, and Mcquillan 2009). The components of 4-bed molecular sieve assembly are a blower, an air save pump, bed heaters, heat exchanger, valves, and sensors. The two desiccant-adsorbent beds operate on a cycle with one adsorbing $CO_2$ from the cabin air while the other desorbs previously accumulated $CO_2$ to space vacuum, before exposing the heated bed to space vacuum, the ullage air is pumped out (James C Knox et al. 2005; Matty 2010). Figure 1.6 shows the CDRA-4BMS schematically. The benefit of using the any kind of zeolites, here is zeolite 5A is that they can be easily regenerable and continuously re-used. The two beds for $CO_2$ removal operate in such a way that one bed uses a fan to pass cabin air through the bed to remove $CO_2$ and water vapor, while the second bed is exposed to space vacuum to regenerate the sorbent (Satyapal et al. 2001; J. C. Knox et al. 2012; J. C. Knox et al. 2013; J. C. Knox et al. 2014; James C. Knox et al. 2015). Although the CDRA has been proven to be very effective, there are some major drawbacks to this current system. The first one is generation of dust that contaminates equipment on the space station. Having temperature oscillation in TSA system generates dust because the clay binder and the crystal have different thermal expansion and contraction that leads generation of cracking then eventually dust (Do 1998). The next drawback is that the dust buildup inside the packed beds results in increased pressure drop during the beds. The last one is requirement of a large amount of energy to regenerate the material; because the clay binder is a poor thermal

conductor that limits the escape of heat generated from the heat of adsorption (Mattox and Bardot 2011).

#### 1.3.3.5 Carbon Dioxide Reduction

Currently, $CO_2$ is heat and vacuum desorbed to space because there is no need to process it further for short-duration missions, but it could be supplied to a $CO_2$ reduction assembly to recover $O_2$ for longer duration missions (Council 1997; Wieland 1994; Ewert, Barta, and Mcquillan 2009; James C Knox et al. 2005). Because the loss of mass in $O_2$ will lead to increased storage or resupply requirements which will be expensive and weight penalty for long duration missions (Wieland 1994). Therefore, this subsystem of AR system as well as $CO_2$ removal system has an essential role to have closed-loop flow diagram for long duration missions. Currently, the ISS does not include $CO_2$ reduction assembly (Council 1997; Ewert, Barta, and Mcquillan 2009; R. L. Carrasquillo 2008). There are several methods such as Sabatier reactor, Bosch reactor, electrochemical separation of $O_2$ from $CO_2$ or biological methods to recover this $O_2$ (Council 1997; Wieland 1994; Ewert, Barta, and Mcquillan 2009; R. L. Carrasquillo 2008). $CO_2$ reacts with hydrogen (H2) at high temperature in the presence of a catalyst to produce methane (CH4) and water (H2O) in the exothermic Sabatier process for $CO_2$ reduction (Ewert, Barta, and Mcquillan 2009; Council 1997; Wieland 1994; James C Knox et al. 2005). $O_2$ can be produced for the cabin atmosphere by water electrolysis by using this produced H2O and the by-product of water electrolysis, hydrogen (H2), can be recycled to the Sabatier. The CH4 can theoretically be used for attitude control or can be vented overboard as a waste product (Council, 1997; Knox et al., 2005). Another process is the exothermic Bosch process. In this reactor $CO_2$ again reacts with H2 at high temperature in the presence of a

catalyst to produce solid carbon (C) and water (H2O). This process, the catalyst bed should be replaced periodically because of carbon accumulation (Council 1997; Wieland 1994). And the other process is $CO_2$ electrolysis and it has been still investigated. In that process, $CO_2$ converts to carbon and $O_2$ directly. The last possible $CO_2$ reduction technology is biological methods; plants can also reduce $CO_2$ through photosynthesis (Council 1997). ISS is planning to use Sabatier reactor for $CO_2$ reduction along those technologies because it is more mature technology than others. There are two modes of operation (process and standby) in the planning Sabatier assembly. In Process mode, inlet gas flows through the system and methane and water were produced operated at sub-ambient to avoid combustible gasses leaking out to the atmosphere. In Standby mode, the unit was evacuated to below 1 psia by isolated supply gasses and stopped coolant air (James C Knox et al. 2005).

### 1.3.4 Water Recovery and Management

Potable (drinking) and washing water has been provided from the stored water tanks, filled prior to launch, on all human space missions so far. To recover water from wastewater and urine for long-term missions has an essential role to potentially reduce the net mass of required water, thus weight because having limited storage space, having larger crews or, it would be prohibitive to store or resupply all of the water required for longer duration missions (Wieland 1994; Council 1997; NASA Facts 2004). A simplified water recovery and management (WRM) system schematic is shown in Figure.1.7

Several methods including filtration, distillation, evaporation, absorption, adsorption, catalytic oxidation, and biological methods are available to process humidity condensate, urine, and hygiene and wash water for reuse as potable water or for other uses

on space habitats (Council 1997; Wieland 1994). Therefore, the water recovery system (WRS) is designed to recycle crewmember urine, cabin humidity condensate, wastewater, and Extra Vehicular Activity (EVA) wastes for reuse as clean water (Council 1997; NASA Facts 2004). The distillation techniques are vapor compression distillation (VCD), thermoelectric integrated membrane evaporation, vapor phase catalytic ammonia removal, and simple air evaporation and the filtration methods are reverse osmosis, multifiltration, and electrodialysis (Council 1997). The ISS Water Recovery System (WRS) includes urine processor assembly (UPA) and water processor assembly (WPS) (R. L. Carrasquillo 2008; NASA Facts 2004). The urine processor, a phase change process, recovers water from urine through an ambient-temperature Vapor Compression Distillation (VCD) technology, which is a low-pressure evaporation in a rotating distillation assembly that compensates the absence of gravity and aids in the separation of liquids and gases in space(R. L. Carrasquillo 2008; Council 1997; NASA Facts 2004; Wieland 1994). Distillate water from the VCD is combined with all other wastewaters and delivered to the Water Processor for treatment. The advantage of VCD is being a power-efficient process while having complex mechanical design with limited water recovery as a disadvantage (R. L. Carrasquillo 2008). The other subsystem of water recovery system is the water processor assembly which produces potable water from urine distillate, cabin air humidity condensate, and other hygiene and miscellaneous waste waters (R. L. Carrasquillo 2008; NASA Facts 2004). The technology uses includes multi-filtration, adsorption, ion exchange, and heterogeneous catalytic oxidation, and gas/liquid membrane separators (NASA Facts 2004; R. L. Carrasquillo 2008; Wieland 1994). The Water Processor first removes free gas and solid materials such as hair and lint, then operates a series of multi-filtration beds for further

purification and uses a high-temperature catalytic reactor assembly to remove any remaining organic contaminants and microorganisms (NASA Facts 2004; Wieland 1994; Council 1997). The main drawbacks are logistics penalties, required bed replacement, higher power, and complexity of temperature catalytic reaction process (NASA Facts 2004; R. L. Carrasquillo 2008).

Monitoring of the product water quality is needed to ensure that the water is with acceptable quality and is done by the Process Control and Water Quality Monitor in the ISS(NASA Facts 2004; Council 1997). The recovered water must meet purity standards before it can be reused by crew members. To check the purity of product water electrical conductivity sensors have been used because the conductivity of water is increased by the presence of typical contaminants. If the water is acceptable, it is delivered to product water storage, while unacceptable water is reprocessed through the system again (NASA Facts 2004; Council 1997; R. L. Carrasquillo 2008; NASA, n.d.; Wieland 1994).

### 1.3.5 Waste Management

Waste Management subsystem must deal with the sources of wastes in a space habitat, which are metabolic wastes consisting of moist solids including feces and vomitus, other solid wastes (paper and plastics), liquid wastes including urine and waste hygiene water, and gaseous wastes (metabolic gaseous wastes ($CH_4$, $H_2S$, $H_2$, CO, and $CO_2$) and by products from various chemical processes), which shown in Figure 1.8 with the products of waste processing (Wieland 1994). The goal of the waste management system is to develop waste management technologies to recover resources, and to increase crew safety and performance while decreasing mission cost.

The Waste Management includes a toilet subsystem for collecting urine and feces and an overall housekeeping system for collecting and storing other wastes; liquid, solid, and concentrated wastes such as food waste, refuse, and biomass (Council 1997). Waste Collection System consists of a commode, urinal, fan separators, odor and bacterial filter (vacuum vent quick disconnect), and waste collection controls. The commode processes the fecal wastes with bag liner, and the urinal is a flexible hose with attachable funnels for storage in waste water tank. The ISS Segment utilizes a commode/urinal system (Daues 2006). In the ISS for short-duration missions recycling is less of an issue, so feces and refuse are collected in a bag and compacted in a cylindrical canister for storage and disposal for eventual by sending it back to Earth with a visiting Shuttle crew, or by placing it into a Progress rocket (Council 1997; Daues 2006). For more advanced long-duration missions, it is necessary to recover for reuse the mass, both liquid and solid, of the metabolic waste. The Heat Melt Compactor, sterile, compact, plastic encapsulated disks, might be the technology for waste stabilization and storage and volume reduction of waste as well as for water recovery. In the heat melt compactor, to compress the waste pneumatic pistons can be used and the waste is heated, plastic is melted as well as the water is vaporized with electric heaters, the that vaporized water might be condensed and recovered (Ewert, Barta, and Mcquillan 2009). Another technology for stabilizing the waste and providing recovered methane fuel as well as water is pyrolysis technology, (Ewert, Barta, and Mcquillan 2009).

### 1.3.6 Food Management

Food currently provided on space vehicles is produced and packaged on the ground. Stored food must be preserved until needed and will either be dehydrated, refrigerated (for

short-term storage), or frozen (for long-term storage) (Wieland 1994). The technologies to preserve the food include freeze-drying, canning, radiation-stabilization, thermo-stabilization (heat processed, canned, and stored at room temperature), and other methods (Council 1997). On the ISS, the electrical power is produced by solar arrays, which does not produce water (Casaburri, Gardner, and George 1999). Food management in the ISS provides frozen foods, refrigerated foods, rehydratable foods (soups, casseroles, appetizers, breakfast foods), thermo-stabilized foods (meats, vegetables, fish, fruit), irradiated foods (meats), natural-form foods (nuts, granola bars, cookies) because no addition water required before consumption of the foods (Daues 2006; Casaburri, Gardner, and George 1999). All daily menu food is single-service, disposable containers to eliminate the need for a dishwasher (Daues 2006). Food production in space through biological processes might be needed for long-duration missions, but it raises new issues in food processing, storage, and preparation and also requirement for the additional power, mass, and volume (Council 1997).

### 1.3.7 Fire Detection and Suppression

Fire Detection and Suppression subsystem of ECLSS detects incipient fires regardless of location or type (fire detection sensors), proves a system of alarms and automatic software actions to alert the crew and automatically respond to a fire, suppresses of fires while minimizing toxic effects on the crew (fire extinguishers, portable breathing equipment), and cleans up after a fire (Wieland 1994; NASA Facts 2004). Methods to detect the fire include flame detectors based on visible, infrared, and ultraviolet emissions, smoke detectors based on detecting the particles emitted by burning materials, ionization detectors, and photoelectric flame detectors; ISS is using the smoke detector is based on

photoelectric technology. Suppression methods are water, foam, $CO_2$, and Halon in general, but in space some of them are not useful such as water because of possibility of being related to electrical failures, and foam because of cleanup problems. Halon and $CO_2$ can be used as a suppressant; ISS is using portable $CO_2$ fire suppression bottles. The reason to choose $CO_2$ suppressant is due to its effectiveness and ability to be easily removed by the atmosphere revitalization system (Gatens and Ruff 2013; Wieland 1994; R. L. Carrasquillo 2008; Daues 2006).

### 1.4 Pressure Swing Adsorption (PSA)

In the last decades, pressure swing adsorption (PSA) technology has been developed with tremendous progress and it is one of the more efficient gas separation and purification technologies because of its low energy requirement and low capital investment costs (Yoshida et al. 2003). PSA technology is being widely used in industry for air-drying, $CO_2$ capture, hydrogen purification or recovery, air separation, and various other separations such as methane recovery from landfill gas (Yoshida et al. 2003). There are excellent reviews available in the literature (Diagne, Goto, and Hirose 1995; Tondeur, D.; Wankat 1985; Kawai 1986; Ruthven, D. M.; Farooq 1994; Suzuki 1991; Yang 1987; Ebner and Ritter 2009).

In this thesis, the $CO_2$ removal and concentration from trace amount of $CO_2$ containing stream during closed-loop human space exploration missions has been achieved via pressure swing adsorption technology.

**Table 1.1** ECLSS functions and sub-functions (Wieland 1994; Council 1997).

| Function | Details |
|---|---|
| Temperature and Humidity Control | Temperature Control<br>Humidity Control<br>Ventilation<br>Equipment cooling |
| Atmosphere Control and Supply | Monitoring Major Constituents<br>Atmosphere Composition Control<br>Atmosphere Constituents Storage<br>Partial and Total Pressure Control |
| Atmosphere Revitalization | $CO_2$ Removal<br>$CO_2$ Reduction<br>$O_2$ Replacement<br>$N_2$ Replacement<br>Trace Contaminant and Particulate Monitoring and Removal |
| Water Recovery and Management | Humidity condensate, urine, hygiene and wash wastewater processing<br>Water storage and distribution<br>Water Recovery<br>Water Quality Monitoring |
| Waste Management | Fecal Collection<br>Urine Collection and Pretreatment<br>Waste processing |
| Food Management | Food production, processing, storage |

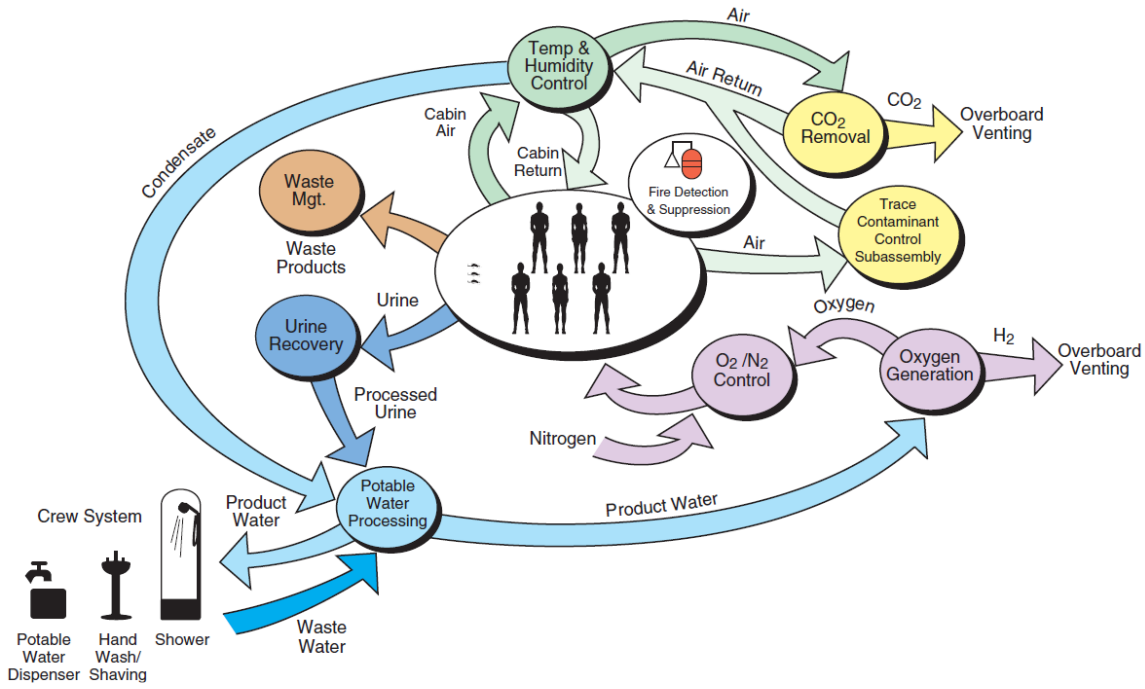


**Figure 1.1** Current space station regenerative environmental control and life support system (ECLSS) flow diagram, open system (NASA Facts 2004).

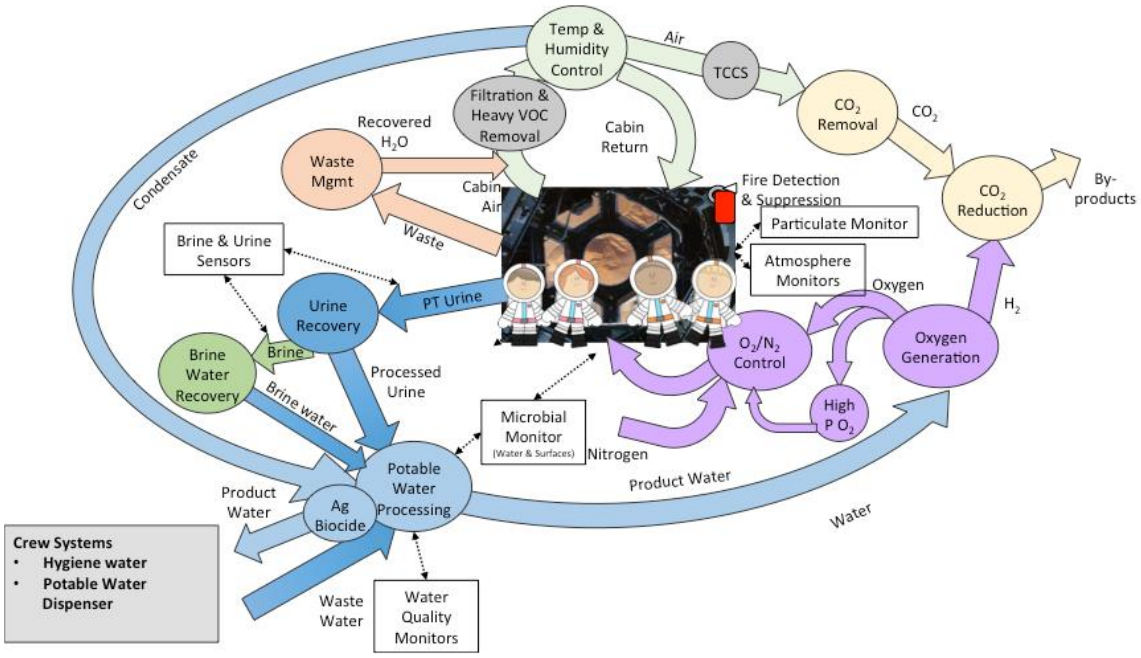


**Figure 1.2** Future space station regenerative environmental control and life support system (ECLSS) flow diagram, closed-loop system (NASA Facts, 2004).

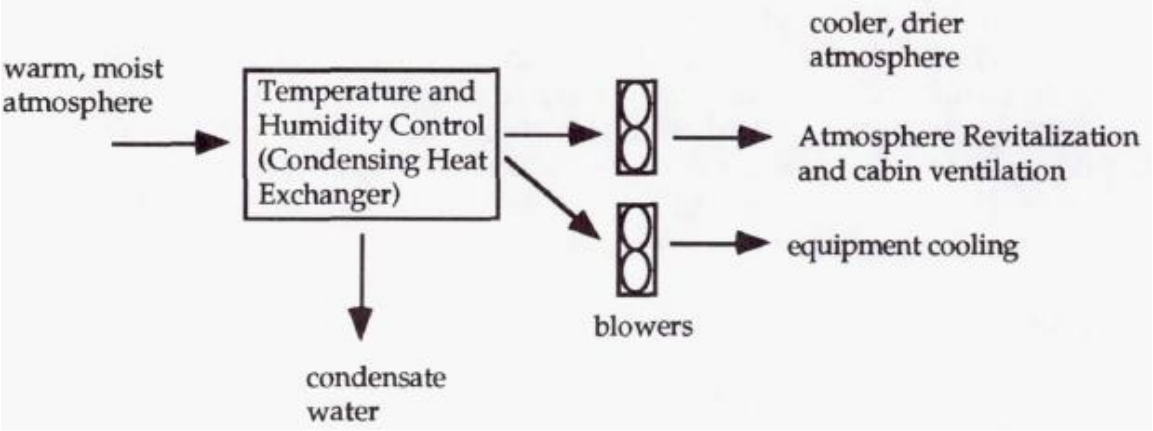


**Figure 1.3** Temperature and humidity control system (Wieland 1994).

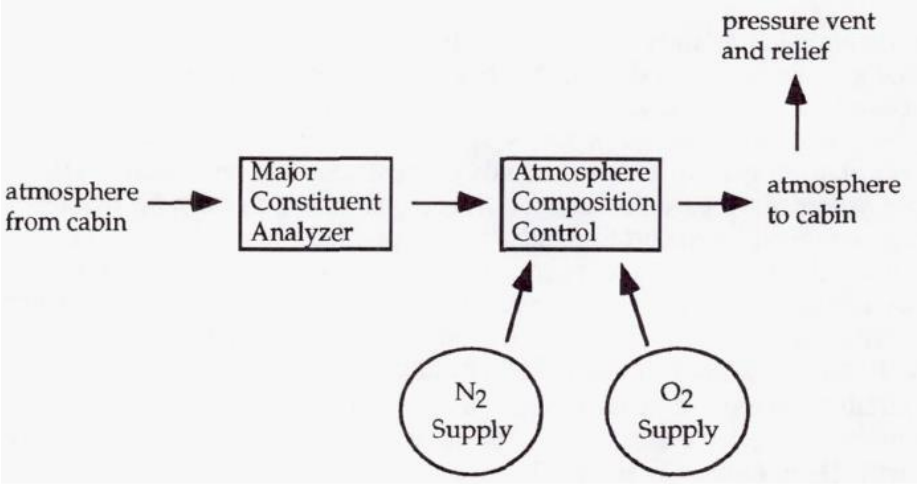


**Figure 1.4** Atmosphere Control and Supply (Wieland 1994).

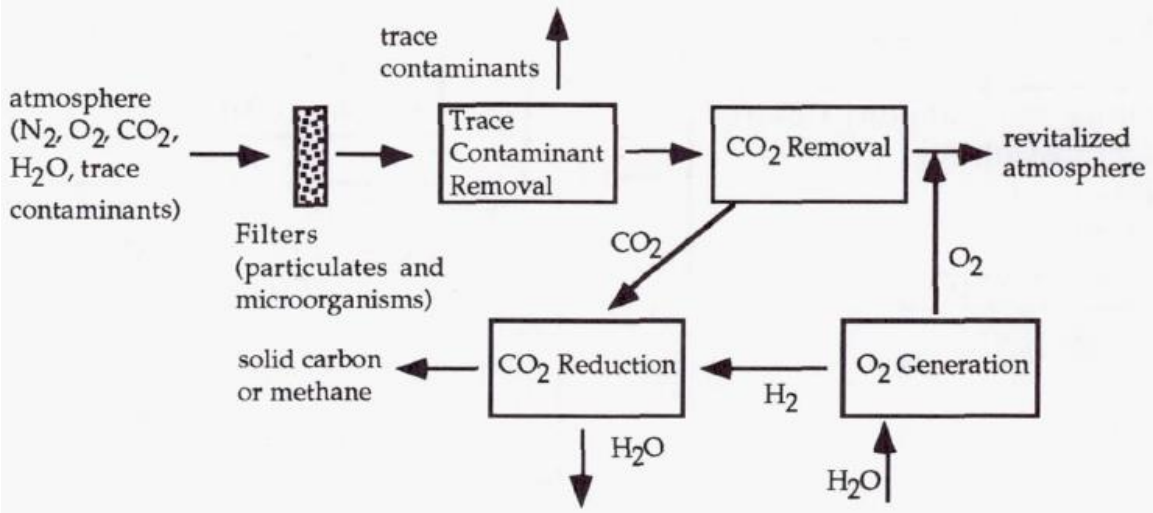


**Figure 1.5** Atmosphere revitalization subsystems (Wieland 1994).

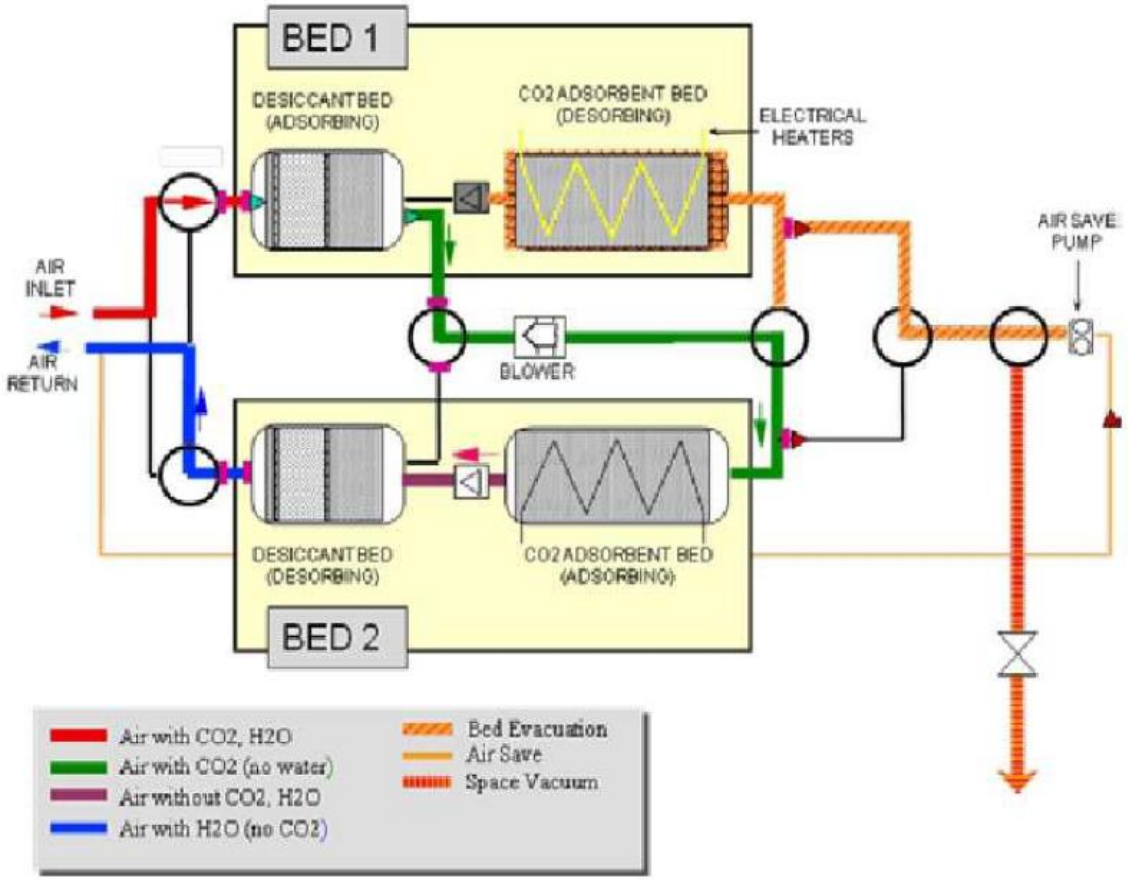


**Figure.1.6** CDRA-4BMS schematic. Desiccant-adsorbent Bed 2 adsorbing $CO_2$ from the cabin and desiccant-adsorbent Bed 1 desorbing to the space vacuum (Matty 2010; James C Knox et al. 2005).

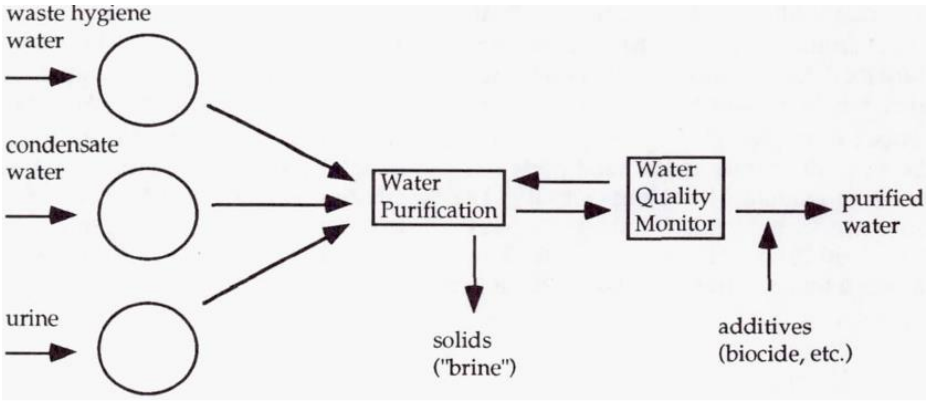


**Figure.1.7** Water recovery and management (Wieland 1994).

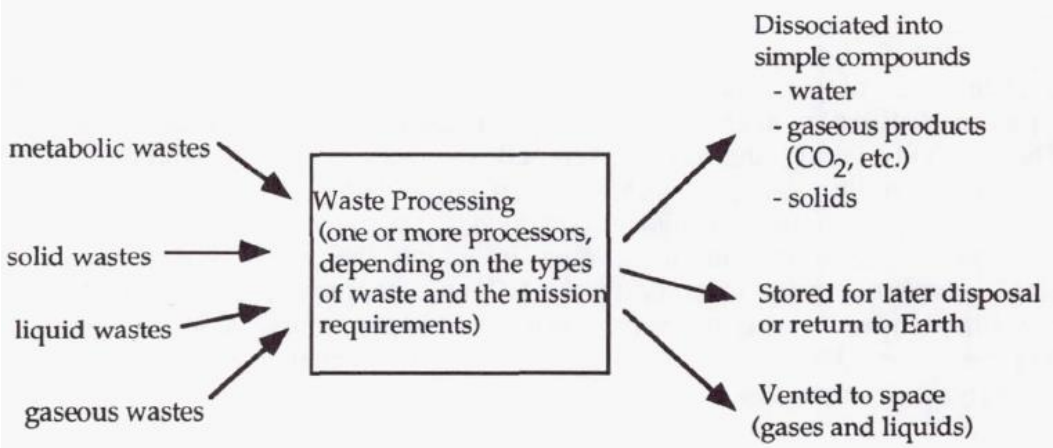


**Figure.1.8** Waste management system (Wieland 1994)

# CHAPTER 2

# MODEL DESCRIPTION

## 2.1 Model Description

Simulations of all PSA cycles were carried out using a FORTRAN based in house dynamic adsorption process simulator (DAPS) that uses DASPK as a solver platform, which is built for solving complex partial differential equations via method of lines and a time adaptive integration technique (Brown, Hindmarsh, and Linda 1994). The nature dynamic PSA simulation models can be described by mass and energy balances, mass and energy transfer equations, and equilibrium isotherm. Table 2.1 shows the main equations included in the present model: component mass balances, an overall mass balance, a pellet mass balance through a linear driving force (LDF) mechanism, an energy balance, a momentum balance represented by Ergun's equation and an equilibrium isotherm model represented by Three Process Langmuir model. For the current study, following simplifying assumptions are imposed: 1) gas phase concentration is represented by ideal gas law; 2) negligible gradients of velocity, pressure, temperature and concentrations in the radial directions; 3) negligible second order mechanisms such as bed mass dispersion or thermal conduction; 4) negligible heat transfer limitation between different phases within the bed, i.e., pellet, gas and bed walls; 5) the gas phase concentration in both bulk and pellet porosity is identical; 6) constant cross section area and wall properties and exterior

temperature along the bed; 7) the mass transfer between solid and gas defines by the linear driving force (LDF) approach.

The equations given in Table 2.1 constitute a complete mathematical model for multi-component pressure swing adsorption process once the initial and boundary conditions for particular steps are specified. For a system containing N components, there are a total of 2N+3 variables and equations that have to be solved at each node. The initial conditions of a step in a cycle are taken as those that occurred at the end of the previous step. Table 2.2 shows all the initial and boundary conditions for the PSA cycles, those conditions are applied at the first (z/L = 0) and last (z/L = 1) nodes of the bed. Component mass balances, overall mass balances and energy balances are applied in those nodes whenever the gas stream leaves the bed, otherwise, gas concentrations, temperatures and gas velocities (or flows) are defined based on the corresponding values of the feed stream. In addition, pressures along the bed are evaluated relative to the pressure of the gas where the gas stream leaves the bed. At this location, the pressure in the bed is evaluated relative to a defined pressure outside the bed through a valve equation. When concentrations, flows, temperatures and valve equations are not specified or required, consistency at the boundary is maintained by utilizing the corresponding balances identified in the equations (C.M.B., O.M.B., LDF, E.B., M.B.) in Table 2.1. The pressure at the other end of the bed is simply evaluated via a momentum balance equation (i.e., Ergun's equation).

The component and overall mass, energy, momentum balance and LDF equations with equilibrium isotherm constitute a complete mathematical model for multi-component PSA process once the initial and boundary conditions for particular steps are specified.

## 2.2 Adsorption Isotherm Measurements

Pure component adsorption equilibrium isotherms for nitrogen ($N_2$), oxygen ($O_2$), and carbon dioxide ($CO_2$) on zeolite 13X were measured at three different temperatures (25, 50 and 75$^oC$) by using a volumetric system from micromeritics (ASAP 2010 , shown in Figure 2.1, located at the University of South Carolina) by Mohammadi et al., 2016. Volumetric method involves measuring the pressure change in a known volume of sample gas exposed to an adsorbent sample. As the gas is adsorbed and allowed to come to equilibrium with the adsorbent, the measured decrease of pressure in the closed system indicates the amount of gas adsorbed under the given isothermal conditions. Prior to each isotherm measurement, the zeolite 13X was regenerated at 350 $^oC$ for under a vacuum of less than $1.33*10^{-5}$ kPa and sample temperature was gradually increased up to the regeneration temperature in order to prevent structural damage caused by desorbing water steam. Free space or available volume was measured by ASAP2010 using non-adsorbing He gas then helium was evacuated from the system by applying vacuum for 1 hour. All three gases have purities higher than 99.99%. A water bath connected to a chiller was used to keep the sample at a desired temperature throughout the experiment for a particular temperature. Data were collected for the equilibrium pressure range of 0.001 to 110 kPa with the help of the molecular drag pump to reach the lowest pressure (e.g. $1.3*10^{-6}$) (Mohammadi et al. 2016).

Three Process Langmuir (TPL) model has been used to correlate the experimental adsorption equilibrium data with simultaneously regressing all of the experimental single-gas data by minimizing $\sum_{i=1}^{n}\left(n_{i,model} - n_{i,experimental}\right)^2$ using Solver in MS Excel. The TPL model describes the adsorption of a gas on a heterogeneous adsorbent composed of

three energetically different but homogeneous sites with the assumption that the free energy of adsorbate-adsorbent on each site is constant. The TPL isotherm parameters for pure gas were obtained by fitting the experimental data by using Equation 2.1 and the fitted equilibrium parameters are summarized in Table 2.3. The resulting equilibrium adsorption isotherms for $CO_2$, $N_2$ and $O_2$ both experimental and TPL model fits are shown in Figure 2.2 for three different temperatures. The Triple Process Langmuir (TPL), pure gas isotherm:

$$q_i = \sum_{j=1}^{3} \left( \frac{{q^s}_{j,i} b_{j,i} P y_i}{(1 + b_{j,i} P y_i)} \right)_j \; with \; b_{j,i} = {b^0}_{j,i} exp\left(\frac{B_{j.i}}{T}\right) \tag{2.1}$$

where $q^s_{j,i}$ is the saturation capacity for component i on site j and $b_{j,i}$ affinity parameter for component i on site j, and P is the absolute pressure. $B_{j,i}$ and ${b^0}_{j,i}$ are the adsorption energy of the component i on site j and the pre-exponential factor for component i on site j, respectively. While obtaining TPL isotherm parameters for all three pure gas by using Equation 2.1, there are nine parameters to be fitted for $CO_2$, while there are three parameters for $N_2$ and three parameters for $O_2$. The reason to have just three parameters for $N_2$ and for $O_2$ is based on an assumption, which indicates that they have the same affinity ($b_{j,i}$) for all three sites since adsorption isotherms of $N_2$ and $O_2$ are linear in the range of working pressure in this thesis.

After having the fitting parameters for pure gases, the Triple Process Langmuir (TPL) mixed gas isotherm equation (Equation 2.2) has been used in the DAPS because in the real PSA process all three gases are available together. Therefore, Equation 2.2 has been used in the simulation for mixed gas isotherms with the parameters coming from pure gas isotherm fittings.

$$q_i^* = \sum_{j=1}^{3} \frac{b_{j,i} P y_i q^s{}_{j,i}}{\left(1 + \sum_{k}^{m} b_{j,k} P y_k\right)} \quad with \quad b_{j,i} = b^0{}_{j,i} \exp\left(\frac{B_{j,i}}{T}\right) \tag{2.2}$$

Toth model has been used in order to calculate heat of adsorption ($\Delta H_i$) for each gas. The Toth model is an empirical expression and was developed to yield an improved fit versus traditional Langmuir isotherm modelling. It is used to describe a monolayer adsorption with assuming adsorption on energetically heterogeneous surfaces with most sites having adsorption energy lower than the maximum. The Toth isotherm model approaches the Henry region at infinite dilution. Experimental isotherms for each pure gas were fitted by using Equation 2.3 to calculate heat of adsorption $\Delta H_i$.

$$q_i = \frac{q_i{}^s b_i P}{(1+(b_i P)^t)^{1/t}} \; with \; b_i = b^o{}_i ex\, p\left(\frac{\Delta H_i}{T}\right) \; and \; q_i{}^s = q_0^s + q_i^s T \tag{2.3}$$

where $q_i{}^s$ and $b_i$ are the saturation capacity and affinity parameters for component i, respectively. P is the absolute pressure. t is the parameter that indicates the heterogeneity of the adsorbent. $\Delta H_i$ and $b^o{}_i$ are the adsorption energy of component i and the pre-exponential factor of component i, respectively. The obtained heat of adsorption values of each gas are shown in Table 2.3.

### 2.3 Mass Transfer Model

The mass transfer between solid and gas phases is defined by the modified linear driving force (LDF) approach for macropore limited diffusion because 3mm 13X beds have been used in the 4-Bed Pressure Swing Adsorption Apparatus, which is going to be used to run experiments in the next chapters. The macropore mass transfer coefficients for $CO_2$,

$N_2$ and $O_2$ were experimentally obtained from the single bed rapid PSA apparatus (located at the University of South Carolina), shown in Figure 2.3, by Rahman et.al., 2016.

The experiments to obtain the macropore mass transfer coefficients for each gases have been done with the following orders; 1) After adsorbent regeneration at 350 °C with flowing helium, measured amount of adsorbent was loaded to the adsorbent column of the RPSA apparatus then was activated in situ at 350 °C by flowing helium. 2) Two step adsorption-desorption cyclic study was carried out with loaded bed using He to determine the excluded volume. 3) Same two step cyclic studies were carried out with the loaded bed with pure $CO_2$, $N_2$, and $O_2$ at different cycle times, temperature and bed pressures to determine the mass transfer coefficients between these gases and the zeolite. The experiments were performed at bed temperatures of 25, 50 and 75 °C (Rahman 2016). Pressure history of the adsorbent bed in the cyclic experiments of $CO_2$, $N_2$, and $O_2$ was fitted with LDF approach with macropore limited diffusion, given in Equation 2.4.

$$\frac{\partial \bar{\bar{q}}}{\partial t} = k_{M,eff}(q^*(P,T) - \bar{\bar{q}}) \; with \; k_{M,eff} = \frac{1}{1+\frac{RT\rho_p}{\varepsilon_p}\frac{\partial q^*}{\partial P}_{T,\bar{P}}} k_M \qquad (2.4)$$

where $k_{M,eff}$ is the overall effective macropore mass transfer coefficient, q* is the adsorbed equilibrium concentration, i.e., q* = f (P,T) given by the isotherm and $\bar{\bar{q}}$ is the average adsorbed concentration. $\rho_P$ is the particle density, $\varepsilon_P$ is the particle porosity, $\frac{\partial q^*}{\partial P}_{T,\bar{P}}$ is the slope of the isotherm, $k_M$ is the macropore mass transfer fitting parameter, shown in Table 2.4 for each gas.

On the other hand, micropore limited LDF approach has been also used for the preliminary study to find a novel PSA cycle for Stage 2, will be shown in next chapters.

Micropore limited LDF approach equation is given in Equation 2.5 with the micropore mass transfer parameters shown in Table 2.4 .

$$\frac{\partial \bar{\bar{q}}}{\partial t} = k_m(q^*(\bar{P}, T) - \bar{\bar{q}}) \tag{2.5}$$

where $k_m$ is micropore mass transfer coefficient, q* is the adsorbed equilibrium concentration, and $\bar{\bar{q}}$ is the average adsorbed concentration.

**Table 2.1** Mathematical model governing equations used in Dynamic Adsorption Process Simulator (DAPS).

Component Mass Balances (C.M.B.):

$$\left(\varepsilon_b + (1-\varepsilon_b)\varepsilon_P\right)C_T \frac{\partial y_i}{\partial t} + \varepsilon_b C_T v \frac{\partial y_i}{\partial z} - y_i \sum_{j=1}^{n} S_j + S_i = 0 \qquad \text{i = 1 to n-1}$$

$$y_i + \sum_{j=1,\, j\neq i}^{n} y_j = 0 \qquad \text{i = n}$$

with $C_T = \dfrac{P}{RT}$; $S_i = (1-\varepsilon_b)\rho_P \dfrac{\partial q_i}{\partial t}$

Overall Mass Balance (O.M.B.):

$$\left(\varepsilon_b + (1-\varepsilon_b)\varepsilon_P\right)C_T\left(\frac{1}{P}\frac{\partial P}{\partial t} - \frac{1}{T}\frac{\partial T}{\partial t}\right) + \varepsilon_b \frac{\partial v C_T}{\partial z} + \sum_{j=1}^{n} S_j = 0$$

LDF equation (L.D.F.E): $\dfrac{\partial q_i}{\partial t} = k^*_{M,i}\left(q_i^* - q_i\right)$, where $k^*_{M,i} = \dfrac{1}{1 + \dfrac{RT\rho_p}{\varepsilon_p}\dfrac{\partial q_i}{\partial t}} * k_{M,i}$

Energy Balance (E.B.):

$$\left(\varepsilon_b + (1-\varepsilon_b)\varepsilon_P\right)\left(Cp_g C_T \frac{\partial T}{\partial t} - \frac{\partial P}{\partial t}\right) + \left((1-\varepsilon_b)\rho_P Cp_p + (\frac{r_{b,o}^2}{r_{b,i}^2} - 1)\rho_w Cp_w\right)\frac{\partial T}{\partial t} +$$

$$\varepsilon_b Cp_g C_T v \frac{\partial T}{\partial z} + (1-\varepsilon_b)\rho_P \sum_{j=1}^{n}\left(Cp_{a,j} q_j \frac{\partial T}{\partial t} + \Delta H_i \frac{\partial q_i}{\partial t}\right) + \frac{2r_{b,o}}{r_{b,i}^2} h_w (T - T_o) = 0$$

with $Cp_g = \sum_{j=1}^{n}\left(y_j Cp_{g,j}\right)$

Momentum Balance (M.B.): $\dfrac{\partial P}{\partial z} + 150 \cdot \mu_g \left(\dfrac{1-\varepsilon}{2r_P \varepsilon}\right)^2 v + 1.75\rho_g v_{sign}\left(\dfrac{1-\varepsilon_P}{2r_P\varepsilon_P}\right)v^2 = 0$

Equilibrium Isotherm:

Triple Process Langmuir Isotherm: $q_i^* = \sum_{j=1}^{3} \dfrac{b_{j,i} P y_i q^s{}_{j,i}}{\left(1 + \sum_{k}^{m} b_{j,k} P y_k\right)}$ with $b_{j,i} = b^0{}_{j,i} \exp\left(\dfrac{B_{j,i}}{T}\right)$;

$q^s{}_{j,i} = q^0{}_{j,i}$

Valve Equation (V.E.):

$F = c_v v_{sign} \dfrac{1}{\sqrt{S_g T}} \min\left(49.08\left|P^2 - P_o^2\right|^{0.5}, 41.63 P^*\right)$ where the comma is to identify choking from non-choking conditions

$P^* = P_o \quad z/L = 0,\ v_{sign} = 1 \ \text{ or } \ z/L = 1,\ v_{sign} = -1$

$P^* = P \quad z/L = 0,\ v_{sign} = -1 \ \text{ or } \ z/L = 1,\ v_{sign} = 1$

**Table 2.2** Initial conditions, boundary conditions and balances for the PSA cycle.

| Step | Time & | Initial conditions, boundary conditions and balances |
|---|---|---|
| F | t = 0, 0 < | $y_{i,F} = y_{i,LPP,f}$, $v_F = v_{LPP,f}$, $q_{i,F} = q_{i,LPP,f}$, $T_F = T_{LPP,f}$, $P_F = P_{LPP,f}$ |
| | z/L = 0, t | $y_{i,F} = y^F{}_i$, T = $T^F$, F = $F^F$, L.D.F.E.(i=1,m), M.B. |
| | z/L = 1, t | C.M.B.(i=1,m), O.M.B., L.D.F.E.(i=1,m), E.B., V.E.($P_o = P_H$, $c_v$>0) |
| I | t = 0, 0 < | $y_{i,I} = y_{i,F,f}$, $v_I = v_{F,f}$, $q_{i,I} = q_{i,F,f}$, $T_I = T_{F,f}$, $P_I = P_{F,f}$ |
| | z/L = 0, t | C.M.B.(i=1,m), L.D.F.E.(i=1,m), E.B., M.B. |
| | z/L = 1, t | C.M.B.(i=1,m), v = 0, L.D.F.E.(i=1,m), E.B. |
| HR | t = 0, 0 < | $y_{i,HR} = y_{i,I,f}$, $v_{HR} = v_{I,f}$, $q_{i,HR} = q_{i,I,f}$, $T_{HR} = T_{I,f}$, $P_{HR} = P_{I,f}$ |
| | z/L = 0, t | $y_{i,HR} = y_{i,LR,z/L=0}$, $F_{HR} = -RR_{HR}*F_{LR,z/L=0}$, L.D.F.E.(i=1,m), M.B. |
| | z/L = 1, t | C.M.B.(i=1,m), O.M.B., L.D.F.E.(i=1,m), E.B., V.E.($P_o = P_I$) |
| Eq | t = 0, 0 < | $y_{i,Eq} = y_{i,HR,f}$, $v_{Eq} = v_{HR,f}$, $q_{i,Eq} = q_{i,HR,f}$, $T_{Eq} = T_{HR,f}$, $P_{Eq} = P_{HR,f}$ |
| | z/L = 0, t | C.M.B.(i=1,m), L.D.F.E.(i=1,m), E.B., M.B., V.E.($P_o = P_{Eq}$, $c_v = 0$) |
| | z/L = 1, t | C.M.B.(i=1,m), O.M.B., L.D.F.E.(i=1,m), E.B., V.E.($P_o = P_{Eq}$, $c_v > 0$) |
| CoD | t = 0, 0 < | $y_{i,CoD} = y_{i,Eq,f}$, $v_{CoD} = v_{Eq,f}$, $q_{i,CoD} = q_{i,Eq,f}$, $T_{CoD} = T_{Eq,f}$, $P_{CoD} = P_{Eq,f}$ |
| | z/L = 0, t | C.M.B.(i=1,m), L.D.F.E.(i=1,m), E.B., V.E.($P_o = P_{CoD,}$ $c_v = 0$), M.B. |
| | z/L = 1, t | C.M.B.(i=1,m), O.M.B., L.D.F.E.(i=1,m), E.B., V.E.($P_o = P_{CoD,}$ $c_v > 0$) |
| CnD | t = 0, 0 < | $y_{i,CnD} = y_{i,CoD,f}$, $v_{CnD} = v_{CoD,f}$, $q_{i,CnD} = q_{i,CoD,f}$, $T_{CnD} = T_{CoD,f}$, $P_{CnD} = P_{CoD,f}$ |
| | z/L = 0, t | C.M.B.(i=1,m), O.M.B., L.D.F.E.(i=1,m), E.B., V.E.($P_o = P_{L,}$ $c_v > 0$) |
| | z/L = 1, t | C.M.B.(i=1,m), L.D.F.E.(i=1,m), E.B., V.E.($P_o = P_{L,}$ $c_v = 0$) |
| LR | t = 0, 0 < | $y_{i,LR} = y_{i,CnD,f}$, $v_{LR} = v_{CnD,f}$, $q_{i,LR} = q_{i,CnD,f}$, $T_{LR} = T_{CnD,f}$, $P_{LR} = P_{CnD,f}$ |
| | z/L = 0, t | C.M.B.(i=1,m), L.D.F.E.(i=1,m), E.B. |
| | z/L = 1, t | $y_{i,LR} = y_{i,F,z/L=1}$, $F_{LR} = -LRR*F_{F,z/L=1}$, L.D.F.E.(i=1,m), M.B. |
| Eq* | t = 0, 0 < | $y_{i,Eq^*} = y_{i,LR,f}$, $v_{Eq^*} = v_{LR,f}$, $q_{i,Eq^*} = q_{i,LR,f}$, $T_{Eq^*} = T_{LR,f}$, $P_{Eq^*} = P_{LR,f}$ |
| | z/L = 0, t | C.M.B.(i=1,m), L.D.F.E.(i=1,m), E.B., M.B., V.E.($P_o = P_{Eq}$, $c_v = 0$) |
| | z/L = 1, t | $y_{i,Eq^*} = y_{i,Eq,z/L=1}$, $F_{Eq^*} = -F_{Eq,z/L=1}$, L.D.F.E.(i=1,m), T = $T^F{}_{z/L=1}$, M.B. |
| LPP | t = 0, 0 < | $y_{i,LPP} = y_{i,Eq^*,f}$, $v_{LPP} = v_{Eq^*,f}$, $q_{i,LPP} = q_{i,Eq^*,f}$, $T_{LPP} = T_{Eq^*,f}$, $P_{LPP} = P_{Eq^*,f}$ |
| | z/L = 0, t | C.M.B.(i=1,m), L.D.F.E.(i=1,m), E.B., M.B, V.E.($P_o = P_{L,}$ $c_v = 0$) |
| | z/L = 1, t | $y_{i,LPP} = y_{i,F,z/L=1}$, $F_{LPP} = -RR_{LPP}*F_{F,z/L=1}$, L.D.F.E.(i=1,m), $T_{LPP} = T_{F,z/L=1}$ |

**Table 2.3** The TPL isotherm parameters for the pure gases

| **Equilibrium isotherm properties** | | | |
|---|---|---|---|
| | $CO_2$ | $N_2$ | $O_2$ |
| **$q^s_{1,i}$, mol/kg** | 1.338 | 0.438 | 0.149 |
| **$q^s_{2,i}$, mol/kg** | 2.238 | 0.733 | 0.248 |
| **$q^s_{3,i}$, mol/kg** | 1.853 | 0.607 | 0.206 |
| **$b^0_{1,i}$, $10^{-8}$ $kPa^{-1}$** | 2.4417 | 75.95 | 408.33 |
| **$b^0_{2,i}$, $10^{-7}$ $kPa^{-1}$** | 5.4204 | 75.95 | 408.33 |
| **$b^0_{3,i}$, $10^{-7}$ $kPa^{-1}$** | 1.3737 | 75.95 | 408.33 |
| **$B_{1,i}$, K** | 5757.03 | 2370.32 | 1833.21 |
| **$B_{2,i}$, K** | 4606.08 | 2370.32 | 1833.21 |
| **$B_{3,i}$, K** | 4224.86 | 2370.32 | 1833.21 |
| **Heat of adsorption ($\Delta H_i$), kJ/mol** | 39.57 | 19.54 | 15.33 |

**Table 2.4** Kinetic properties, used in LDF approach both for macropore and micropore limited diffusion.

| **Kinetic Properties** | | | |
|---|---|---|---|
| | $CO_2$ | $N_2$ | $O_2$ |
| Macropore mass transfer coefficient, $k_{M,i}$, $s^{-1}$ | 47 | 70 | 70 |
| Micropore mass transfer coefficients, $k_{m,i}$, $s^{-1}$ | 1.0 | 1.0 | - |


**Figure 2.1** Picture of ASAP 2010

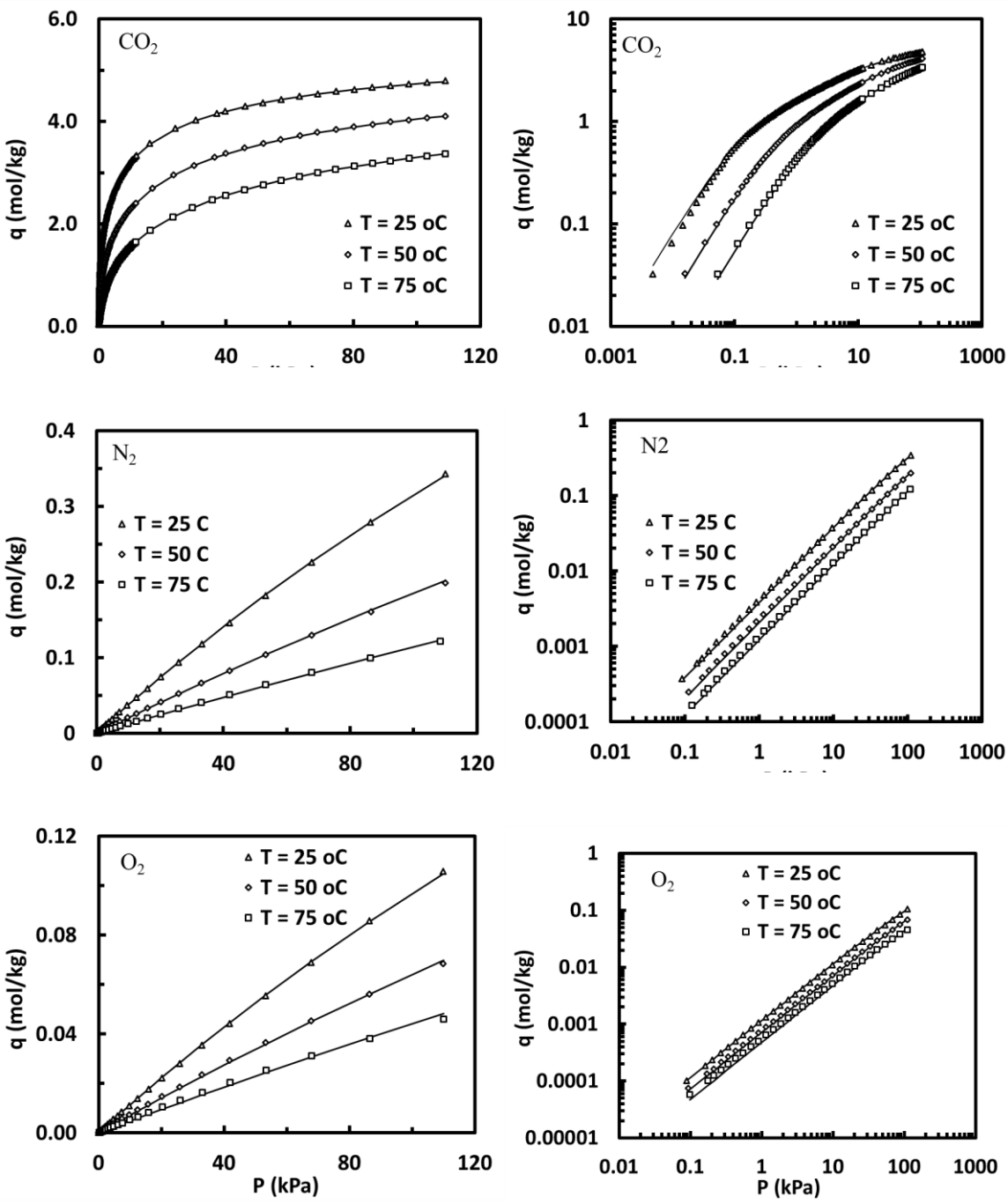


**Figure 2.2** Isotherms of Carbon dioxide, Nitrogen and Oxygen at three different temperatures in linear (left) and log-log scale (right). The solid lines represent the model fits and the markers represent the experimental data.

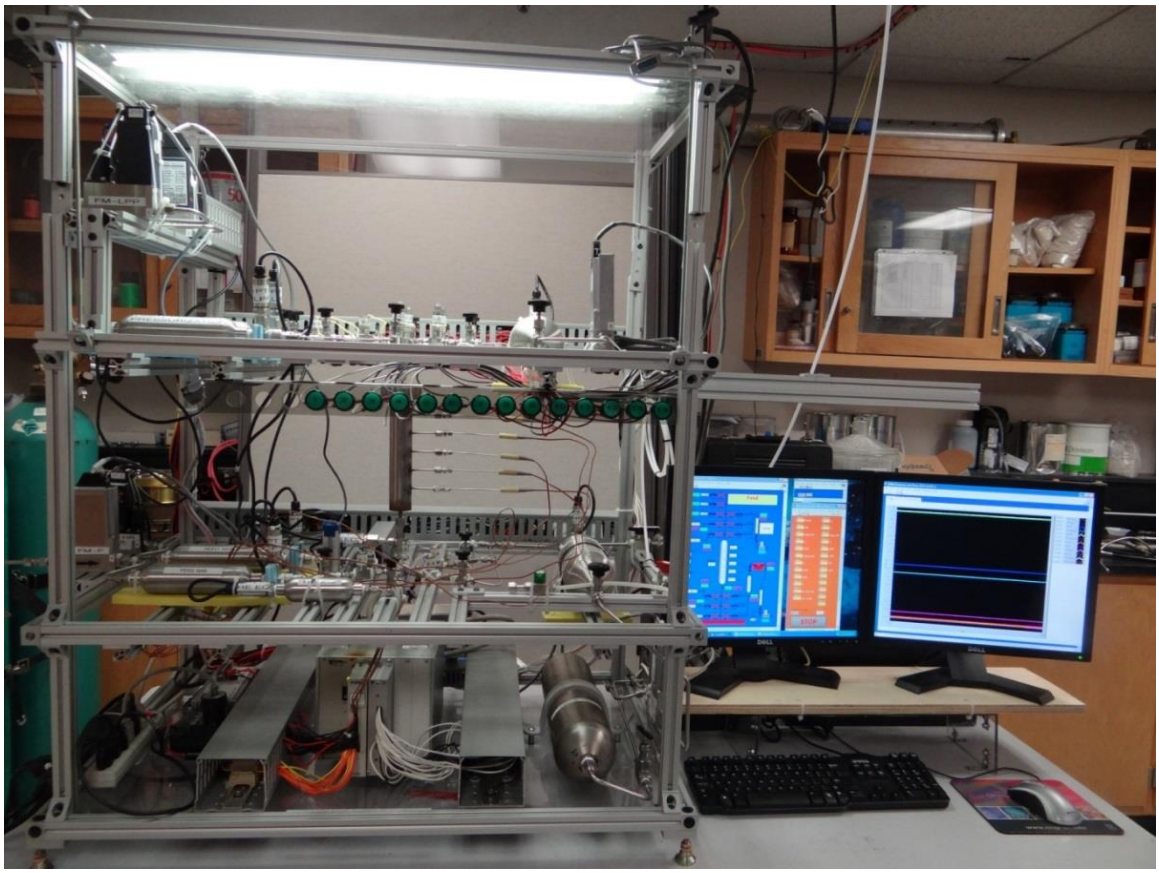

**Figure 2.3** Single bed rapid pressure swing adsorption (RPSA) apparatus (Rahman 2016).

CHAPTER 3

# A PARAMETRIC STUDY ON PRESSURE SWING ADSORPTION PROCESS TO ENRICH TRACE AMOUNT OF $CO_2$ FROM AIR BY USING 13X ZEOLITE

## 3.1 Summary

Simulations of a 3-bed 9-step pressure swing adsorption (PSA) cycles were carried out to study the enrichment and recovery trace amount of $CO_2$ from a $CO_2$-air mixture using 13X zeolite using dynamic adsorption process simulator DAPS. The PSA sequence includes feed (F), idle (I), heavy reflux (HR), co-current equalization depressurization (Eq), co-current depressurization (CoD), counter-current depressurization (CnD), light reflux (LR), counter-current equalization pressurization (Eq*) and Light Product Pressurization (LPP) steps. These 3-bed DAPS simulations were carried out at high feed flow rate with 0.4% $CO_2$ concentration in air. Extensive parametric studies were investigated using an in-house built dynamic adsorption process simulator (DAPS) in order to determine how process performances are affected by process parameters such as HR/LR step time (thus cycle time), light reflux ratio, co-current and counter-current depressurization pressures, and light reflux pressure. Simulation results show that more than 96% $CO_2$ purity with more than 87% $CO_2$ recovery have been achieved with this new PSA cycle as a preliminary study. The best run resulted in this PSA process performance of 96.26% $CO_2$ purity, 87.76

% $CO_2$ recovery, 0.017% $N_2$ loss in the heavy product with the conditions of 4500s cycle time, $P_{CnD}$ = 1kPa, LRR = 0.1, $P_{LR}$ = 3kPa, $P_{CoD}$ = 5kPa and 570slpm feed flow rate.

### 3.2 PSA Cycle Description

A typical PSA process involves a cyclic process where a number of interconnected vessels containing adsorbent/adsorbents undergo successive pressurization and depressurization steps in order to produce a continuous stream of purified product. The steps of the PSA cycle include feed (F), idle (I), heavy reflux (HR), equalization down (E), co-current depressurization (CoD), counter-current depressurization (CnD), light reflux (LR), equalization up (E*) and light product pressurization (LPP). The operation of 3-bed 9-step PSA cycle is described in Figure 3.1 along with the cycle sequence. Each row in the cycle sequence represents all the different cycle steps a given bed undergoes over the entire cycle, whereas each column represents which cycle step is being run by which bed at a particular $t_s$. The sequence of operation is developed by following a simple methodology called graphical approach (Mehrotra et al., 2011). The unit block shown in the Figure 3.1 by a shaded area consists of four ($t_{s,1}$, $t_{s,2}$, $t_{s,3}$ and $t_{s,4}$) unit step times where all steps are being run by one of the three beds and the total cycle time is composed of multiple consecutive unit blocks where the operations are repeated again and again. Therefore, the cycle shown in Figure 3.1 with the unit block is used to perform the parametric study.

The operation of first unit block, bed 1 is fed from bottom at atmospheric pressure for a period equivalent to the sum of all unit step times ($t_{s,1}$, $t_{s,2}$, $t_{s,3}$ and $t_{s,4}$). The reason of covering all the unit step times by feed (F) step during the operation of bed 1 is to maintain a continuous feed flow throughout the cycle. During this operation, the preferentially

adsorbed species ($CO_2$) is captured by the adsorbent in the bed and a product stream is collected from the top of bed 1.

Next, bed 2 undergoes an idle (I) step for a period of $t_{s,1}$ where valves at both ends of the bed is physically closed so that no gas can come in or go out of the bed. The reason of having an idle step in a cycle sequence is to maintain the alignment of coupled steps heavy reflux (HR) and light reflux (LR) in this case. During $t_{s,2}$, the bed has heavy reflux (HR) step which is ringed with heavy gas providing from another bed undergoing light reflux (LR) step. Heavy reflux (HR) step is operated in this case at atmospheric pressure like feed step. The purpose of having HR step in the sequence is to enhance the loading of heavy component in the column by using heavy product enriched stream coming from light reflux (LR) step. It is important to mention that a compressor is necessary to provide feed to HR step by pulling gas from LR step. During $t_{s,3}$, bed 2 undergoes a co-current equalization depressurization (E) step where it is co-currently blown down to another intermediate pressure to provide gas from its light end to another bed undergoing equalization pressurization (E*) step. Finally, bed 2 is co-currently blown down (CoD) from an atmospheric pressure to an intermediate pressure for a period of $t_{s,4}$. The rate of CoD is controlled by a valve coefficient ($Cv_{CoD}$) in order to reduce the loss of adsorbent material due to attrition.

Finally, bed 3 is in counter-current blow down (CnD) step during $t_{s,1}$, which bed 3 is depressurized counter-currently to a low pressure and the pressure at the end of this step is controlled by a valve coefficient ($Cv_{CnD}$). During CnD, heavy gas is collected as product from the bottom of bed. Next during $t_{s,2}$, the bed undergoes light reflux (LR) step. In this step, the bed is fed from light end with a portion of the light gas (LRR) coming from another

bed undergoing feed (F) step. The pressure at the end of this step is controlled by a valve coefficient ($Cv_{LR}$) associated with the step. The entire heavy product collected during LR step is sent back to HR step. The purpose of having LR step in the sequence is to regenerate the bed. Then during $t_{s,3}$, the bed is equalized with another bed from the light end to bring the pressure up to an intermediate level. This equalization pressurization (E*) step helps to reduce operating cost as well to improve PSA performance. Finally during $t_{s,4}$, the bed is re-pressurized to atmospheric pressure using the light gas from the light end of the bed undergoing feed step to prepare the bed to the next cycle. After this phase same operation is repeated to complete the overall cycle.

Simulations of a 3-bed 9-step PSA cycles were carried out using a FORTRAN based in house dynamic adsorption process simulator (DAPS), detailed information is given in Chapter 2.

In the current PSA cycle, the desired product is $CO_2$ which is the preferentially adsorbed species. Therefore, the performance of the process is evaluated on the basis of $CO_2$ recovery and $CO_2$ purity in the heavy product. Recovery of $CO_2$ is defined as the number of moles of $CO_2$ withdrawn as product during production step (CnD) divided by the number of moles of $CO_2$ fed to the PSA process during the feed step. On the other hand, $CO_2$ purity is defined as the mole fraction of $CO_2$ leaving the bed during the CnD step.

Finally, the performance of a PSA process is calculated in terms of purity, recovery and productivity. In this study, these are defined are follows:

$$Throughput\left[\frac{L(STP)}{kg.h}\right] = \frac{Fresh\ total\ Feed(SLPM)\ in\ Feed\ step*60}{Mass\ of\ adsorbent(kg) in\ all\ beds} \qquad (3\text{-}1)$$

$$Purity[\%] = \frac{CO_2(mol)obtained\ as\ product\ during\ CnD\ step}{total\ Product(mol)obtained\ during\ CnD\ step} * 100 \quad (3\text{-}2)$$

$$Recovery[\%] = \frac{CO_2(mol)obtained\ as\ product\ during\ CnD\ step}{Fresh\ CO_2(mol)fed\ in\ Feed\ step} \times 100 \quad (3\text{-}3)$$

In addition to recovery and purity, energy which is an indicator of the operation cost of the process was calculated by following equations for a given step:

$$E[J] = \sum_i^S \int_{t=0}^{t_{step}} \left(\frac{\gamma}{\gamma-1}\right) RT \left[\left(\frac{P_H}{P(t)}\right)^{\frac{\gamma-1}{\gamma}} - 1\right] \frac{1}{\eta} m_{step}(t)dt \quad (3\text{-}4)$$

$$m_{step}(t)\left[mol/_S\right] = \frac{P_{step}(t)\ 1000\ v_{step}(t)\ A\ \varepsilon_b}{R\ T(t)} \quad (3\text{-}5)$$

$$P[W] = \frac{E[J]}{t_{cycle}/_{number\ of\ bed}} \quad (3\text{-}6)$$

In the cycle studied in this work, the energy consuming steps are CnD, LR, and CoD and the value of $P_H$ is 101.325 kPa.

Cumulative $CO_2$ gas phase concentration equation, given in below, has been used to explain the $CO_2$ breaking through during the particular step.

$$\overline{y_{CO_2,cum}} = \frac{\int_0^{t_{step}} y_{CO_2}(t).v(t).C_T(t)dt}{\int_0^{t_{step}} v(t).C_T(t).dt}, C_T(t) = \frac{P_{step}(t)*1000}{RT_{step}(t)} \quad (3\text{-}7)$$

### 3.3 Bed and Adsorbent Characteristics

An overview of the bed and adsorbent characteristics used as input parameters in the simulations as well as process characteristics are summarized in Table 3.1. The feed stream contains 0.4vol % $CO_2$ with 79 vol % $N_2$, and 20.6 vol % $O_2$ (given in Table 3.1).

The adsorbent utilized here is 13X zeolite. The TPL isotherm parameters were obtained by fitting the experimental data and the fitted equilibrium parameters are summarized in Table 2.3. The mass transfer coefficients for $CO_2$, $N_2$ and $O_2$ were obtained experimentally from the single bed rapid PSA apparatus and macropore mass transfer parameters are summarized in Table 2.4.

### 3.4 Parametric Study

A detailed parametric study is conducted in order to investigate the effects of various process parameters on process performance indicators such as purity and recovery of heavy component. The parameters studied include HR/LR/F step time, thus cycle time (by variable x in Table 3.2), light reflux ratio (LRR), counter-current depressurization pressure ($P_{CnD}$), light reflux pressure ($P_{LR}$), and co-current depressurization pressure ($P_{CoD}$). The ranges of all the parameters during the parametric study are summarized in Table 3.2.

### 3.5 Result and Discussion

The PSA cycles performances at the periodic behavior for 13 different simulations are summarized in Table 3.3. In the simulation the varied conditions include HR/LR/F step time (thus cycle time), light reflux ratio (LRR), counter-current depressurization pressure ($P_{CnD}$), light reflux pressure ($P_{LR}$), and co-current depressurization pressure ($P_{CoD}$). The overall process performance was judged in terms of the purity and recovery of $CO_2$ in the heavy product and the required energies. The $CO_2$ purity was defined as the average mole fraction of $CO_2$ in the heavy product, equation 3.2. $CO_2$ recovery was defined as the moles of $CO_2$ in the heavy product divided by the moles of $CO_2$ fed to the process cumulatively

during the feed, equation 3.3. Another process performance, required energy which is an indicator of the operation cost of the process was calculated by equations 3.4-3.6.

### 3.5.1 Effect of HR/LR/F Step Time, (Thus Cycle Time)

To study this effect the parameters that being held constant are light reflux ratio (0.1), counter-current blow down pressure (1kPa), light reflux pressure (5kPa), and co-current blow down pressure (5kPa) as shown in Table 3.2. To have different the HR/LR/F step time, x values in Table 3.2 has been changed 0, 250, 500, and 750s (run numbers: 1-4). The pressures for other steps are 101.325kPa at the end of feed, heavy reflux and light product pressurization steps, 44.13kPa for Run1, 42.88kPa for Ru$N_2$, 41.68kPa for Run3 and 40.50kPa for Run4 at the end of equalizations steps as shown in Table 3.6.

In a typical PSA process, cycle time determines the length of operation of a particular step in a fixed cycle schedule. As increasing the cycle time increases proportionally the length of associated cycle steps for a fixed cycle schedule; HR/LR steps as well as feed step in this paper. Results shown in Figure 3.2-a) indicate that the purity of heavy product increases with increasing x. Longer cycle time helps to increase the length of corresponding step proportionally, the longer duration forces more $CO_2$ to adsorb by the adsorbent at a certain temperature and pressure. In other words, the bed gets saturated higher with $CO_2$ at the end of HR step as shown in Figure 3.3, which shows bed profiles at the end of HR step for each run at periodic steady state. From Figure 3.3, it can be easily seen that the front is moving through the end of bed by increasing x. Hence, the purity shows an increasing trend with increasing x.

On the other hand, recovery of $CO_2$ increases for x = 250s then decreases by increasing x as shown in Figure 3.2-b). In a typical PSA cycle, recovery of heavy product decreases by increasing cycle time. It is important to notice that feed step time, heavy reflux step time and light reflux step time, thus cycle time have been changed at the same time by changing x value in Table 3.2. A likely explanation for the observed trend is that the depth of penetration of mass transfer zone of $CO_2$ into the bed increases with the increase of cycle time which in turn enhances the loss of $CO_2$ in the light end. To understand which particular step is causing an increase in heavy product recovery, $CO_2$ losses from light end for each step (Feed, HR, CoD, LR, and LPP) can be seen from Figure 3.4, which shows relative $CO_2$ losses versus x for aforementioned steps. In Figure 3.4, a relative loss of $CO_2$ in HR step is increasing by increasing x. A basic explanation for this increase is that the bed is saturated with more $CO_2$, which can be seen from (Figure 3.3) that causes $CO_2$ to break through from light end. Therefore, $CO_2$ loss increases by increasing x. $CO_2$ loss during CoD step decreases slightly by increasing x (Figure 3.4). CoD step time for these runs is not changing so the amount of $CO_2$ leaving the bed at the end of CoD step does not have a big change, but the amount of $CO_2$ into the bed during feed step is increasing as can be seen form Table 3.4. Therefore, $CO_2$ loss during CoD decreases by increasing x. These two steps do not have the same trend that $CO_2$ recovery has, so these steps are not the main reason of the king in $CO_2$ recovery. The other steps that cause the loss of $CO_2$ from light end are feed, LR, and LPP. Since some portion of light product from feed end goes to light reflux and light product pressurization steps, the combination of these steps needs to be count to investigate $CO_2$ losses in light end as shown in Figure 3.4. In this combination step, $CO_2$ losses decrease at the beginning of increased x, then increase as well as $CO_2$

recovery increases first then decreases by increased x, so it can be said that the main reason for the trend that $CO_2$ recovery has is feed steps. To better understanding, cumulative $CO_2$ gas phase concentration ($\bar{y}CO_{2,\,cum}$) from the beginning to the end of feed step needs to be investigated deeply for the runs 1-4 as shown in Figure 3.5. It can be seen from Figure 3.5 that $\bar{y}CO_{2,\,cum}$ at the end of feed step is decreasing for x = 250s compare to x = 0s, which causes an increase in $CO_2$ recovery that means that the bed gets better saturated with $CO_2$ in the feed step by increasing x. For x = 500s, $\bar{y}CO_{2,\,cum}$ is decreasing slightly compare to x = 250s, so $CO_2$ recovery is increasing slightly; $CO_2$ recoveries are 76.94 and 77.01 for x = 250s and for x = 500s, respectively. For x = 750s in Figure 3.5, $\bar{y}CO_{2,\,cum}$ increasing compare to x = 250 and 500s, which causes a decrease in $CO_2$ recovery that means that $CO_2$ starts breaking through during the feed steps and the bed loses some of the $CO_2$ from light end. It is important to notice that $\bar{y}CO_{2,\,cum}$ for x = 750 is still lower that the value for x = 0, so the $CO_2$ recovery for x = 750 is still higher than the one x = 0. Therefore, the recovery of $CO_2$ increases for x = 250 and 500s compare to x = 0s, then it decreases for further increased x (750s). To explain the main reason that $CO_2$ starts breaking through for x=750s, which is Run number 4, during the feed step the time ratios of feed step and light reflux step for all four x values have an essential role. The time ratios of these two steps are 0.7, 0.76, 0.8, and 0.83 for run number 1 through 4, respectively. The increase of this ratio decreases by increasing x values. It can be said that during the light reflux step, the bed is regenerated as much as like clean bed for x=500s, run number 3, but for x=750s, run number 4, the bed has the maximum regeneration level that achieved at x=500s while still increasing time for both light reflux and feed steps. That situation leads $CO_2$ to breaking through during feed step.

The total energy for run numbers 1-4 is increasing by increasing x as can be seen from Figure 3.2-b). This figure shows the effect of x in all energy consuming steps, which are CnD, CoD, and LR in this work. CoD and CnD energies are decreasing slightly by increasing x compare to the LR energy. For this parametric study, CoD and CnD time is not changing while total cycle time increasing, so the time fractions of these steps are decreasing which causes a decrease in energy for these steps. The main time portion of the cycle from energy consumption steps is LR. LR energy is increasing by increasing x (Figure 3.2-b)). Time fractions of LR to total cycle are 0.23, 0.25, 0.27, and 0.28 for run 1 through run 4, respectively. Since the pump pulls gases which are coming from LR in 5kPa to HR in 101.325kPa for longer time, more energy is needed with the increasing time fraction of LR. Therefore, energy needed for LR step is increasing, so total energy increases by increasing x.

### 3.5.2 Effect of Light Reflux Ratio (LRR)

Figure 3.6 summarizes the net results for $CO_2$ recovery and purity in heavy product and energies as a function of light reflux ratio (LRR). The parameters that are held constant during the simulation include x (500s), counter-current blow down pressure (1kPa), light reflux pressure (5kPa), flow rate (570 slpm), and co-current blow down pressure (5kPa) as shown in Table 3.2. The pressures for those runs are 101.325kPa at the end of feed, heavy reflux and light reflux pressurization steps, 42.37kPa for Run5, 41.68kPa for Run3, 41.15kPa for Run6 and 40.71 for Run7 at the end of equalizations steps (Table 3.6). The light reflux ratio values for this parametric study are 0.08, 0.1, 0.12, and 0.14; corresponding runs are 5, 3, and 6, and 7 in Table 3.2.

Figure 3.6-a) shows that purity of $CO_2$ increases slight while recovery of $CO_2$ increases dramatically with increasing light reflux ratio. As HR and LR steps are coupled together, any increase in the number of moles produced from LR step will increase the partial pressure of $CO_2$ during the constant total pressure operation of HR step. This increased partial pressure of $CO_2$ causes the higher saturated bed with $CO_2$ in HR step, so the front is moving to the end of bed during HR step as can be seen from Figure 3.7. Operating the light reflux step with higher flow rate of light product regenerated the adsorbent better but might be diluted the heavy product. That might be the reason of having a slight increase in purity of heavy product compare to recovery. The other reason of increasing recovery of heavy product by increasing light reflux ratio is having more regenerated bed during HR step; less $CO_2$ is leaving the bed at the end of HR step by increasing light reflux ratio as can be seen from Table 3.5. The capacity of the bed has been used more with increasing light reflux ratio. Therefore, recovery of $CO_2$ increases by increasing light reflux ratio.

Figure 3.6-b) shows the effect of LRR in all energy consuming steps. The total energy for the corresponding runs (3, 5-7) is increasing by increasing light reflux ratio. Total energy means in this work is required energies for CoD, CnD, and LRR to increase the stream pressure from the pressure at the end of these steps to atmospheric pressure. Required energy for CoD from 5kPa to 101.325 kPa is decreasing slightly by increasing LRR because the amount of $CO_2$ leaving the bed at the end of CoD is decreasing as can be seen from Table 3.5. Since the amount of $CO_2$ leaving the bed at the end of CnD is increasing, as can be seen from Table 3.5, energy required for CnD step from 1kPa to 101.325kPa is increasing slightly by increasing LRR. The other step that causes energy

consumption is LR step; LR energy is increasing dramatically by increasing light reflux ratio. The amount of gases leaving the bed during the LR step is increasing by increasing light reflux ratio (Table 3.5). That causes the pump to pull more gases, which need more energy. Therefore, total energy increases by increasing light reflux ratio.

### 3.5.3 Effect of Counter-Current Depressurization Pressure ($P_{CnD}$)

Figure 3.8 shows the effect of counter-current desorption pressure ($P_{CnD}$) on cyclic steady state performance for the PSA cycle. To study the effect of $P_{CnD}$, the simulations were performed at a constant x (500s), light reflux ratio (0.1), co-current blow down pressure (5kPa), light reflux pressure (5kPa), flow rate (570 slpm) as shown in Table 3.2. The only parameter that is changed was $P_{CnD}$ (0.8, 1, 1.2kPa); corresponding simulations are Run numbers 8, 3, and 9, respectively. The other pressures for those runs are 101.325kPa at the end of feed, heavy reflux and light reflux pressurization steps, 42.04kPa for Run8, 41.68kPa for Run3, 41.42kPa for Run9 at the end of equalizations steps as can be seen from Table 3.6.

In general, the bed is better regenerated by lowering the desorption pressure. In other words, the desorption pressure enhances the working capacity of the bed for a fixed high pressure. The valve coefficient during CnD step in adjusted in such a way that the final pressure at the end of step reaches a desired low pressure. It can be seen from Figure 3.8-a) purity of $CO_2$ decreases with the decrease of desorption pressure for a particular cycle time. The observed behavior in Figure 3.8-a) for $CO_2$ purity can be described with the help of Figure 3.9, which shows bed profiles at the end of HR step. The $CO_2$ front is moving backward by decreasing low pressure, which causes decrease in purity of $CO_2$. On the other hand, recovery of $CO_2$ increases by decreasing CnD final pressure. To decrease

the low pressure, more $CO_2$ is leaving the bed as a heavy product as can be seen from Table 3.5, which leads increasing $CO_2$ recovery.

The total energy for run numbers 3, 8, and 9 stays almost constant by decreasing CnD final pressure as can be seen from Figure 3.8-b). This figure shows the effect of $P_{CoD}$ in all energy consuming steps, which are CnD, CoD, and LR in this work. The energy required for CoD is almost constant and for LR step is decreasing slightly while for CnD step is increasing slightly by decreasing CnD final pressure. Required energy for CnD step is increasing by decreasing CnD final pressure because the pumps needs to pull more gases to get the lower pressures at the end of CnD step. Since the next step after CnD is LR, there was less gasses in the bed pulled by the pump during LR, energy required for LR decreases by decreasing $P_{CnD}$. Because of the neutral effect of these two steps total energy stays almost constant.

### 3.5.4 Effect of Light Reflux Pressure ($P_{LR}$)

Figure 3.10 summarizes the net results for $CO_2$ recovery and purity in heavy product and energies as a function of light reflux pressure ($P_{LR}$). The parameters that are held constant during the simulation include x (500s), light reflux ratio (0.1), counter-current blow down pressure (1kPa), flow rate (570 slpm), and co-current blow down pressure (5kPa) as shown in Table 3.2. The only parameter that is changed was $P_{LR}$ (3, 4, 5kPa); corresponding simulations are Run11, 10, 3, respectively. The other pressures for those runs are 101.325kPa at the end of feed, heavy reflux and light reflux pressurization steps, 39.51kPa for Run11, 40.56kPa for Run10 and 41.68kPa for Run3 at the end of equalizations steps (Table 3.6).

From Figure 3.10-a), purity of $CO_2$ increases slight while recovery of $CO_2$ increases dramatically by decreasing the pressure at the end of the light reflux. Low pressure for light reflux step means more regenerated bed with light product gases, in other words, more $CO_2$ is coming from the bed. Since heavy reflux step is being fed from this stream that causes moving the $CO_2$ front to the end of bed during heavy reflux step (Figure 3.11). That means that the bed is being used more than with high $P_{LR}$ case which causes an increase in purity and recovery of $CO_2$. It can be also seen from Table 3.5 that amount of $CO_2$ leaving the bed at the end of HR step from light end decreasing by increasing $P_{LR}$, which causes increase in recovery of $CO_2$. The reason of having a slight increase in purity of heavy product might be diluted the heavy product stream with light products ($N_2$, $O_2$) to reach lower pressures.

Figure 3.10-b) shows the effect of $P_{LR}$ in all energy consuming steps. The total energy for the corresponding runs is increasing by decreasing LR pressure. Required energy for CoD and CnD is increasing slightly by decreasing $P_{LR}$. Required energy for LR step is increasing with decreasing $P_{LR}$. The pump is pulling more gases to reach the low LR pressures, so energy needed for LR increases by decreasing LR final pressure. Therefore, total energy increases by decreasing $P_{LR}$.

### 3.5.5 Effect of Co-Current Depressurization Pressure ($P_{CoD}$)

The parameters that are held constant during the simulations to study this effect include x (500s), light reflux ratio (0.1), counter-current blow down pressure (1kPa), light reflux pressure (5kPa), flow rate (570 slpm) as shown in Table 3.2. The pressures at the end of each step for these three simulations (Run #3, 12, and 13) were constant except $P_{CoD}$. Those pressures are 101.325kPa at the end of feed, heavy reflux and light reflux

pressurization steps, ~41.7kPa at the end of equalizations steps, 1kPa at the end of counter-current blowdown, 5kPa at the end of light reflux (Table 3.5). In other words, the only parameter that is changed was $P_{CoD}$; 4, 5, 7kPa for runs 12, 3, and 13, respectively. Figure 3.12 shows the effect of co-current blow down pressure ($P_{CoD}$) on purity and recovery of $CO_2$ and energies.

It is clear from Figure 3.12-a) that purity of heavy product stream is dramatically increasing while recovery of $CO_2$ is slightly decreasing by decreasing the final pressure of co-current depressurization. The decrease in final pressure of CoD step results desorption of more $CO_2$ (heavy component) along with the light components ($N_2$ and $O_2$). In other words, the reason of decreasing the recovery of $CO_2$ with decreasing CoD final pressure is that the bed is losing adsorbed phase $CO_2$ in light end to reach the low pressures (Table 3.5). Besides $CO_2$, more $N_2$ and $O_2$ are also leaving the bed from light end by decreasing CoD final pressure that causes less $N_2$ and $O_2$ in the system at the end of CoD. Since the next step after CoD is CnD, which is production step, more pure $CO_2$ is coming out from the bed as heavy product. That causes an increase in purity of heavy product.

The total energy for run numbers 3, 12, and 13 stays almost constant by decreasing CoD final pressure as can be seen from Figure 3.12-b). This figure shows the effect of $P_{CoD}$ in all energy consuming steps, which are CnD, CoD, and LR in this work. The energies required for CnD and LR steps are almost constant while for CoD step is increasing slightly by decreasing CoD final pressure. The reason of an increase of required energy for CoD step is that the pump pulls more gases from the bed to reach low pressures at the end of CoD step. Since the time portion of CoD step to cycle time is very low (0.02), total energy stays almost constant by decreasing CoD final pressure.

### 3.6 Conclusion

An in-house process simulator was used to study 3 beds 9 steps PSA process for the enrichment and recovery trace amount of $CO_2$ from a $CO_2$-air mixture using 13X zeolite**.** The practical feasibility of carbon dioxide separation and recovery from air-$CO_2$ mixtures was demonstrated by means of a new PSA cycle. A 3-bed 9-step PSA system was configured and utilized to study concentration and separation of $CO_2$ from air (0.4% $CO_2$, 79% $N_2$, and 20.6% $O_2$) using Zeolite 13X as adsorbent. PSA Cycle, which included feed (F), idle (I), heavy reflux (HR), co-current equalization depressurization (Eq), co-current depressurization (CoD), counter-current depressurization (CnD), light reflux (LR), counter-current equalization pressurization (Eq*) and Light Product Pressurization (LPP) steps was able to produce carbon dioxide with purities more than 96.2% and recoveries more than 87.7%.

The effects of HR/LR step time (thus cycle time), light reflux ratio, co-current and counter-current depressurization pressures, and light reflux pressure were investigated. The simulations revealed that the purity of heavy product increases with increasing HR/LR step time while recovery of $CO_2$ increases first then starts decreasing by increasing HR/LR step time. This trend in recovery of $CO_2$ is because $CO_2$ starts breaking through during the feed steps and the bed loses some of the $CO_2$ from light end. This is the reason of picking the run3 as a base case with 95.75% $CO_2$ purity and 77% $CO_2$ recovery process performances. The effect of light reflux ratio study indicated that the $CO_2$ purity is not sensitive to this parameter while it has a relatively big effect on recovery of $CO_2$. Parametric study on $P_{CnD}$ shows that purity of $CO_2$ decreases while recovery of $CO_2$ increases by decreasing CnD final pressure. Purity of heavy product stream is dramatically increasing while recovery of

$CO_2$ is slightly decreasing by decreasing the final pressure of co-current depressurization. The final parametric study on $P_{LR}$ indicated that purity of $CO_2$ increases slight while recovery of $CO_2$ increases dramatically by decreasing the pressure at the end of the light reflux. And that also revealed that optimizing this parameter ($P_{LR}$) is vital for the best performance.

**Table 3.1** PSA bed and adsorbent properties with process characteristics.

| **Bed characteristics** | |
|---|---|
| Bed radius ($r_i$), m | 0.1143 (4.5in) |
| Bed length (L), m | 0.3048 (12in) |
| Bed porosity ($\varepsilon_b$) | 0.3403 |
| Bulk density, kg/m$^3$ | 725.7 |
| Wall density, kg/m$^3$ | 8000 |
| Wall thickness, m | 0.006 |
| Heat transfer coefficient ($h_w$), kW/m$^2$.K | 0.01 |
| Heat of adsorption of $CO_2$, $N_2$, $O_2$ ($\Delta H_i$), kJ/mol | 39.57, 19.54, 15.33 |
| **Adsorbent characteristics** | |
| Adsorbent | 13X Zeolite |
| Pellet radius ($r_p$), m | 0.0015 |
| Pellet density ($\rho_p$), kg/m$^3$ | 1100 |
| Pellet porosity ($\varepsilon_p$) | 0.45 |
| Pellet heat capacity ($Cp_p$), kJ/kg.K | 1.1 |
| **Process characteristics** | |
| Feed mole fraction for $CO_2$, $N_2$, $O_2$ ($yi^F$) | 0.004, 0.79, 0.206 |
| Feed temperature ($T^F$), K | 294.25 |
| Outside wall temperature ($T_o$), K | 294.25 |
| High pressure ($P_H$), kPa | 101.325 |
| Feed Flow ($F^F$), SLPM | 570 |
| Throughput (L(STP)/kg/h) | 1264 |
| Cycle time ($t_{cycle}$), s | See Table 3.2 |
| Low pressure ($P_L$), kPa | See Table 3.2 |
| Light Reflux Ratio (LRR) | See Table 3.2 |
| CoD pressure ($P_{CoD}$), kPa | See Table 3.2 |
| Light Reflux Pressure ($P_{LR}$), kPa | See Table 3.2 |

**Table 3.2** Input parameters of 3-Bed 9-Step PSA process for parametric study using the cycle depicted below. Run no. 3 is taken as the base case for each parametric study.

| | | | | | |
|---|---|---|---|---|---|
| Bed1 | FEED | | | | |
| Bed2 | I | HR | | E | CoD |
| Bed3 | CnD | LR | | E* | LPP |
| Step time | 200 | 700+x | | 25 | 75 |

| Run No. | x (s) | $t_{cycle}$ (s) | LRR | $P_L$ (kPa) | $P_{LR}$ (kPa) | $P_{CoD}$ (kPa) |
|---|---|---|---|---|---|---|
| Effect of HR/LR step time, thus cycle time, x | | | | | | |
| 1 | *0* | *3000* | 0.1 | 1 | 5 | 5 |
| 2 | *250* | *3750* | 0.1 | 1 | 5 | 5 |
| **3*** | ***500*** | ***4500*** | **0.1** | **1** | **5** | **5** |
| 4 | *750* | *5250* | 0.1 | 1 | 5 | 5 |
| Effect of light reflux ratio (LRR) | | | | | | |
| 5 | 500 | 4500 | *0.08* | 1 | 5 | 5 |
| **3*** | **500** | **4500** | ***0.10*** | **1** | **5** | 5 |
| 6 | 500 | 4500 | *0.12* | 1 | 5 | **5** |
| 7 | 500 | 4500 | *0.14* | 1 | 5 | 5 |
| Effect of CnD pressure ($P_L$) | | | | | | |
| 8 | 500 | 4500 | 0.1 | *0.8* | 5 | 5 |
| **3*** | **500** | **4500** | **0.1** | ***1*** | **5** | 5 |
| 9 | 500 | 4500 | 0.1 | *1.2* | 5 | **5** |
| Effect of LR pressure ($P_{LR}$) | | | | | | |
| **3*** | **500** | **4500** | **0.1** | **1** | ***5*** | 5 |
| 10 | 500 | 4500 | 0.1 | 1 | *4* | 5 |
| 11 | 500 | 4500 | 0.1 | 1 | *3* | **5** |
| Effect of CoD pressure ($P_{CoD}$) | | | | | | |
| 12 | 500 | 4500 | 0.1 | 1 | 5 | *4* |
| **3*** | **500** | **4500** | **0.1** | **1** | **5** | ***5*** |
| 13 | 500 | 4500 | 0.1 | 1 | 5 | *7* |

*: Values in bold correspond to base case.

**Table 3.3** Parameter ranges investigated and performances in terms of $CO_2$ purity and recovery obtained for the PSA cycle.

| Conditions | | | | | | | | HP | | |
|---|---|---|---|---|---|---|---|---|---|---|
| **Run #** | **x (s)** | **Cycle time (s)** | **LRR** | **$P_{CnD}$ (kPa)** | **$P_{LR}$ (kPa)** | **Feed (slpm)** | **$P_{CoD}$ (kPa)** | $CO_2$ **Purity (%)** | $CO_2$ **Recovery (%)** | $N_2$ **Losses (%)** |
| 1 | 0 | 3000 | 0.1 | 1 | 5 | 570 | 5 | 92.13 | 74.83 | 0.032 |
| 2 | 250 | 3750 | 0.1 | 1 | 5 | 570 | 5 | 94.32 | 76.94 | 0.023 |
| **3** | **500** | **4500** | **0.1** | **1** | **5** | **570** | **5** | **95.75** | **77.01** | **0.017** |
| 4 | 750 | 5250 | 0.1 | 1 | 5 | 570 | 5 | 96.75 | 76.06 | 0.013 |
| 5 | 500 | 4500 | 0.08 | 1 | 5 | 570 | 5 | 94.77 | 70.41 | 0.020 |
| **3** | **500** | **4500** | **0.1** | **1** | **5** | **570** | **5** | **95.75** | **77.01** | **0.017** |
| 6 | 500 | 4500 | 0.12 | 1 | 5 | 570 | 5 | 96.18 | 81.20 | 0.016 |
| 7 | 500 | 4500 | 0.14 | 1 | 5 | 570 | 5 | 96.47 | 83.85 | 0.016 |
| 8 | 500 | 4500 | 0.1 | 0.8 | 5 | 570 | 5 | 95.30 | 77.40 | 0.019 |
| **3** | **500** | **4500** | **0.1** | **1** | **5** | **570** | **5** | **95.75** | **77.01** | **0.017** |
| 9 | 500 | 4500 | 0.1 | 1.2 | 5 | 570 | 5 | 96.12 | 76.66 | 0.016 |
| **3** | **500** | **4500** | **0.1** | **1** | **5** | **570** | **5** | **95.75** | **77.01** | **0.017** |
| 10 | 500 | 4500 | 0.1 | 1 | 4 | 570 | 5 | 96.21 | 82.74 | 0.016 |
| 11 | 500 | 4500 | 0.1 | 1 | 3 | 570 | 5 | 96.26 | 87.76 | 0.017 |
| 12 | 500 | 4500 | 0.1 | 1 | 5 | 570 | 4 | 96.79 | 76.25 | 0.013 |
| **3** | **500** | **4500** | **0.1** | **1** | **5** | **570** | **5** | **95.75** | **77.01** | **0.017** |
| 13 | 500 | 4500 | 0.1 | 1 | 5 | 570 | 7 | 93.24 | 77.15 | 0.028 |

* The highlighted run (#11) corresponds to the best results.

**Table 3.4** Moles of $CO_2$, and $N_2+O_2$ into the bed step by step for each runs.

| **Run** | **Feed** | | **LR** | | **Eq*** | | **LPP** | |
|---|---|---|---|---|---|---|---|---|
| **no** | $CO_2$ | $N_2+O_2$ | $CO_2$ | $N_2+O_2$ | $CO_2$ | $N_2+O_2$ | $CO_2$ | $N_2+O_2$ |
| 1 | 1.695 | 422.171 | 0.030 | 29.641 | 0.002 | 1.040 | 0.002 | 1.151 |
| 2 | 2.119 | 527.714 | 0.037 | 40.231 | 0.002 | 1.033 | 0.002 | 1.192 |
| **3** | **2.543** | **633.256** | **0.046** | **50.818** | **0.002** | **1.024** | **0.002** | **1.236** |
| 4 | 2.967 | 738.799 | 0.058 | 61.403 | 0.002 | 1.011 | 0.002 | 1.275 |
| 5 | 2.543 | 633.256 | 0.048 | 40.643 | 0.003 | 1.031 | 0.002 | 1.215 |
| **3** | **2.543** | **633.256** | **0.046** | **60.992** | **0.002** | **1.016** | **0.002** | **1.261** |
| 6 | 2.543 | 633.256 | 0.045 | 71.165 | 0.002 | 1.007 | 0.002 | 1.274 |
| 7 | 2.543 | 633.256 | 0.045 | 50.819 | 0.001 | 1.032 | 0.001 | 1.237 |
| 8 | 2.543 | 633.256 | 0.045 | 50.817 | 0.002 | 1.017 | 0.002 | 1.248 |
| **3** | **2.543** | **633.256** | **0.046** | **50.829** | **0.002** | **1.040** | **0.002** | **1.276** |
| 9 | 2.543 | 633.256 | 0.047 | 50.840 | 0.002 | 1.057 | 0.002 | 1.313 |
| **3** | **2.543** | **633.256** | **0.046** | **50.817** | **0.002** | **1.021** | **0.002** | **1.238** |
| 10 | 2.543 | 633.256 | 0.035 | 50.818 | 0.002 | 1.024 | 0.001 | 1.238 |
| 11 | 2.543 | 422.171 | 0.024 | 29.641 | 0.001 | 1.040 | 0.001 | 1.151 |
| 12 | 2.543 | 527.714 | 0.047 | 40.231 | 0.002 | 1.033 | 0.002 | 1.192 |
| **3** | **2.543** | **633.256** | **0.046** | **50.818** | **0.002** | **1.024** | **0.002** | **1.236** |
| 13 | 2.543 | 738.799 | 0.046 | 61.403 | 0.002 | 1.011 | 0.002 | 1.275 |

**Table 3.5** Moles of $CO_2$, and $N_2+O_2$ leaving the bed step by step for each runs.

| Run no | Feed | | HR | | Eq | | CoD | | CnD | | LR | |
|---|---|---|---|---|---|---|---|---|---|---|---|---|
| | $CO_2$ | $N_2+O_2$ | $CO_2$ | $N_2+O_2$ | $CO_2$ | $N_2+O_2$ | $CO_2$ | $N_2+O_2$ | $CO_2$ | $N_2+O_2$ | $CO_2$ | $N_2+O_2$ |
| 1 | 0.418 | 422.093 | 0.037 | 29.760 | 0.002 | 1.040 | 0.006 | 1.004 | 1.269 | 0.108 | 2.310 | 29.484 |
| 2 | 0.479 | 527.677 | 0.050 | 40.427 | 0.002 | 1.033 | 0.005 | 0.937 | 1.631 | 0.098 | 3.049 | 40.067 |
| **3** | **0.570** | **633.259** | **0.066** | **51.095** | **0.002** | **1.024** | **0.005** | **0.873** | **1.959** | **0.087** | **3.788** | **50.648** |
| 4 | 0.685 | 738.832 | 0.087 | 61.763 | 0.002 | 1.011 | 0.006 | 0.811 | 2.257 | 0.076 | 4.548 | 61.228 |
| 5 | 0.734 | 633.243 | 0.068 | 40.869 | 0.003 | 1.031 | 0.007 | 0.913 | 1.791 | 0.099 | 3.299 | 40.480 |
| **3** | **0.570** | **633.259** | **0.066** | **51.095** | **0.002** | **1.024** | **0.005** | **0.873** | **1.959** | **0.087** | **3.788** | **50.648** |
| 6 | 0.465 | 633.280 | 0.065 | 71.526 | 0.002 | 1.007 | 0.004 | 0.814 | 2.065 | 0.078 | 4.208 | 70.985 |
| 7 | 0.398 | 633.267 | 0.065 | 51.054 | 0.001 | 1.032 | 0.004 | 0.896 | 2.132 | 0.097 | 4.587 | 50.645 |
| 8 | 0.560 | 633.267 | 0.065 | 51.054 | 0.002 | 1.032 | 0.005 | 0.896 | 1.968 | 0.097 | 3.475 | 50.645 |
| **3** | **0.570** | **633.259** | **0.066** | **51.095** | **0.002** | **1.024** | **0.005** | **0.873** | **1.959** | **0.087** | **3.788** | **50.648** |
| 9 | 0.578 | 633.265 | 0.067 | 51.127 | 0.002 | 1.017 | 0.005 | 0.856 | 1.950 | 0.079 | 4.036 | 50.651 |
| **3** | **0.570** | **633.259** | **0.066** | **51.095** | **0.002** | **1.024** | **0.005** | **0.873** | **1.959** | **0.087** | **3.788** | **50.648** |
| 10 | 0.430 | 633.279 | 0.049 | 51.163 | 0.002 | 1.040 | 0.004 | 0.842 | 2.104 | 0.083 | 4.042 | 50.690 |
| 11 | 0.306 | 633.294 | 0.034 | 51.227 | 0.001 | 1.057 | 0.003 | 0.815 | 2.232 | 0.087 | 4.280 | 50.732 |
| 12 | 0.577 | 633.258 | 0.067 | 51.105 | 0.002 | 1.021 | 0.006 | 0.903 | 1.939 | 0.064 | 3.878 | 50.647 |
| **3** | **0.570** | **633.259** | **0.066** | **51.095** | **0.002** | **1.024** | **0.005** | **0.873** | **1.959** | **0.087** | **3.788** | **50.648** |
| 13 | 0.567 | 633.261 | 0.066 | 51.091 | 0.002 | 1.024 | 0.004 | 0.821 | 1.962 | 0.142 | 3.758 | 50.648 |

**Table 3.6** Bed pressures in kPa at the end of each steps for each run.

| run no | Feed | I | HR | Eq | CoD | CnD | LR | Eq* | LPP |
|---|---|---|---|---|---|---|---|---|---|
| 1 | 101.325 | 100.97 | 101.325 | 44.13 | 5 | 1.0 | 5 | 44.13 | 101.325 |
| 2 | 101.325 | 100.99 | 101.325 | 42.88 | 5 | 1.0 | 5 | 42.88 | 101.325 |
| **3** | **101.325** | **100.99** | **101.325** | **41.68** | **5** | **1.0** | **5** | **41.68** | **101.325** |
| 4 | 101.325 | 101.03 | 101.325 | 40.50 | 5 | 1.0 | 5 | 40.50 | 101.325 |
| 5 | 101.325 | 101.13 | 101.325 | 42.37 | 5 | 1.0 | 5 | 42.37 | 101.325 |
| **3** | **101.325** | **100.99** | **101.325** | **41.68** | **5** | **1.0** | **5** | **41.68** | **101.325** |
| 6 | 101.325 | 100.88 | 101.325 | 41.15 | 5 | 1.0 | 5 | 41.15 | 101.325 |
| 7 | 101.325 | 100.80 | 101.325 | 40.71 | 5 | 1.0 | 5 | 40.72 | 101.325 |
| 8 | 101.325 | 100.98 | 101.325 | 42.04 | 5 | 0.8 | 5 | 42.03 | 101.325 |
| **3** | **101.325** | **100.99** | **101.325** | **41.68** | **5** | **1.0** | **5** | **41.68** | **101.325** |
| 9 | 101.325 | 100.00 | 101.325 | 41.42 | 5 | 1.2 | 5 | 41.42 | 101.325 |
| **3** | **101.325** | **100.99** | **101.325** | **41.68** | **5** | **1.0** | **5** | **41.68** | **101.325** |
| 10 | 101.325 | 100.85 | 101.325 | 40.56 | 5 | 1.0 | 4 | 40.57 | 101.325 |
| 11 | 101.325 | 100.69 | 101.325 | 39.52 | 5 | 1.0 | 3 | 39.51 | 101.325 |
| 12 | 101.325 | 100.99 | 101.325 | 41.59 | 4 | 1.0 | 5 | 41.59 | 101.325 |
| **3** | **101.325** | **100.99** | **101.325** | **41.68** | **5** | **1.0** | **5** | **41.68** | **101.325** |
| 13 | 101.325 | 100.99 | 101.325 | 41.72 | 7 | 1.0 | 5 | 41.71 | 101.325 |

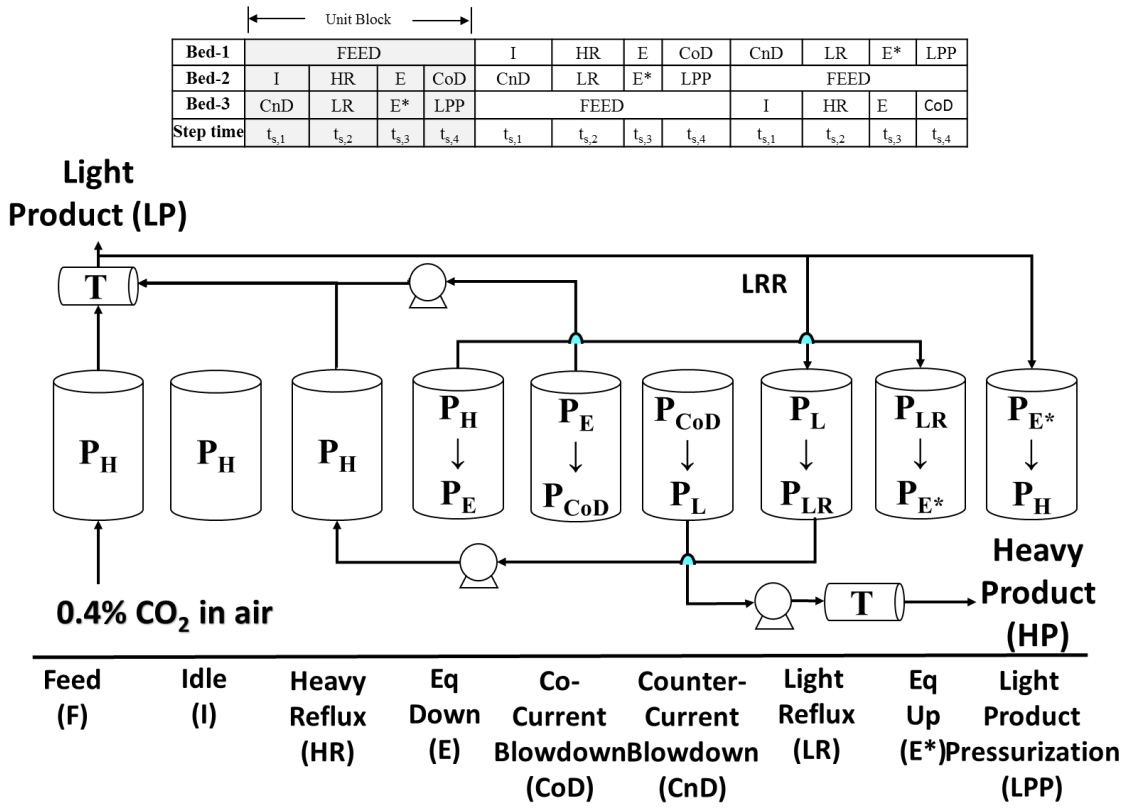


**Figure 3.1** Cycle sequence of preliminary simulations: 3-Bed 9-Step PSA Cycle.

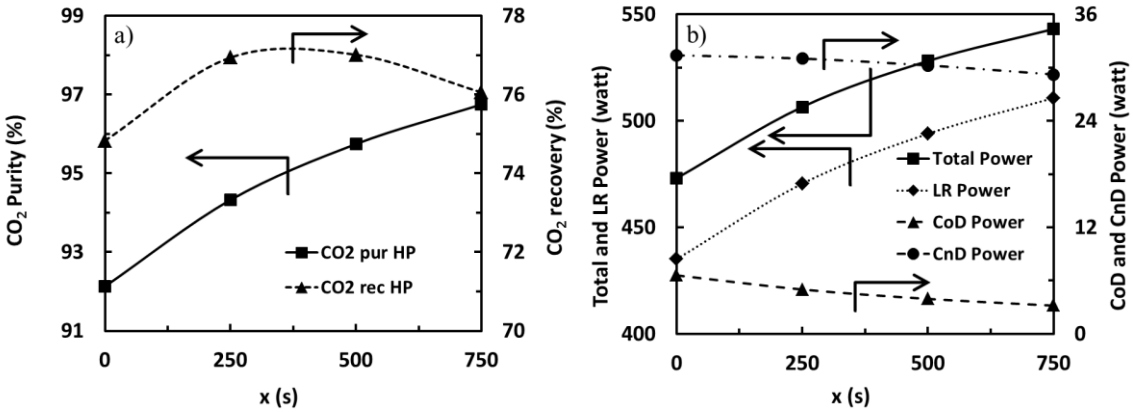


**Figure 3.2** Effect of HR/LR/F step time (thus cycle time) on cyclic steady state performance for the runs 1-4 in Table 3.2. a) $CO_2$ purity and recovery, b) Power.

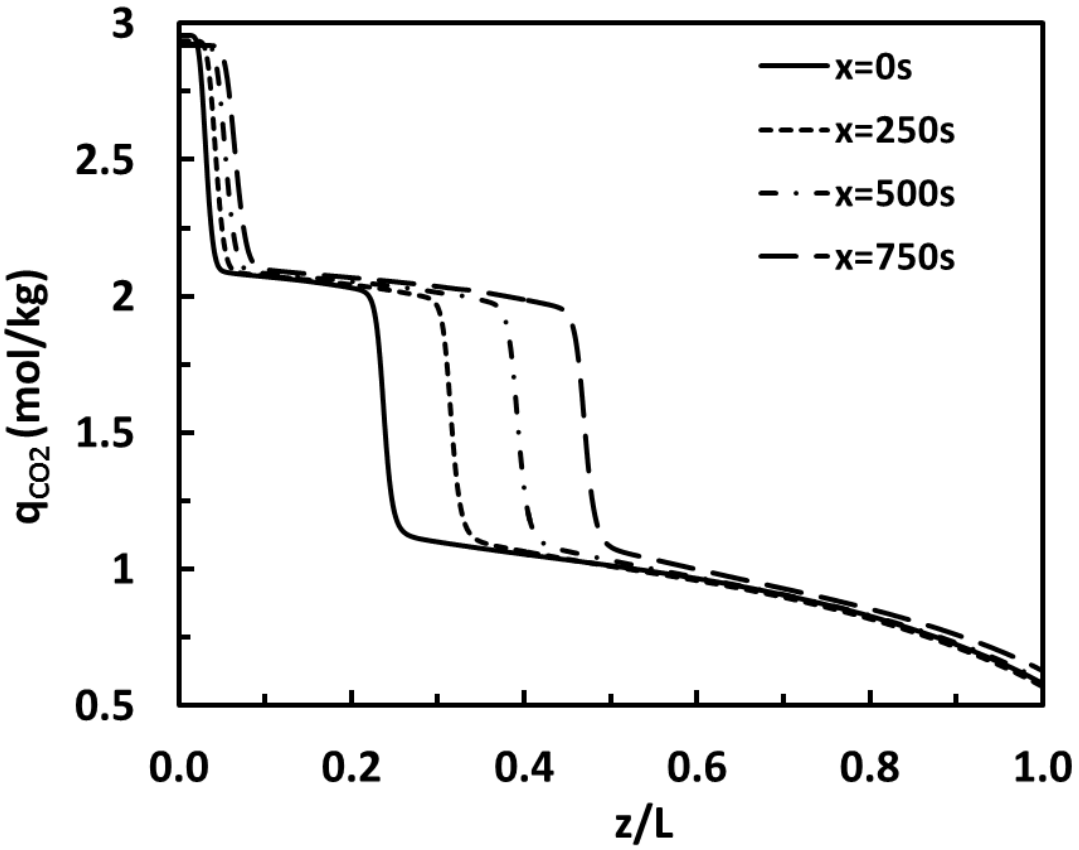


**Figure 3.3** Bed profiles at the end of HR step for each run (1-4 in Table 3.2) at periodic steady state.

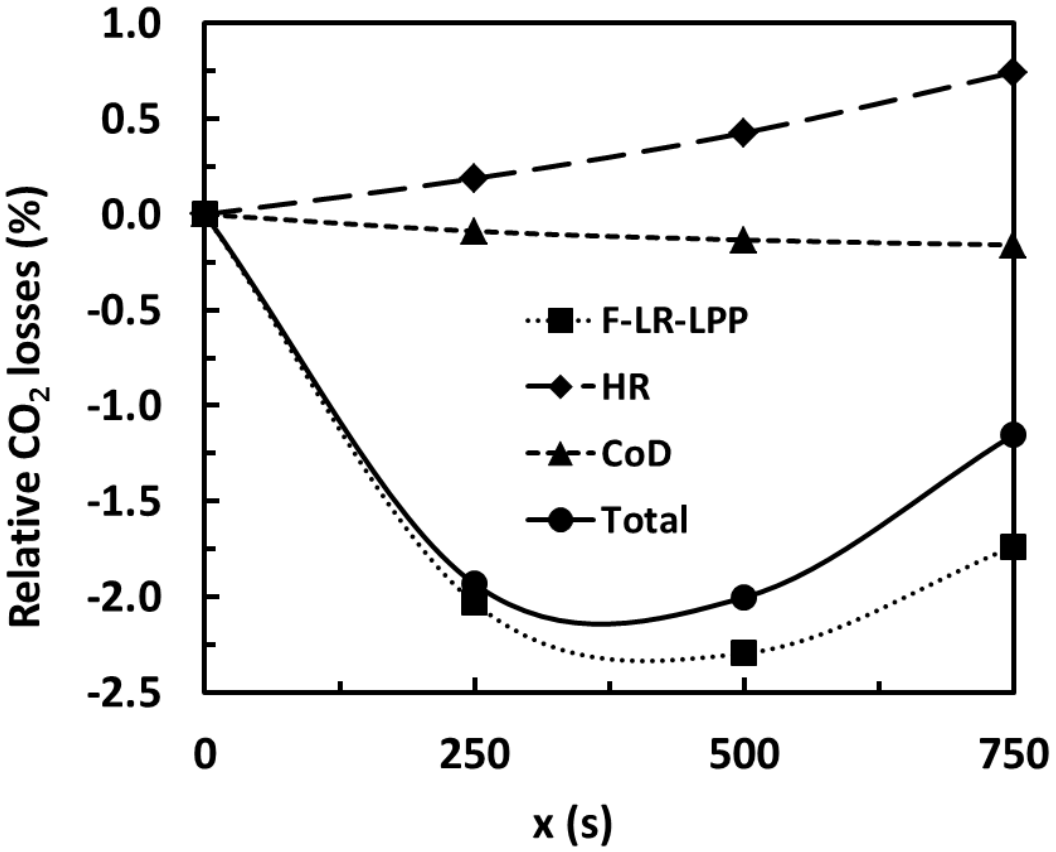


**Figure 3.4** Relative losses of $CO_2$ from light end (minus: decrease in $CO_2$ loss, +: increase in $CO_2$ loss relative to x=0). Run numbers 1-4 in Table 3.2.

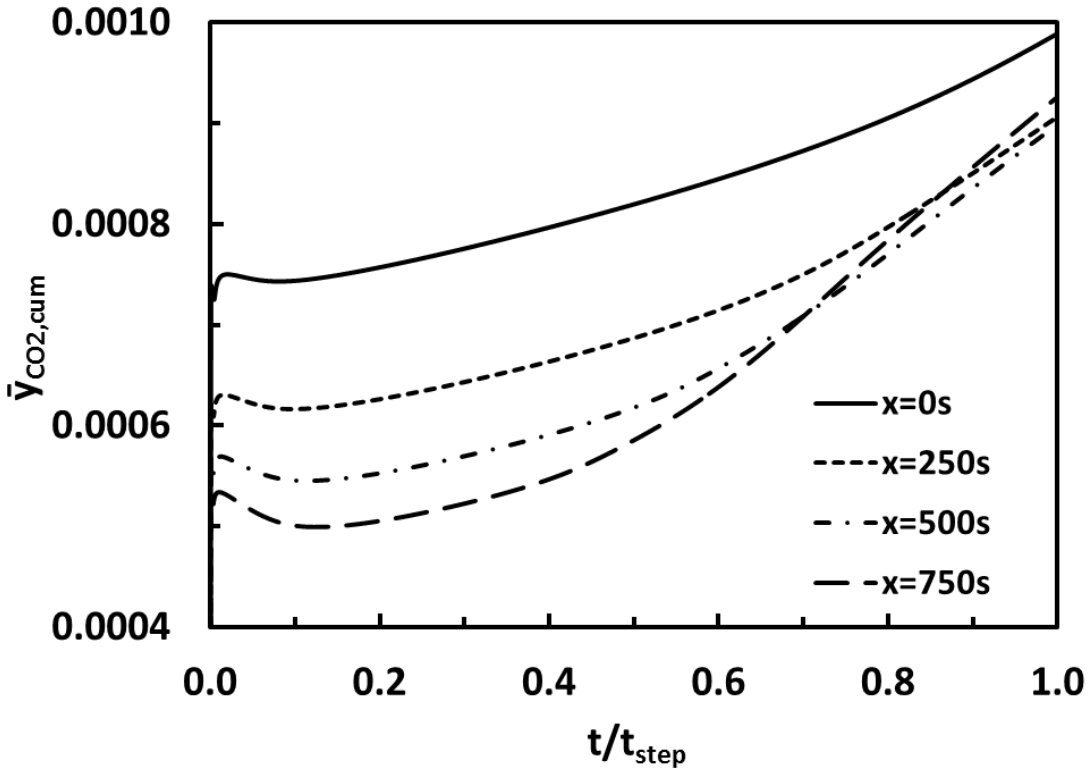


**Figure 3.5** Cumulative $CO_2$ gas phase concentration ($\bar{y}CO_{2,}$ cum) from the beginning to the end of feed step. Run numbers 1-4 in Table 3.2.

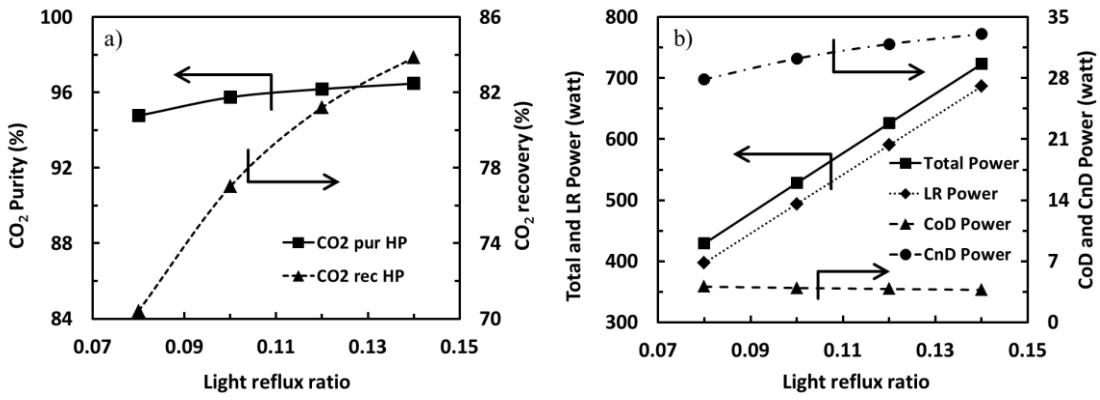


**Figure 3.6** Effect of light reflux ratio (LRR) on cyclic steady state performance for the PSA cycle. Run numbers 3 and 5-7 in Table 3.2. a) $CO_2$ purity and recovery, b) Power.

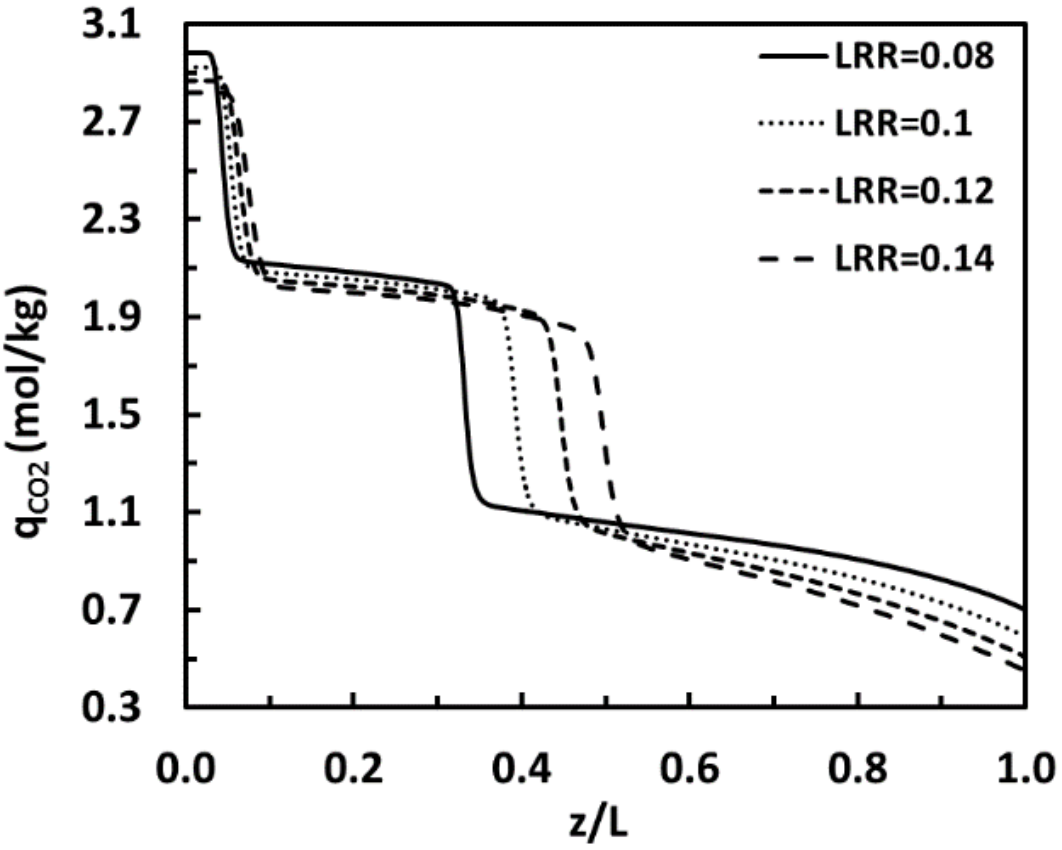


**Figure 3.7** Bed profiles at the end of HR step for each run (3 and 5-7 in Table 3.2) at periodic steady state.

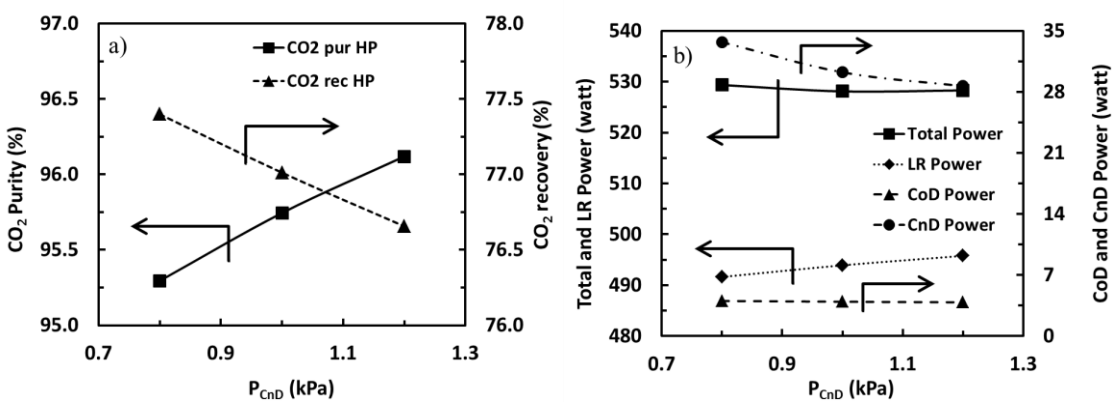


**Figure 3.8** Effect of counter-current depressurization pressure ($P_{CnD}$) on cyclic steady state performance for the PSA cycle. Run numbers 3, 8, and 9 in Table 3.2. a) $CO_2$ purity and recovery, b) Power.

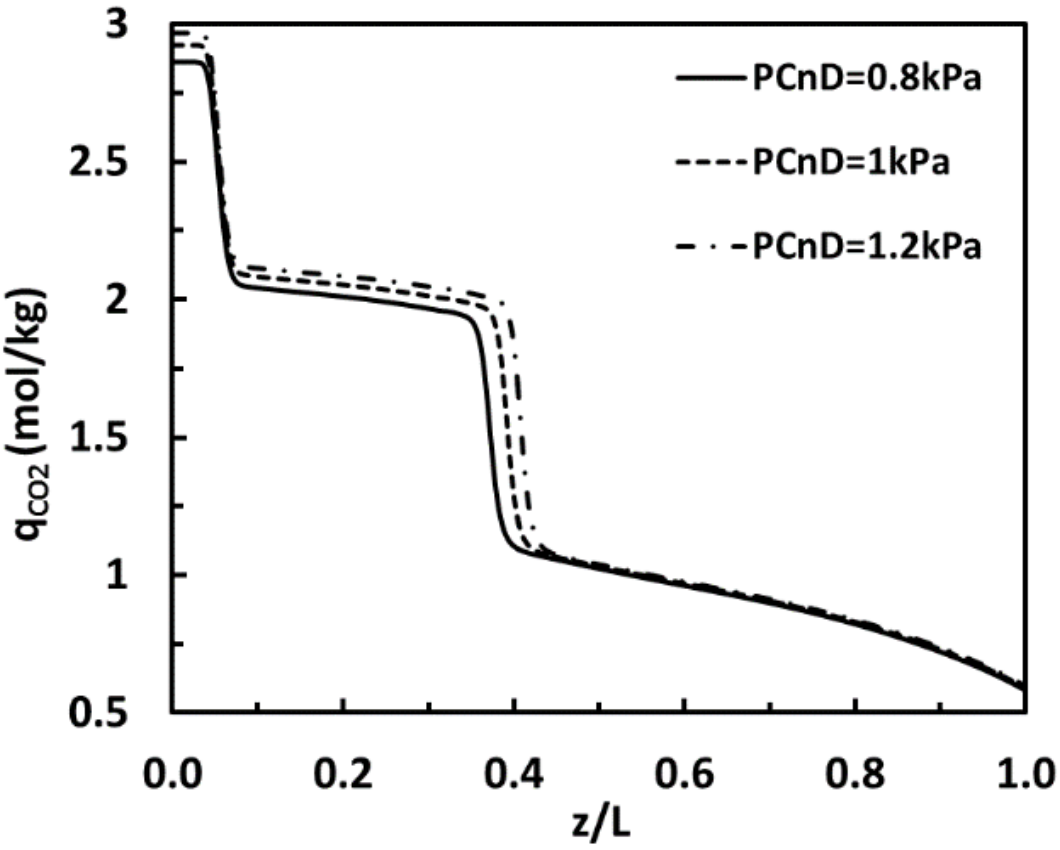


**Figure 3.9** Bed profiles at the end of HR step for each run (3, 8-9 in Table 3.2) at periodic steady state.

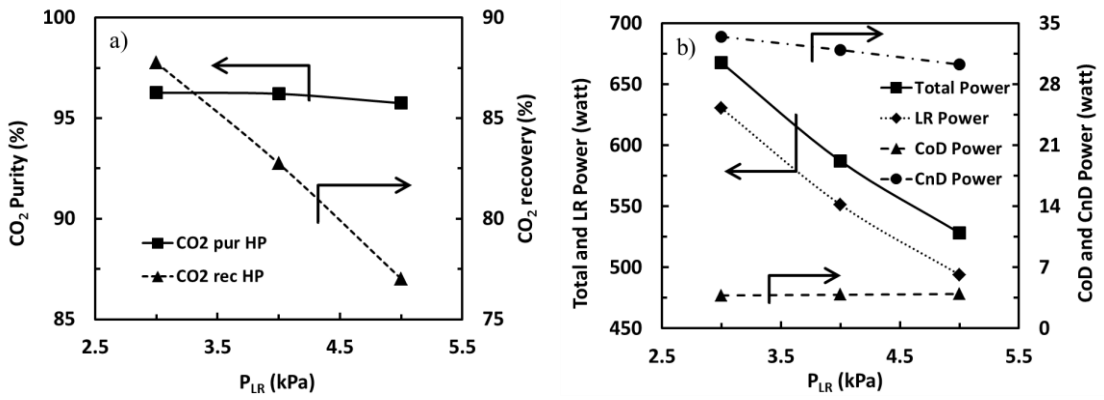


**Figure 3.10** Effect of light reflux pressure ($P_{LR}$) on cyclic steady state performance for the PSA cycle. Run numbers 3, 10-11 in Table 3.2. a) $CO_2$ purity and recovery, b) Power.

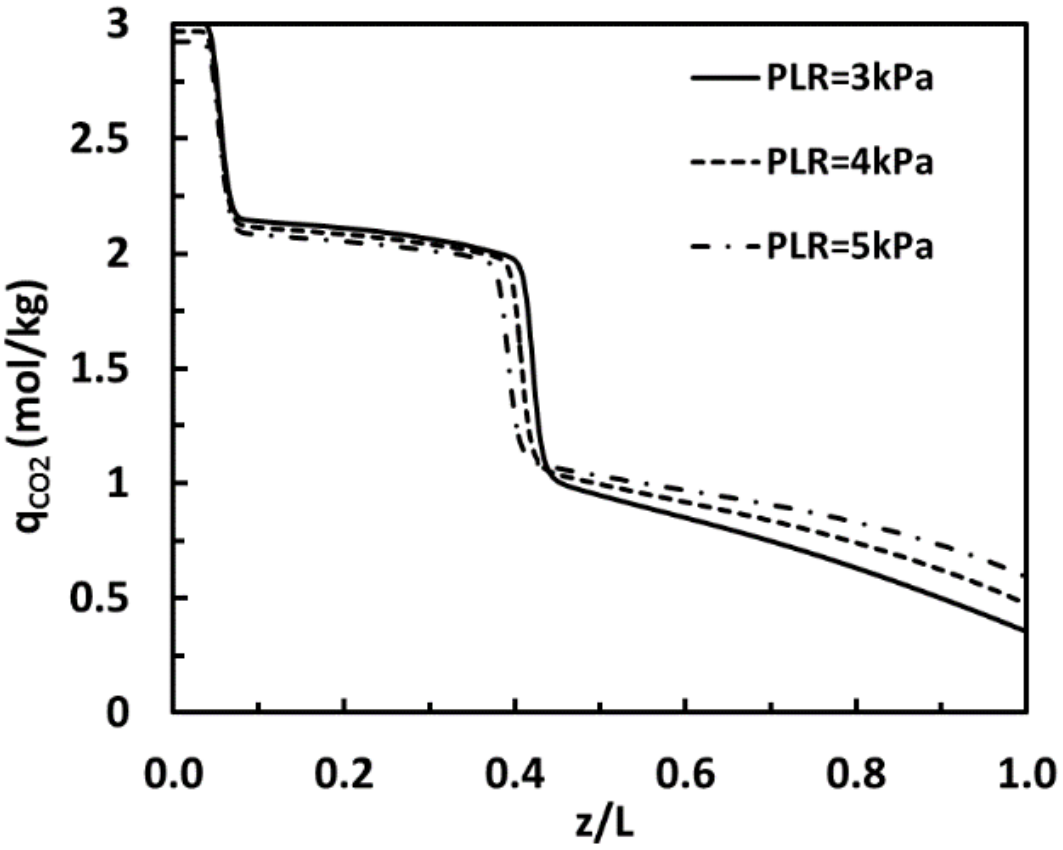


**Figure 3.11** Bed profiles at the end of HR step for each run 3, 10-11 in Table 3.2) at periodic steady state.

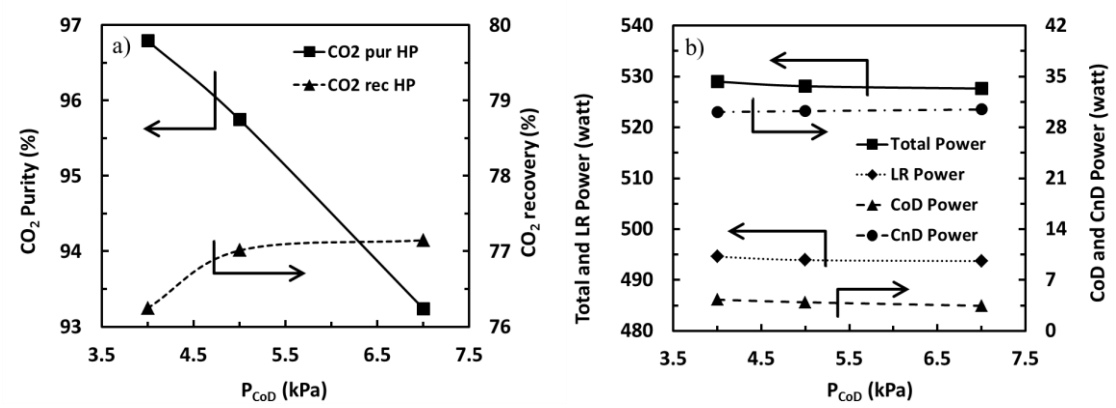


**Figure 3.12** Effect of co-current depressurization pressure ($P_{CoD}$) on cyclic steady state performance for the PSA cycle. Run numbers 3, 12-13 in Table 3.2. a) $CO_2$ purity and recovery, b) Power

# CHAPTER 4

# PRELIMINARY STUDY TO DEVELOP A NEW PSA CYCLE FOR $CO_2$ REMOVAL AND CONCENTRATION DURING CLOSED-LOOP HUMAN SPACE EXPLORATION MISSIONS

## 4.1 Summary

In this study, a new 3-bed PSA cycle sequence and schedule were developed and studied using dynamic adsorption process simulator DAPS. This novel PSA application is being evaluated as part of an effort to develop a next generation $CO_2$ Removal system, which is part of the life support system that will be used on future long duration spaceflights. Initial results obtained with a dynamic adsorption process simulator (DAPS) utilizing a beaded 13X zeolite. The preliminary DAPS results were then used to determine the 3-bed experimental conditions. 3-bed experiments were carried out, accordingly. After having the experimental results model validation has been done by DAPS.

A next generation $CO_2$ removal system for life support is to separate, enrich and recover $CO_2$ from spacecraft cabin air for current and future long duration spaceflights. The current ISS $CO_2$ removal system that utilizes zeolite 5A in a temperature swing adsorption (TSA) process did not operate as designed, so replacements are being

explored. So, the next generation air revitalization system may utilize a PSA process with 13X zeolite to remove $CO_2$ from cabin air. Because of these reasons a new 3-bed PSA cycle step sequence and schedule were thus conceived and studied using DAPS. Initial simulations using the full scale flow rates in search of the bed size, light reflux ratio, cycle time and vacuum pressure that lead to the desired performance with a 3-bed 8-step pressure swing adsorption (PSA) cycles (0.4% $CO_2$ from a $CO_2$-$N_2$ mixture) were carried out by using 13X zeolite as an adsorbent using dynamic adsorption process simulator DAPS. The initial DAPS results were then used to determine the 3-bed experimental conditions. Experimental runs have been done by using a 4-bed PSA apparatus using the PSA schedule and conditions determined from the initial simulations but restricted by conditions defined by the unit (namely, bed size, vacuum pump capacity and vacuum level). Model validation was carried out via running simulations with no adjustable parameters against experimental results. The PSA sequence includes feed (F), heavy reflux (HR), co-current equalization depressurization (Eq), co-current depressurization (CoD), counter-current depressurization (CnD), light reflux (LR), counter-current equalization pressurization (Eq*) and Light Product Pressurization (LPP) steps. The main goal of this chapter is to remove 6kg $CO_2$/day (>93% recovery) with more than 97% $CO_2$ enrichment. Full scale feed flow rate is 570slpm with 0.4% $CO_2$ and 99.6%$N_2$. As an overall conclusion of this study, large enrichments (>90%) of $CO_2$ from 0.4% can be achieved via adequate PSA schedule and this process has to be designed in two stages with first stage focusing on 100% recovery of $CO_2$ to achieve NASA objectives.

## 4.2 PSA Cycle Description

A typical PSA process involves a cyclic process where a number of interconnected vessels containing adsorbent/adsorbents undergo successive pressurization and depressurization steps in order to produce a continuous stream of purified product. The steps of the PSA cycle include feed (F), heavy reflux (HR), equalization down (E), co-current depressurization (CoD), counter-current depressurization (CnD), light reflux (LR), equalization up (E*) and light product pressurization (LPP). The operation of 3-bed 8-step PSA cycle is described in Figure 4.1 along with the cycle sequence. Each row in the cycle sequence represents all the different cycle steps a given bed undergoes over the entire cycle, whereas each column represents which cycle step is being run by which bed at a particular $t_s$. The sequence of operation is developed by following a simple methodology called graphical approach (Mehrotra et al., 2011). The unit block shown in the Figure 4.1 by a shaded area consists of four ($t_{s,1}$, $t_{s,2}$, $t_{s,3}$ and $t_{s,4}$) unit step times where all steps are being run by one of the three beds and the total cycle time is composed of multiple consecutive unit blocks where the operations are repeated again and again.

The operation of first unit block, bed 1 is fed from bottom at atmospheric pressure for a period equivalent to the sum of all unit step times ($t_{s,1}$, $t_{s,2}$, $t_{s,3}$ and $t_{s,4}$). The reason of covering all the unit step times by feed (F) step during the operation of bed 1 is to maintain a continuous feed flow throughout the cycle. During this operation, the preferentially adsorbed species (in this case $CO_2$) is captured by the adsorbent in the bed and a product stream is collected from the top of bed 1.

Next, bed 2 undergoes a heavy reflux (HR) step for a period of $t_{s,1}$ and $t_{s,2}$ which is ringed with heavy gas providing from another bed undergoing light reflux (LR) step. Heavy reflux (HR) step is operated in this case at atmospheric pressure like feed step. The purpose of having HR step in the sequence is to clean the bed and to enhance the loading of heavy component in the column. It is important to mention that a compressor is necessary to provide feed to HR step by pulling gas from LR step. During $t_{s,3}$, bed 2 undergoes a co-current equalization depressurization (E) step where it is co-currently blown down to another intermediate pressure to provide gas from its light end to another bed undergoing equalization pressurization (E*) step. Finally, bed 2 is co-currently blown down (CoD) to another intermediate pressure for a period of $t_{s,4}$. The rate of CoD is controlled by a valve coefficient ($Cv_{CoD}$) in order to reduce the loss of adsorbent material due to attrition.

Finally, bed 3 is in counter-current blow down (CnD) step during $t_{s,1}$, which bed 3 is depressurized counter-currently to a low pressure and he pressure at the end of this step is controlled by a valve coefficient ($Cv_{CnD}$). During CnD, heavy gas is collected as product from the bottom of bed. Next during $t_{s,2}$, the bed undergoes light reflux (LR) step. In this step, the bed is fed from light end with a portion of the light gas (LRR) coming from another bed undergoing feed (F) step. The pressure at the end of this step is controlled by a valve coefficient ($Cv_{LR}$) associated with the step. The entire heavy product collected during LR step is sent back to HR step. The purpose of having LR step in the sequence is to regenerate the bed. Then during $t_{s,3}$, the bed is equalized with another bed from the light end to bring the pressure up to an intermediate level. This equalization pressurization (E*) step helps to reduce operating cost as well to improve PSA performance. Finally during $t_{s,4}$, the bed is re-pressurized to atmospheric pressure using the light gas from the light end of the bed

undergoing feed step. After this phase same operation is repeated to complete the overall cycle.

Initial simulations of a 3-bed 9-step PSA cycles were carried out using a FORTRAN based in house dynamic adsorption process simulator (DAPS) detailed information about the simulator is given in Chapter 2.

In the current PSA cycle, the desired product is $CO_2$ which is the preferentially adsorbed species. Therefore, the performance of the process is evaluated on the basis of $CO_2$ recovery and $CO_2$ purity in the heavy product. Recovery of $CO_2$ is defined as the number of moles of $CO_2$ withdrawn as product during production step (CnD) divided by the number of moles of $CO_2$ fed to the PSA process during the feed step. On the other hand, $CO_2$ purity is defined as the mole fraction of $CO_2$ leaving the bed during the CnD step.

Finally, the performance of a PSA process is calculated in terms of purity, recovery. In this study, these are defined are follows:

$$Purity[\%] = \frac{CO_2(mol)obtained\ as\ product\ during\ CnD\ step}{total\ Product(mol)obtained\ during\ CnD\ step} * 100 \qquad (4\text{-}1)$$

$$Recovery[\%] = \frac{CO_2(mol)obtained\ as\ product\ during\ CnD\ step}{Fresh\ CO_2(mol)fed\ in\ Feed\ step} \times 100 \qquad (4\text{-}2)$$

### 4.3 Bed and Adsorbent Characteristics

An overview of the bed and adsorbent characteristics used as input parameters in the simulations and process characteristics are summarized in Table 4.1. The feed stream contains 0.4vol % $CO_2$ with 99.6 vol % $N_2$ (given in Table 4.1). The adsorbent utilized here is 13X zeolite. The TPL isotherm parameters were obtained by fitting the experimental

data and the fitted equilibrium parameters are summarized in Table 2.3. The mass transfer coefficients for $CO_2$, $N_2$ and $O_2$ were obtained experimentally from the single bed rapid PSA apparatus and macropore mass transfer parameters are summarized in Table 2.4.

## 4.4 Experimental Section

### 4.4.1 Description of 4-Bed Pressure Swing Adsorption Apparatus

A typical schematic diagram of the PSA experimental system used in this study is shown in Figure 4.4. The system is equipped with four adsorption beds (1, 2, 3 and 4), seven mass flow controllers (FC), F21, F22, F23, F24, F25, F31, F32 in Figure 4.4, three mass flow meters (FM), F11, F12, F13 in Figure 4.4, one light product tank, two heavy product tanks, eighteen thermocouples (nine connected with first three beds and seven with last bed, one with light product tank and one with large heavy product tank), seven pressure transducers (four of them are coupled with four beds and the remaining two are with light product tank and large heavy product tank, and one with vacuum pumps), vacuum pumps and valves (1 to 50). In lower part of the columns, the line connected with the valves 6, 12, 18 and 24 is used to provide feed to the adsorption columns whereas the lines coupled with valves 5, 11, 17, 23 and valves 4, 10, 16, 22 are used as counter-current blow down/light reflux (CnD/LR) and heavy reflux (HR) lines, respectively. Similarly in the upper trend of the columns, the line incorporated with the valves 1, 7, 13 and 19 is used as the product line during feed step, the one coupled with the valves 38, 39, 40, 41, and 25 is for the product line during heavy reflux (HR) step and the line connected with the valves 3, 9, 15, 21 and 28 is used for light product pressurization (LPP) as well as light reflux (LR) steps by closing 28 while opening 27. In addition, the current system has the facility to operate

the PSA cycle by incorporating equalization (EQ) step which is accomplished by using the line connected with the valves 2, 8, 14 and 20, and finally the line with valve 49 in addition to the valves 2, 8, 14, 20 is used for co-current blow down (CoD).

The thermocouples used in the experimental set-up shown in Figure 4.4 are K-type thermocouples which are used to measure the centerline temperatures of the beds as well as the temperatures of the light and heavy product tanks. In each bed, a series of three thermocouples are distributed axially throughout the bed which shows the bed temperature profiles at one quarter, half way and three quarters into the bed from the feed end. In addition, a fifteenth thermocouple which is not shown in the schematic diagram is used to measure the ambient temperature. Also, a total of three heaters coupled with each adsorption bed provided the facility of heating the bed uniformly. The power input to all the heaters is controlled by using twelve variable autotransformers (range 0 to 120/140V, type 3PN1O1O). The signals from all the thermocouples are sent to the signal conditioner as input to the computer which displays real time temperature as the system is running (Bhadra 2012).

The mass flow controllers and mass flow meters used in the system are supplied by Tylan General/Brooks/MKS which have the ability to measure and/or control the mass flow rates of the gas accurately and reliably. All the meters and controllers are digitally controlled by two DX-5 Digital Power Supply instruments from UNIT instruments, Inc and one Hasting Power Supply-Model 200. Each unit of this instrument from UNIT instruments, Inc has five individual channels (eight of them have been using) and Hasting Power Supply unit has two. Each mass flow controller channel controls and displays the set point and actual flow for the channel as a percentage of full scale units. All the seven

pressure transducers used as pressure sensors are supplied by Omega Dyne Inc. The outputs from all the pressure transducers are converted to absolute pressures which are displayed on the screen of the computer. The valves used for the system are all from Swagelok which are opened or closed depending on the duration of each step of a cycle. Valves 1 through 26 are Swagelok® U series bellows-sealed valves which provide enhanced reliability, versatility, and safety with a secondary containment system that prevents leaks to atmosphere even if the primary seal fails. These valves have a very high operating temperature and pressure (343 $^{o}$C and 2500 psig) and are operated on double actuation mode (opened and closed by air). On the other hand, the rest of the valves are operated on single actuation mode (opened by air but closed by spring) except the valves with handle which are metering valves. The pressure and temperature ratings of these valves are about 3220 psig and 65 $^{o}$C, respectively. It is worthwhile to note that all the instruments and devices are controlled by a single CPU which is used to save the outputs from all the devices, if necessary (Bhadra 2012).

The system is designed in such a way that provides the facility to measure the feed (F), light product (LP) during feed, light product (LP) during heavy reflux, mixed light product (LP), heavy product (HP) and heavy reflux (HR) concentrations using a 6-port valve manufactured by Swagelok. This valve is connected to a residual gas analyzer (RGA), a small and usually rugged mass spectrometer, which is basically a vacuum instrument that operates near $10^{-6}$ mbar pressure. At high or atmospheric pressure, the aperture assembly of RGA is insufficient to reduce the pressure while maintaining the response time. In order to facilitate the sampling at this pressure, a pressure reduction device which is actually a capillary is coupled with the RGA. The length of the capillary is

selected on a trial and error basis in order to maintain fast response time (Bhadra 2012). Back and front views of 4-Bed PSA apparatus are shown in Figure 4.5.

LabVIEW program controls the valves and recording pressures, temperatures, and flowrates from different locations of the PSA experimental system. Front Panel of LabVIEW Program is shown in Figure 4.6. MS Excel file is being used for input file in which user can define PSA step properties by deciding flowrates, timing, and on/off position of each valve.

### 4.4.2. PSA Cycle Description for experiments

PSA cycle steps used in the experiments consist of feed (F), idle (I), heavy reflux (HR), equalization down (E), co-current depressurization (CoD), counter-current depressurization (CnD), light reflux (LR), equalization up (E*) and light reflux pressurization (LPP). The operation of 3-bed 8-step PSA cycle is described in Figure 4.1 along with the cycle sequence. As shown in the figure, the cycle sequence is divided into 9 unequally long unit step times of length. The flow schematic of the unit block depicted in gray in cyclic schedule is also described in the figure. The other three unit blocks are just the repetition of the same steps but with different sequence. Therefore, it is noteworthy to describe the cyclic operation of the present cycle more specifically on the basis of the unit block. It is important to mention that only bed number 2, 3, and 4 have been used for 3-bed 8-step PSA experiments from available in-house 4-bed PSA experimental set-up, shown in Figure 4.4.

The adsorption beds 1, 2, 3 and 4 are filled with Zeolite 13X adsorbent. Bed, adsorbent properties for the experiments and model validation were given in Table 4.1. The adsorbent

was prepared for cycling by first regenerating with heating under continuous upward Helium flow (~ 0.1 SLPM) up to 350 $^{o}$C at 101.325kPa and the regenerated (i.e., dry) weight of the adsorbent was obtained from the regeneration data. The adsorbent beds were further regenerated in-situ, under vacuum and continuous Helium flow (~0.1 SLPM) by increasing the temperature around 350$^{o}$C via 8 band heaters connected around the beds prior to each experiment. At the end of regeneration period, the beds were cooled down to the room temperature. The feed gas mixture (0.4% $CO_2$ in $N_2$) has been obtained by using two mass flow controllers for $CO_2$ and $N_2$ separately. These feed stream gases are introduced to the upstream of bed 1 (z/L = 0) at high pressure ($P_H$) through opened valves 12 and 7 and is allowed to pass through for a duration of $t_{s,1}$ s to have preferentially adsorbed species ($CO_2$) adsorbed and the high pressure product stream enriched with less strongly adsorbed species ($N_2$) leaves the column from the other end (z/L = 1.0) of the bed which is sent to the light product tank through needle valves N-9 and N-10. At this moment, bed 2 is under idle step (I) when it is separated from rest of the processes by closing all the valves incorporated with the bed 2. During this operation, $t_{s,1}$, beds 3 undergoes countercurrent blow down step. During this step, one end of the column is closed while the other is exposed to a vacuum pump. Valves 19, 20, 21, 22, 24, 41, and 48 are kept closed and the bed is depressurized to a low pressure ($P_L$) through opened valve 23 and all the desorbed gas is sent to the heavy product tank. As a result of pressure decrease, $CO_2$ from the adsorbent gets desorbed and exits the bed. At the end of the operation in first unit step time of $t_{s,1}$ s, beds 1 undergoes feed step which is conducted according to the procedure described above for duration of next unit step time of $t_{s,2}$ s. During this operation time, $t_{s,2}$, bed 2 undergoes light reflux step (LR) by opening valve 23, 21, and 28 while

valves 19, 20, 41, 22, and 24 are kept closed. Bed 3, light reflux step operated at $P_{LR}$ to facilitate desorption of $CO_2$. This light reflux step helps to clean the bed from heavy product by sending light product gases; therefore, breaking through of heavy gases from light end can be prevented by the help of light reflux step. The $CO_2$ rich effluent from the light reflux purge step enters the heavy reflux step. Bed 2 undergoes this heavy reflux step by closing valves 13, 14, 15 17, 18, and 47 while opening valves 17, 40, and 25. In heavy reflux (HR) step, the blow down gas emanating from this light reflux step is fed to the feed end of the column at high pressure ($P_H$) usually. The purpose of this step is to increase the loading of heavy component in the solid phase. Also, undesirable light gas present in the void space is flushed out of the bed as it is replaced with pure $CO_2$. These factors cumulatively help to increase the enrichment of heavy component during CnD step. During the operation of the next unit step time of the unit block, $t_{s,3}$, bed 1 is at feed step and beds 2 and 3 are at equalization step. The operating procedure of feed step is the same to the procedure described above. With valves 16, 17, 18, 13, 40, 15 of bed 2, valves 22, 23, 24, 19, 41, 21 of bed 3 closed and the remaining valves 14 and 20 of beds 2 and 4 opened, the two beds are connected through their product ends to equalize pressure. In this case, beds 2 and 3 are at co-current equalization pressurization (E) and equalization depressurization (E*), respectively. This equalization pressurization step helps to save energy because the gas, partially depleted of strongly adsorbed species from high pressure bed is used to pressurize the other bed at low pressure to an intermediate pressure. In the last unit step, $t_{s,4}$ bed 1 again undergoes feed step with the same to the procedure described above. Continuous feed flow during entire PSA cycle has been achieved with this way. Bed 2 is at co-current depressurization step while bed 1 is at feed step. In the CoD step, valves 16, 17, 18, 13, 40,

15 closed and the remaining valves 14 and 49 opened. During CoD step, bed 2 goes from an atmospheric pressure to an intermediate pressure. The main purpose of having CoD step in PSA cycle is to purity and recovery of heavy product by getting rid of the light product gases from light end. Bed 3 is at light product pressurization (LPP) step during last unit step time of unit block. The light product pressurization (LPP) step is conducted on bed 3 by closing valves 22, 23, 24, 19, 20, 41 and 27 while opening valves 21 and 28. The light product from light product tank is used for LPP. The purpose of incorporating light product pressurization (LPP) step is to push the concentration wave towards the feed end of the column thereby, enhancing the performance of the process. Similarly, the consecutive operation in each bed of corresponding unit block for particular step is repeated until the periodic steady state is reached. With setting a 6-port valve, the transient as well as periodic steady state concentration profiles of light and heavy products can be monitored by using RGA. An in-house built LabView program and National Instruments data acquisition and control system were used to control valve operation, cycle sequencing, and mass flow controller and to monitor the temperature, pressure and flow rate profiles with time. Depending on the value of parameters and length of step change in parameter values from previous steady state condition, huge numbers of cycles were required to reach a new periodic steady state. To decrease the number of cycle to reach steady state because of having long cycle time, all 4 experiments have been started with 10% $CO_2$ saturated bed. Initial simulations show that starting with clean bed or saturated bed has no effect on the process performance in terms of purity and recovery of $CO_2$ in the heavy product and $N_2$ in the light product. The periodicity was verified by observing the steady temperature

profiles of all thermocouples at different locations of the bed as well as by monitoring the steady heavy and light product concentrations profiles by RGA.

## 4.5. Result and Discussion

### 4.5.1 Initial Simulations Results

A parametric study was conducted to evaluate the effects of various parameters, especially HR/LR time, on the cyclic steady state PSA performance. The conditions of initial simulations have been run in this study and all the initial simulation process performances were given in Table 4.1. In the initial simulations, the varied conditions include HR/LR/F step time (thus cycle time), two different light reflux ratios (LRR), counter-current depressurization pressure ($P_{CnD}$) and time, light reflux pressure ($P_{LR}$), and co-current depressurization pressure ($P_{CoD}$). It can be seen from the Table 4.2 that added HR/LR time x has important role in $CO_2$ concentration in HP for run numbers 1, 5, 9, 13, 17. That effect can be explained by the bed profiles at the end of HR step for these runs, shown in Figure 4.2. From the figure, it can be easily seen that $CO_2$ front in the bed is moving through the end of bed by increasing x. Hence, the purity shows an increasing trend with increasing x. It is important to notice that other parameters such as light reflux ratio (LRR), counter-current depressurization pressure ($P_{CnD}$) and time, light reflux pressure ($P_{LR}$), and co-current depressurization pressure ($P_{CoD}$) have not much effect on purity of $CO_2$ (still around 90%) in heavy product while have negative effect on $CO_2$ recoveries (drop to 60%) in heavy product beside HR/LR time parameter. However in the overall picture, modelling results show that one gets close to the desired performance,

which is Run#18 in Table 4.2. Run #18 has been chosen as a base case for the experiments. However, vacuum pressures for the flows needed are prohibitive in experimental set up.

### 4.5.2 Experimental Results

Four experiments were conducted on the 3-bed PSA system to reach the overall process performance for closed-loop human space exploration missions. In those four experiments, flow and pressures adjusted to smaller beds while maintaining PSA schedule and throughput, shown in Table 4.4. The main difference between experiments and the initial simulations is the final pressure of light reflux step ($P_{LR)}$. $P_{LR}$ was the same with $P_{CnD}$, which is lowest pressure ($P_{L)}$, in the initial simulations, while it is little bit higher than the lowest pressure in the experiments. The reason of that situation is mainly because of having high flow rates during light reflux step, thus the vacuum pump cannot reach the lowest pressure during the light reflux step that it can reach during the counter-current depressurization step because there was no flow feeding the bed.

#### 4.5.2.1. PSA Cycle Process Performance Indicators

Once the system was reached to periodic steady state for a particular set of operating conditions, all the temperature, pressure, flow rate, heavy product and light product profiles were captured to evaluate the periodic state performance indicators. The process performance indicators for the PSA process were evaluated on the basis of enrichment, recovery and throughput. The overall process performance was judged in terms of the purity and recovery of $CO_2$ in the heavy product and $N_2$ in the light product. The $CO_2$ purity was defined as the average mole fraction of $CO_2$ in the heavy product. $CO_2$ recovery was defined as the moles of $CO_2$ in the heavy product divided by the moles of

$CO_2$ fed to the process cumulatively during the feed (Eqn 1, 2). The enrichment and recovery of both heavy and light components were calculated from the concentration profiles captured by RGA after the steady state situation was reached. After every set of experiment, the RGA was trained with running different $CO_2$-$N_2$ standards namely 0, 0.2, 0.5, 1, and 2 % $CO_2$ and from 10% $CO_2$ to 100% $CO_2$ with increment of 10% by using two mass flow controllers for $CO_2$ and $N_2$.

A total of four runs were carried out to study the effect of various process parameters. The parameters studied include the heavy reflux/light reflux, thus total cycle time and CnD time, light reflux ratio, feed flow rate, $P_{CoD}$ and $P_{CnD}$. The conditions used during each run (E1 to 4) are shown in Table 4.4. The process performance in terms of purities and recoveries of $CO_2$ in the heavy product and $N_2$ in the light product is shown in Table 4.5. From Table 4.5, 3-bed 9-step PSA process only recovers ~ 50% $CO_2$ at original model throughputs but higher LR pressures while it can recover ~ 80 % $CO_2$ at half of the original model throughputs. In addition, it is quite significant that the system is able to enrich $CO_2$ from 0.4 to ~ 90%. Therefore, this process will be focused in fully recovering $CO_2$ as a first of a two-step process while enriching less $CO_2$ and utilizing less power for vacuum.

Temperature and Pressure histories of the experiments have been shown in Figure 4.7 and 4.8, respectively. From temperature history of Experiment 4, Figure 4.7, it can be easily seen that major temperatures rises during HR step (35-65) minutes and during this step $CO_2$ front reaches anywhere between 60.75% and 73.41% of the bed. Pressure history during one entire cycle (a) and a zoomed-in view of pressure when equalization down, CoD, CnD steps (b) and when light reflux, equalization up and light product pressurization

steps (c) have shown in Figure 4.8. Small drops at the upper part of the pressure are due to the idle step. After evaluating the recoveries and enrichments of all the components in both heavy and light ends, a material balance calculation was performed to calculate the error associated with the system. In each case, the resulting total error was generally less than 3% for either component. This magnitude of error was considered acceptable for such a process.

### 4.6. Model Validation

The DAPS model was validated against experimental data obtained from Experiment 1-4. Figure 4.9 shows the experimental data and the model predictions for the pressure profiles at periodic state for the entire PSA cycle (top) and zoomed-in (left, right) which encompasses 9 cycle steps namely feed step, idle step, heavy reflux step, equalization down step, counter-current blowdown step, light reflux purge step, equalization up step and a pressurization step. The dashed line indicates the experimental data whereas the solid line shows the model predictions. The Model was adjusted to match the experimental pressures by changing Cvs of valves. From the figure it can be easily seen that model and experimental pressure history overlaps for feed, heavy reflux, equalization down, CnD, and light reflux steps while having little bit difference in equalization up and light product pressurization steps. However, in LPP step the final bed pressure of model at the end of step is the same with experiment. Figure 4.10 shows the temperature profiles at periodic state for seven different thermocouples in the bed for experiment 4. The black solid line indicates the experimental data whereas the gray solid line shows the model predictions. As Figure 4.10 shows, the higher concentration wave front reaches thermocouple T-7 in experiment but T-6 in model validation. Thus, the front's location for

experiment is 86.07% in the bed and for model is anywhere between 73.41% and 86.07% in the bed. The main reason having higher maximum temperature in the model than the experiment is having only one lumped heat transfer coefficient with only one energy balance equation for all gas and solid phases, and the wall. Thus, the model was able to mostly predict the temperature profiles and position of the higher concentration front during the Heavy Reflux step for the entire PSA cycle of experiments without any fitting parameters (kinetic and thermodynamic) and for a wide range of concentrations (0.4-90.0% $CO_2$). The $CO_2$ purity and $CO_2$ recovery in the heavy component and $N_2$ recovery in the light component calculated by DAPS is compared to the experimental results in Table 4.6. The results show a close agreement between experiment and model without any fitting parameters (kinetic and thermodynamic) and for a wide range of concentrations (0.4-90.0% $CO_2$).

The differences between experiment and model performances might be because of not exactly reaching steady state in the experiments due to long cycle times. Model results give more meaningful results than experiments based on the theory. More detailed explanation is in the following: (a) the first comparison is between E1 and E2: the difference is the CnD step time, $t_{CnD}$, thus $P_{CnD}$, by decreasing heavy reflux time at constant cycle time. Recovery of heavy product, here is $CO_2$, increases for both experiments and model, which is expected because more $CO_2$ is coming out from the bed during the CnD step due to longer time. However, purity of heavy product is decreasing in the model results while increasing in the experimental results. The expectation is a decrease in purity because the pump is pulling more gases, $CO_2$ and also more $N_2$ and $O_2$, to reach the lower pressure with having less time for heavy reflux step. That less time in heavy reflux step causes less

$CO_2$ saturation in the bed, which means the bed, is having less $CO_2$. Since the bed is having less $CO_2$ to reach the lower pressure light products are also coming out from the bed. That dilutes the heavy product with light product, which causes a decrease in purity. Bed profiles at end of HR step of modelling results for experiments 1 through 4 have shown in Figure 4.11. As it can be seen from the figure $CO_2$ front at the end of the heavy reflux step is moving backward by increasing CnD step time, which is an another prof of a decrease in purity; (b) Comparison of E1 and E3: the difference is the CnD step time and heavy reflux step time. Recovery of heavy product decreases for both experiments and model because most probably the bed is losing some portion of $CO_2$ during feed step due to having more $CO_2$ saturated bed at the end of heavy reflux step by the time increases. On the other hand, there is again a conflict between model and experimental results. Purity of heavy product is increasing in the model results while decreasing in the experimental results. From Figure 4.11, it can be seen that $CO_2$ front at the end of HR step is moving forward through the end of the bed, which causes an increase in purity of $CO_2$. Therefore, model results seem more reliable than experiments because of not reaching the steady state in the experiments; (c) next comparison is between E1 and E4, with the difference having half feed flow. Recovery of heavy product increases for both experiments and model because having less feed flow rates causes $CO_2$ to not breaking through from light end, so an increase in recovery. Purities for E1 and E4 are almost constant for both modeling and experimental result. From the Figure 4.11, since $CO_2$ front at the end of HR step for the modeling results are the same for experiment 1 and 4, purity stays almost constant.

Therefore, the model behind DAPS was validated and will now be used to simulate a variety of PSA cycles and process conditions for removal and concentrating $CO_2$ during closed-loop human space exploration missions.

### 4.7. Conclusion

The practical feasibility of carbon dioxide separation and recovery from $N_2$-$CO_2$ mixtures was demonstrated by means of a new PSA cycle by using an in-house process simulator and experimentally by using 4-bed PSA experimental set-up. Thereafter, model validation has been done with DAPS, in house simulator. A 3-bed 8-step PSA system was configured and utilized to study concentration and separation of $CO_2$ from $N_2$ (0.4% $CO_2$, 99.6% $N_2$) using Zeolite 13X as adsorbent. PSA Cycle included feed (F), idle (I), heavy reflux (HR), co-current equalization depressurization (Eq), co-current depressurization (CoD), counter-current depressurization (CnD), light reflux (LR), counter-current equalization pressurization (Eq*) and Light Product Pressurization (LPP) steps. Based on initial modeling and experimental efforts, a 3-bed PSA system was developed for metabolic $CO_2$ removal from spacecraft cabin air. Initial simulation runs with the new PSA cycle were able to produce carbon dioxide with purities more than 97% and recoveries more than 90%. Those initial simulation results show that added LR time, X, has important role in $CO_2$ concentration in HP, however, vacuum pressures for the flows needed are prohibitive. Some experiments have been done with 4-bed PSA experimental set up with the help of initial simulation runs. Flow and pressures adjusted to smaller beds while maintaining PSA schedule and throughput. Experimental results pointed that process only recovers around 50% $CO_2$ at original model throughputs but higher LR pressures while recovery of $CO_2$ is around 80 % at half of the original model throughputs. On the other hand it is quite

significant that the system is able to enrich $CO_2$ from 0.4 to around 90%. Model validation has been done via running simulations with no adjustable parameters against experimental results. The Model was adjusted to match the experimental pressures by changing $C_v$s of valves of pressure changing steps. Results show excellent match between modeling and experiments without any fitting parameters (kinetic and thermodynamic) and for a wide range of concentrations (0.4-90.0% $CO_2$). As an overall conclusion, large enrichments (>90%) of $CO_2$ from 0.4% can be achieved via adequate PSA Schedule and this process has to be designed in two stages with first stage focusing on 100% recovery of $CO_2$ to achieve NASA objectives. Overall, results indicate that objectives cannot be achieved in one stage and that future focus should be given toward the complete recovery of $CO_2$ with more modest enrichments (60-80%) from stage one, with a subsequent stage 2 to reach the desired performances.

**Table 4.1** PSA bed, adsorbent, equilibrium and kinetic properties for initial simulation runs.

| | |
|---|---|
| **Bed characteristics** | |
| Bed radius ($r_i$), m | 0.1143 (4.5in) |
| Bed length (L), m | 0.3048 (12in) |
| Bed porosity ($\varepsilon_b$) | 0.3403 |
| Bulk density, kg/m$^3$ | 725.7 |
| Wall density, kg/m$^3$ | 8000 |
| Wall thickness, m | 0.006 |
| Heat transfer coefficient ($h_w$), kW/m$^2$.K | 0.01 |
| Heat of adsorption of $CO_2$, $N_2$ ($\Delta H_i$), kJ/mol | 39.57, 19.54 |
| **Adsorbent characteristics** | |
| Adsorbent | 13X Zeolite |
| Pellet radius ($r_p$), m | 0.0015 |
| Pellet density ($\rho_p$), kg/m$^3$ | 1100 |
| Pellet porosity ($\varepsilon_p$) | 0.45 |
| Pellet heat capacity ($Cp_p$), kJ/kg.K | 1.1 |
| **Process characterictics** | |
| Feed mole fraction for $CO_2$, $N_2$ ($yi^F$) | 0.004, 0.996 |
| Feed temperature ($T^F$), K | 294.25 |
| Outside wall temperature ($T_o$), K | 294.25 |
| High pressure ($P_H$), kPa | 101.325 |
| Feed Flow ($F^F$), SLPM | 570 |
| Throughput (L(STP)/kg/h) | 1264 |
| Cycle time ($t_{cycle}$), s | See Table 4.2 |
| Low pressure ($P_L$), kPa | See Table 4.2 |
| Light Reflux Ratio (LRR) | See Table 4.2 |
| CoD pressure ($P_{CoD}$), kPa | See Table 4.2 |
| Light Reflux Pressure ($P_{LR}$), kPa | See Table 4.2 |

**Table 4.2** Conditions and performances in terms of $CO_2$ purity and recovery of 3-Bed 8-Step PSA process for initial simulations using the cycle depicted below.

| Bed1 | FEED | | | |
|---|---|---|---|---|
| Bed2 | HR | | E | CoD |
| Bed3 | CnD | LR | E* | LPP |
| Step time (s) | $t_{s,1}$: $t_{CnD}$ | $t_{s,2}$: 425 + x - $t_{CnD}$ | $t_{s,3}$: 25 | $t_{s,4}$: 50 |

| Conditions | | | | | | | | | HP | |
|---|---|---|---|---|---|---|---|---|---|---|
| **Run** | **x** | **Cycle** | **$t_{CnD}$** | **LRR** | **$P_{CnD}$** | **$P_{LR}$** | **$P_{CoD}$** | **Feed** | $CO_2$ | $CO_2$ |
| **1** | *0* | *1500* | 50 | 0.1 | 2.0 | 2.0 | 7.0 | 570 | 81.7 | 89.5 |
| **5** | *200* | *2100* | 50 | 0.1 | 2.0 | 2.0 | 7.0 | 570 | 87.8 | 91.7 |
| **9** | *500* | *3000* | 50 | 0.1 | 2.0 | 2.0 | 7.0 | 570 | 92.5 | 92.7 |
| **13** | *900* | *4200* | 50 | 0.1 | 2.0 | 2.0 | 7.0 | 570 | 95.9 | 90.9 |
| **17** | 1300 | 5400 | 50 | 0.1 | 2.0 | 2.0 | 7.0 | 570 | 97.8 | 87.6 |
| **18*** | 1300 | **5400** | ***100*** | **0.1** | **2.0** | **2.0** | **7.0** | **570** | **97.3** | **88.6** |
| **19** | 1300 | 5400 | 50 | 0.1 | *5.0* | *5.0* | *10.0* | 570 | 98.2 | 65.0 |
| **20** | 1300 | 5400 | *100* | *0.05* | *1.0* | *4.0* | *6.0* | 570 | 93.7 | 63.7 |
| **21** | 1300 | 5400 | *200* | *0.05* | *0.5* | *4.0* | *6.0* | 570 | 91.9 | 61.8 |
| **22** | 1300 | 5400 | 50 | *0.05* | *1.0* | *4.0* | *6.0* | 570 | 94.7 | 62.7 |
| **23** | 1300 | 5400 | *150* | *0.05* | *1.0* | *4.0* | *6.0* | 570 | 93.3 | 62.4 |
| **24** | 1300 | 5400 | 50 | 0.1 | *1.0* | *7.0* | *6.0* | 570 | 95.7 | 66.3 |
| **25** | 1300 | 5400 | *100* | 0.1 | *1.0* | *7.0* | *6.0* | 570 | 94.4 | 66.8 |
| **26** | 1300 | 5400 | 50 | *0.05* | *1.0* | *4.0* | 7.0 | 570 | 93.4 | 63.8 |
| **27** | 1300 | 5400 | 50 | 0.1 | *1.0* | *7.0* | 7.0 | 570 | 94.5 | 66.8 |
| **28** | 1300 | 5400 | 100 | 0.1 | *1.0* | *4.0* | 6.0 | 285 | 90.5 | 97.2 |

*: Values in bold correspond to base case for experiments.

**Table 4.3** Bed, adsorbent properties for the experiments and model validation.

| **Bed characteristics** | |
|---|---|
| Bed radius ($r_i$), m | 0.0254 (1in) |
| Bed length (L), m | 0.502 (19.75in) |
| Bed porosity ($\varepsilon_b$) | 0.425 |
| Bulk density, $kg/m^3$ | See Table 4.1 |
| Wall density, $kg/m^3$ | See Table 4.1 |
| Wall thickness, m | See Table 4.1 |
| Heat transfer coefficient ($h_w$), $kW/m^2.K$ | See Table 4.1 |
| Heat of adsorption of $CO_2$, $N_2$, ($\Delta H_i$), kJ/mol | See Table 4.1 |
| **Adsorbent characteristics** | |
| See Table 4.1 | |

**Table 4.4** PSA process conditions for the experiments and model validation.

| | $y_{CO2}{}^{F}$ | $P_H$ **[kPa]** | $\mathbf{T^F}$ **[°C]** | **x** **[s]** | $\mathbf{t_{cycle}}$ **[s]** | $F^F$ **[SLPM]** | $\mathbf{t_{CnD}}$ **[s]** | $\mathbf{P_{CoD}}$ **[kPa]** | $\mathbf{P_{CnD}}$ **[kPa]** | $\mathbf{P_{LR}}$ **[kPa]** | **LRR** |
|---|---|---|---|---|---|---|---|---|---|---|---|
| **E1** | 0.04 | 101.325 | 18.1 | 1300 | 5400 | 40.4 | 100 | 3.72 | 2.25 | 4.70 | 0.05 |
| **E2** | 0.04 | 101.325 | 18.9 | 1300 | 5400 | 40.4 | 200 | 5.32 | 1.06 | 4.65 | 0.05 |
| **E3** | 0.04 | 101.325 | 19.4 | 1600 | 6300 | 40.4 | 250 | 5.08 | 0.85 | 4.75 | 0.05 |
| **E4** | 0.04 | 101.325 | 18.8 | 1300 | 5400 | 20.2 | 100 | 3.95 | 2.20 | 4.62 | 0.10 |

**Table 4.5** Summary of PSA Process Performance. Experiments (E1-4).

| | Conditions | | | | | | | | | Performance | | |
|---|---|---|---|---|---|---|---|---|---|---|---|---|
| | | | | | | | | | | HP | | LP |
| | $t_{cycle}$ [s] | Flow [SLPM] | x [s] | $t_{CnD}$ [s] | $t_{HR/LR}$ [s] | $P_{CoD}$ [kPa] | $P_{CnD}$ [kPa] | $P_{LR}$ [kPa] | LRR | $YCO_2$ [%] | $ReCO_2$ [%] | $ReN_2$ [%] |
| **E1** | 5400 | 40.4 | 1300 | 100 | 1625 | 3.72 | 2.25 | 4.70 | 0.05 | 90.2 | 42.9 | 99.95 |
| **E2** | 5400 | 40.4 | 1300 | 200 | 1525 | 5.32 | 1.06 | 4.65 | 0.05 | 96.6 | 52.4 | 99.94 |
| **E3** | 6300 | 40.4 | 1600 | 250 | 1725 | 5.08 | 0.85 | 4.75 | 0.05 | 95.8 | 50.6 | 99.94 |
| **E4** | 5400 | 20.2 | 1300 | 100 | 1625 | 3.95 | 2.20 | 4.62 | 0.10 | 90.8 | 81.9 | 99.90 |

**Table 4.6** Comparison of experiment and model PSA process performances

| | Conditions | | | | | | | | HP | | | | LP | |
|---|---|---|---|---|---|---|---|---|---|---|---|---|---|---|
| | | | | | | | | | **Y**$CO_2$ [%] | | **Re**$CO_2$ [%] | | **Re**$N_2$ [%] | |
| | $t_{cycle}$ [s] | Flow [SLPM] | $t_{CnD}$ [s] | $t_{HR/LR}$ [s] | $P_{CoD}$ [kPa] | $P_{CnD}$ [kPa] | $P_{LR}$ [kPa] | LRR | Exp | M | Exp | M | Exp | M |
| **1** | 5400 | 40.4 | 100 | 1625 | 3.72 | 2.25 | 4.70 | 0.05 | 90.2 | 98.9 | 42.9 | 39.8 | 99.95 | 100.0 |
| **2** | 5400 | 40.4 | 200 | 1525 | 5.32 | 1.06 | 4.65 | 0.05 | 96.6 | 93.5 | 52.4 | 51.3 | 99.94 | 99.99 |
| **3** | 6300 | 40.4 | 250 | 1725 | 5.08 | 0.85 | 4.75 | 0.05 | 95.8 | 94.0 | 50.6 | 49.8 | 99.94 | 99.98 |
| **4** | 5400 | 20.2 | 100 | 1625 | 3.95 | 2.20 | 4.62 | 0.10 | 90.8 | 98.6 | 81.9 | 75.2 | 99.90 | 100.0 |

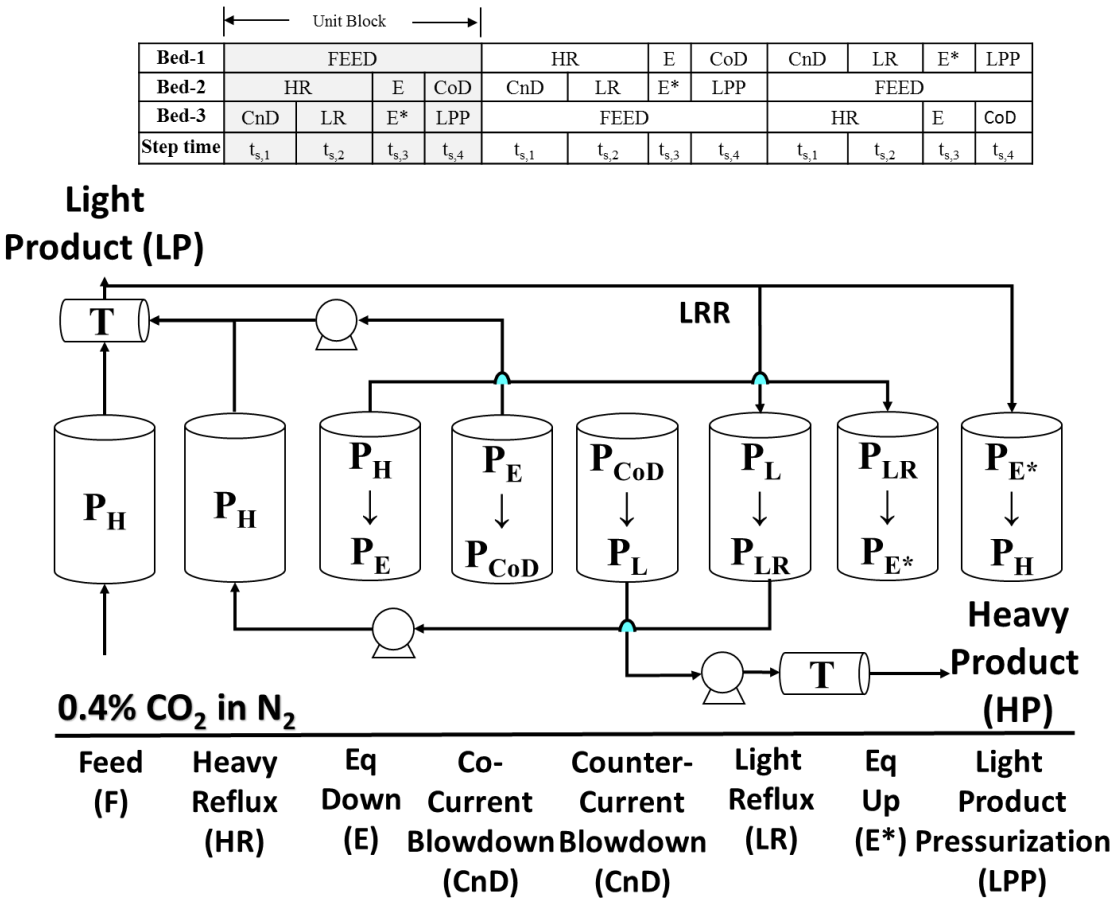


**Figure 4.1** Cycle sequence of initial simulations: 3-Bed 8-Step PSA Cycle.

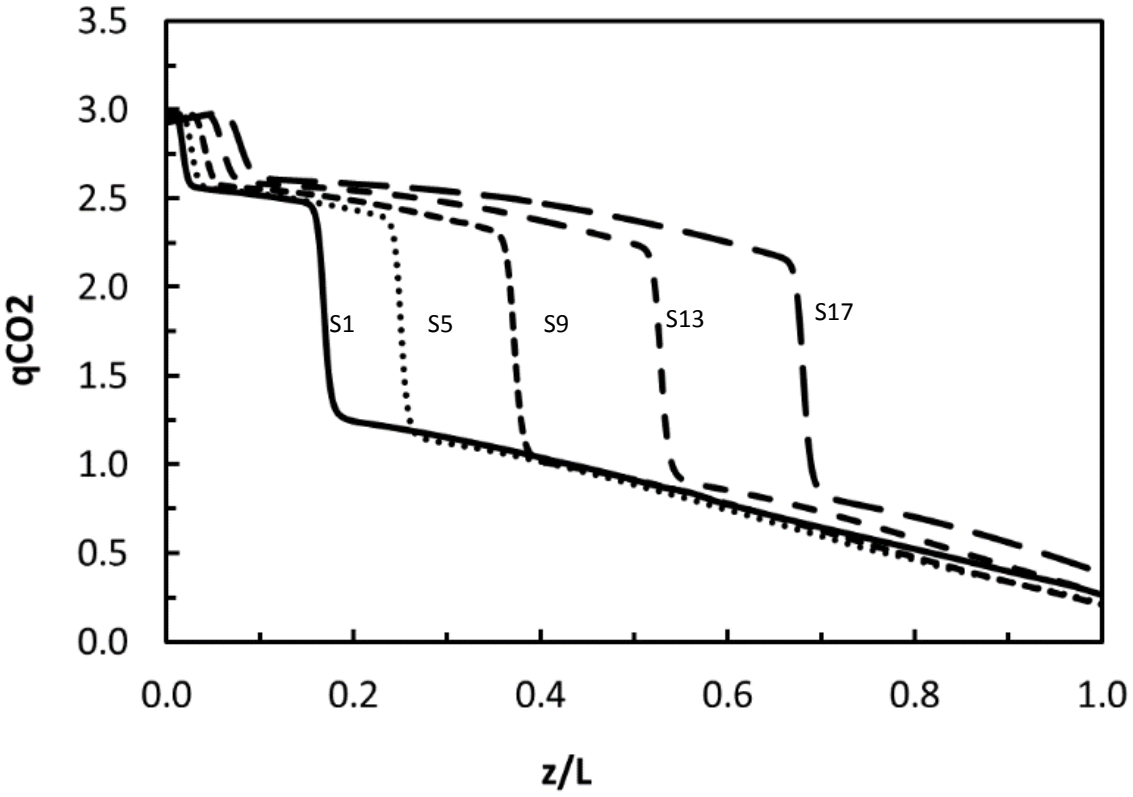


**Figure 4.2** Bed profiles at end of HR step for different x times

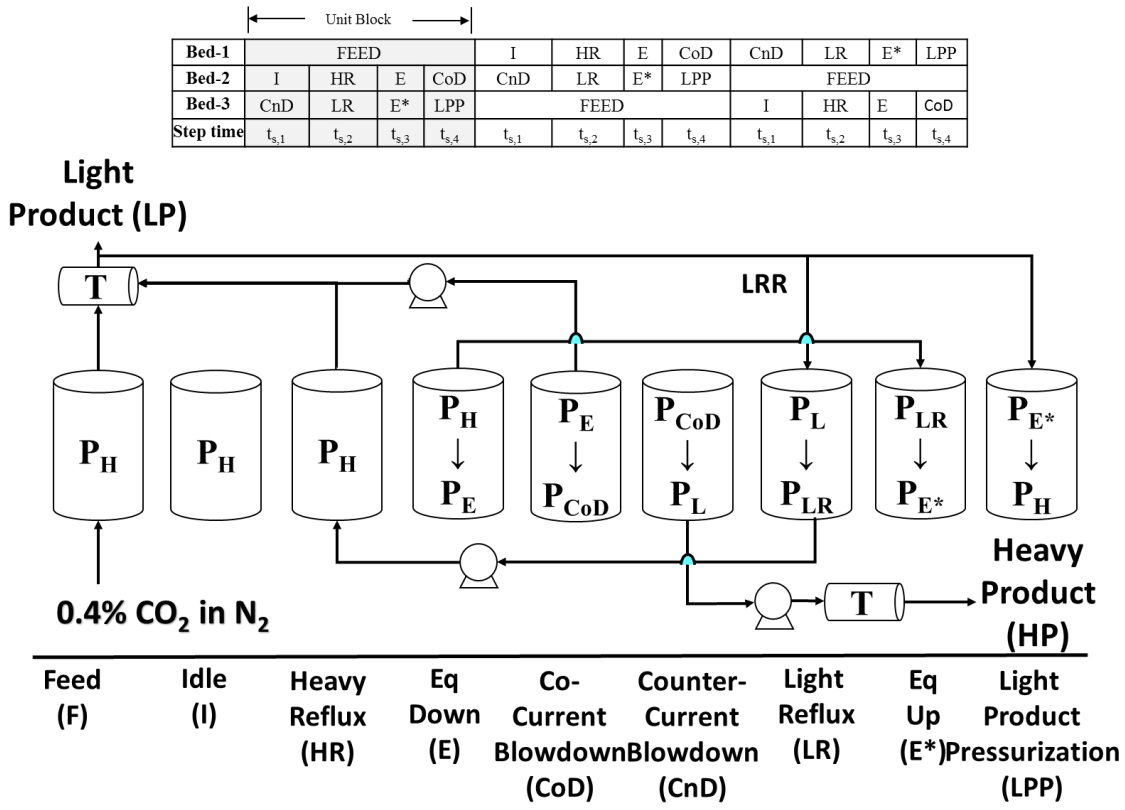


**Figure 4.3** Cycle sequence for the experiments and model validation: 3-Bed 9-Step PSA Cycle.

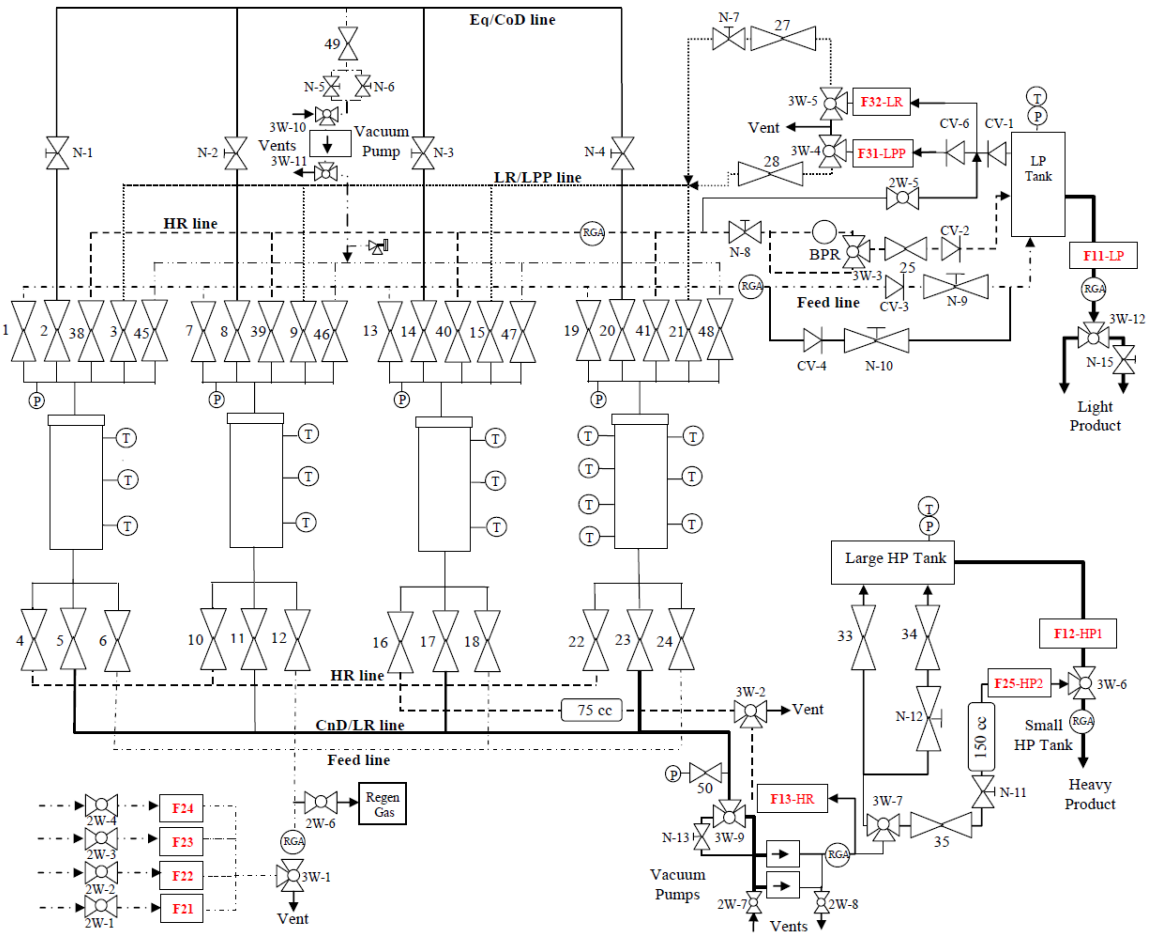


**Figure 4.4** Schematic diagram of the 4-Bed PSA system, showing all the valves, mass flow controllers and mass flow meters, pressure-vacuum pump, heavy product tank and light product tank.

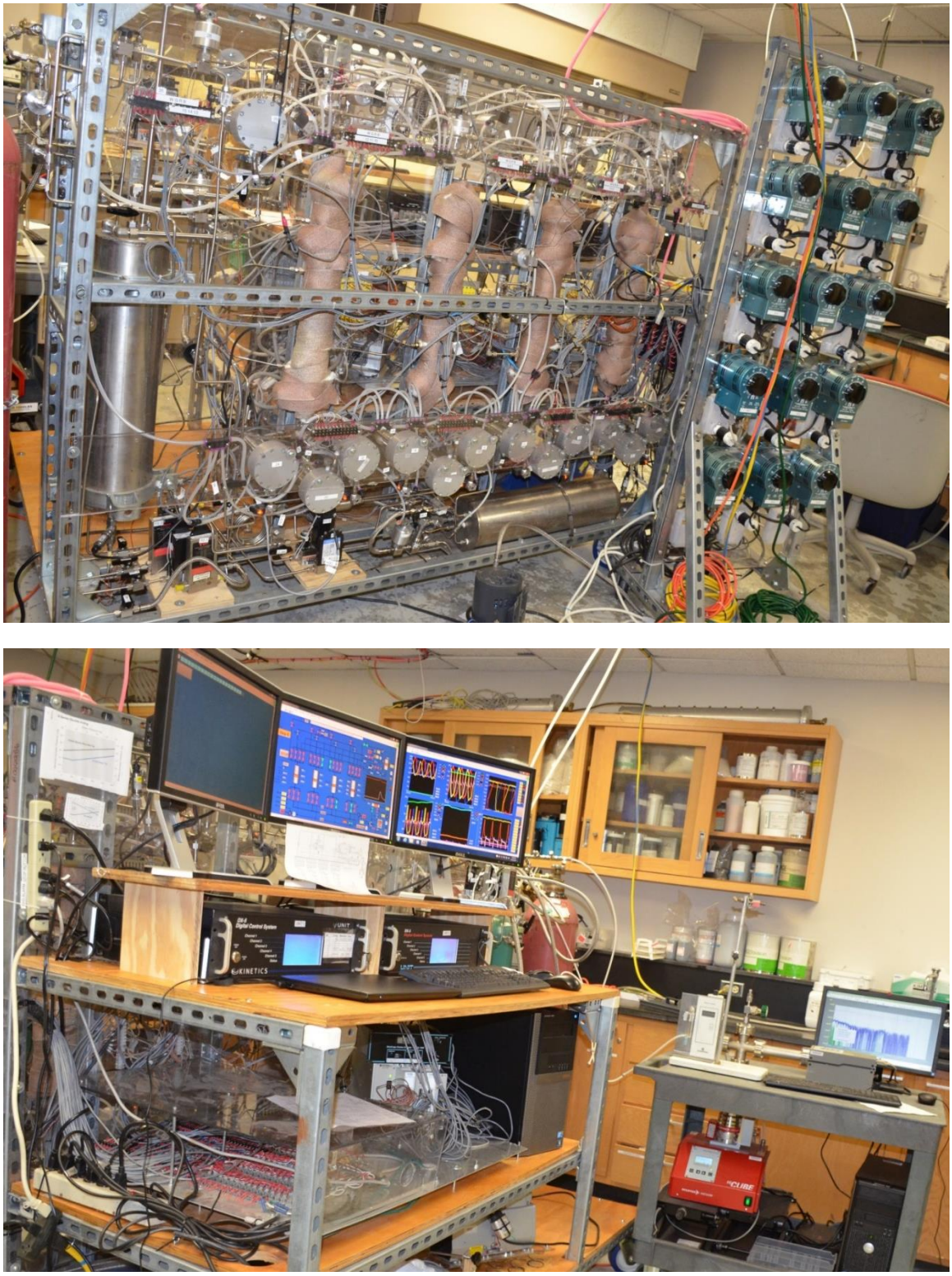

**Figure 4.5** Back and front views of 4-Bed PSA system.

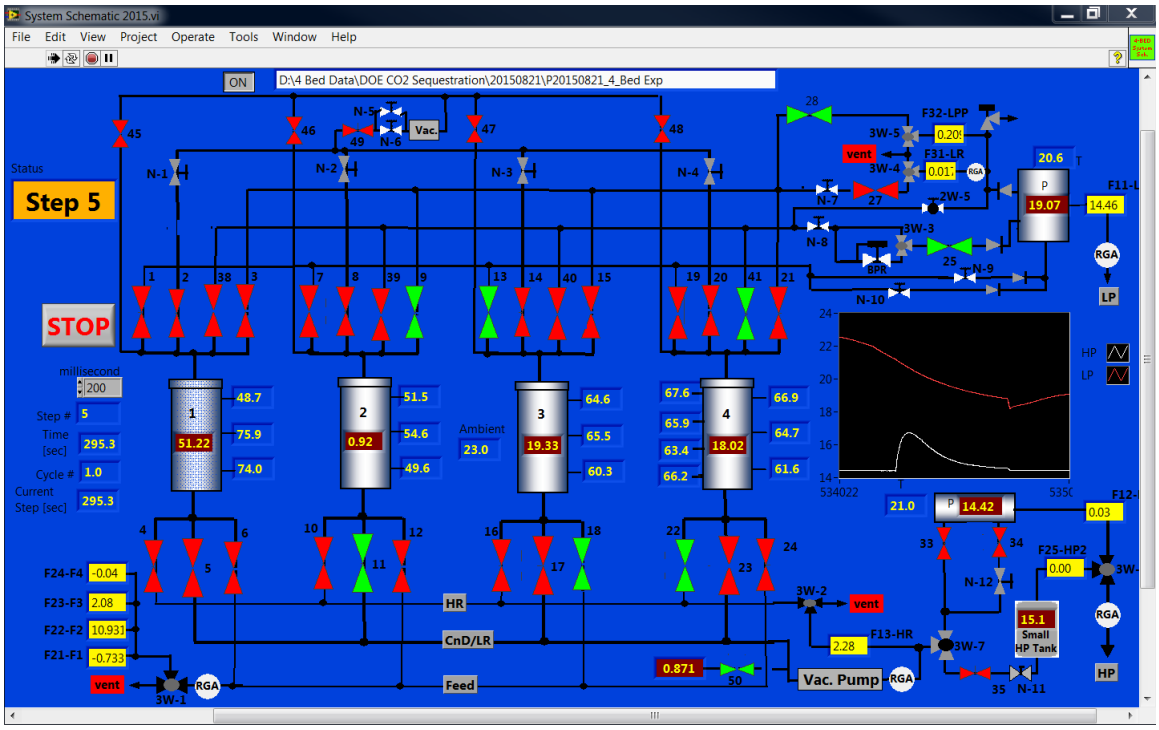


**Figure 4.6**.Front Panel of LabVIEW Program

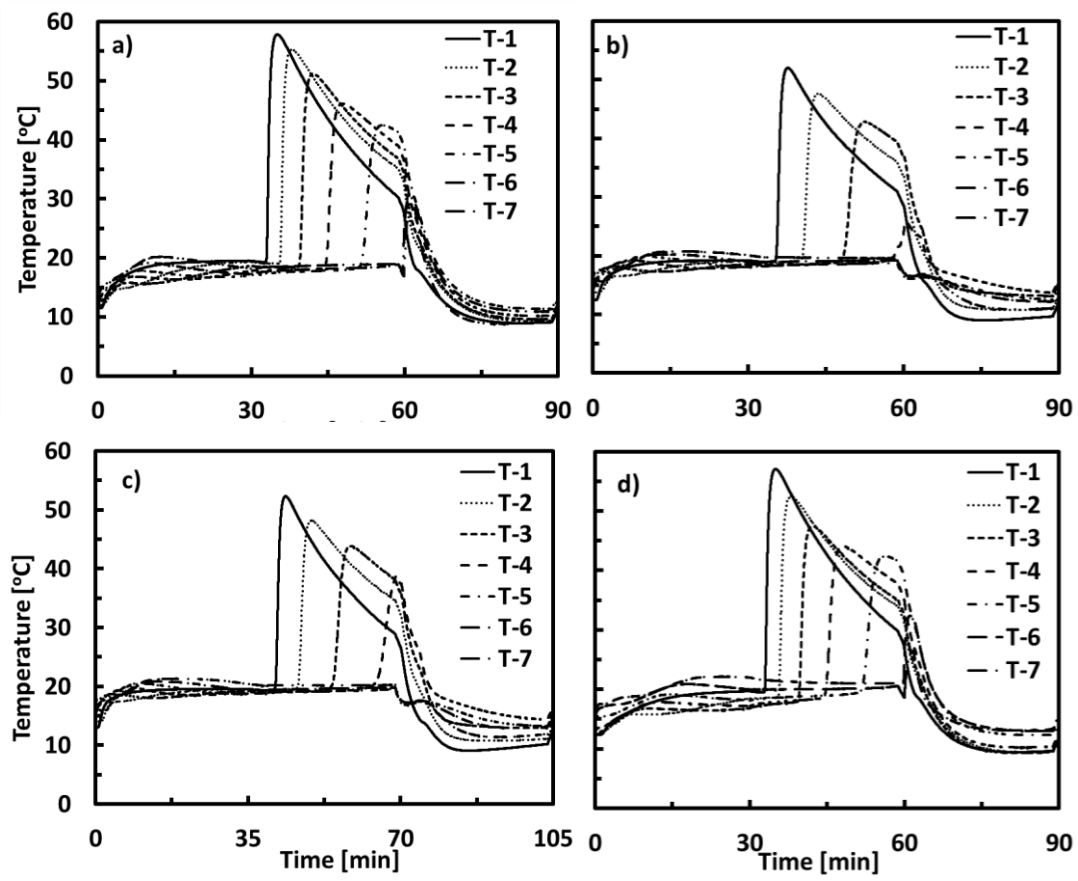


**Figure 4.7** Temperature history of one bed for the E1-4 (a-d, recpectively) during one entire cycle. T1-7 (10.12%, 22.78%, 35.44%, 48.10%, 60.75%, 73.41%, 86.07%) are locations of thermocouples from feed end.

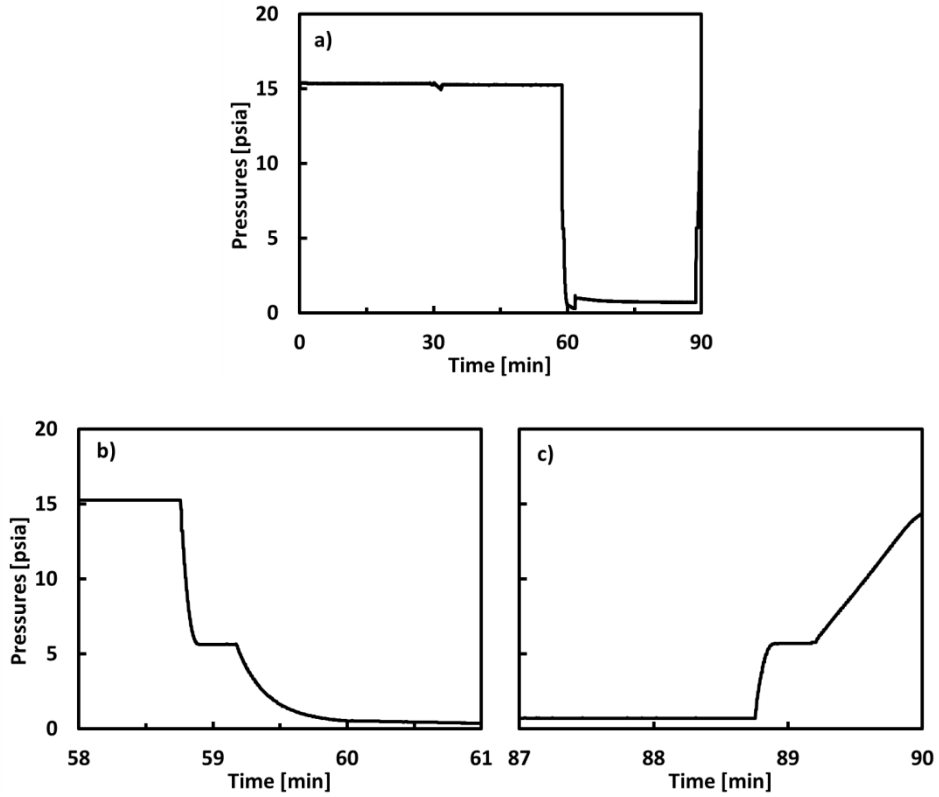


**Figure 4.8** Pressure history during one entire cycle for E4 (a) and a zoomed-in view of pressure when equalization down, CoD, CnD steps (b) and light reflux, equalization up and light product pressurization steps (c) occur.

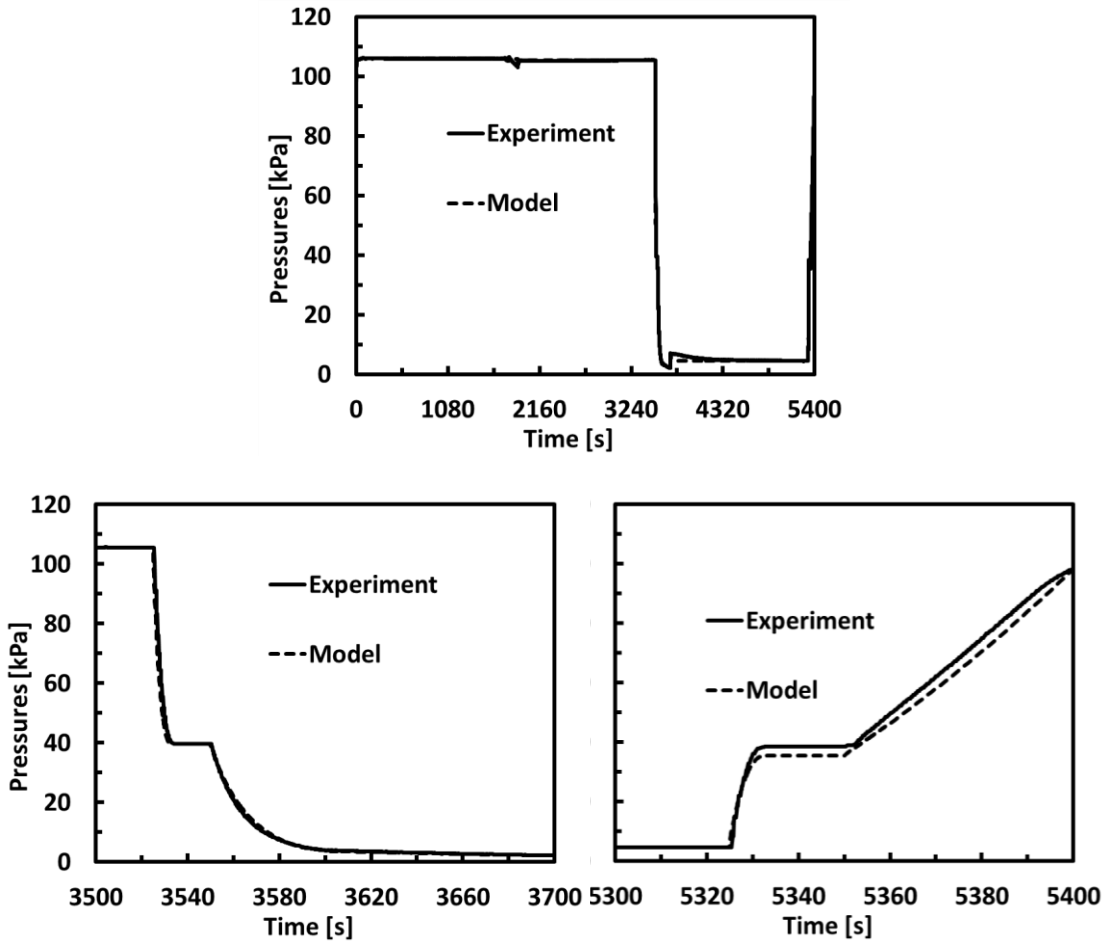


**Figure 4.9** Pressure history during one bed with one-third of entire cycle (Top) and zoomed-in view of pressure during Eq down, CoD and CnD steps (left) and zoomed-in view during Eq up and LPP steps (right) for E4&M4.

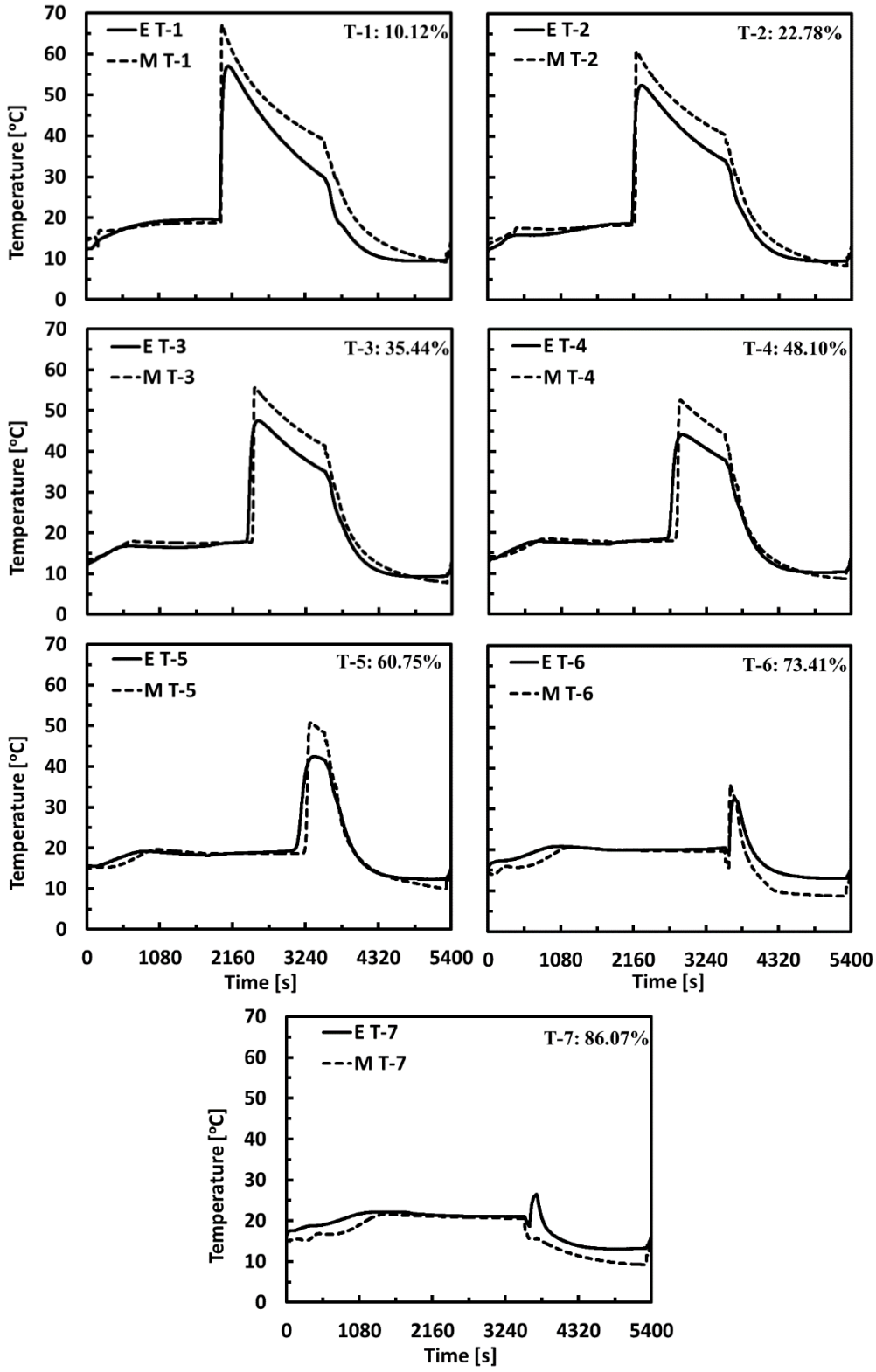


**Figure 4.10** Comparison of temperature histories of experiment 4, E, (solid) and model 4, M (dashed). T1-7 (10.12%, 22.78%, 35.44%, 48.10%, 60.75%, 73.41%, and 86.07% from T1 through T-7, respectively) are locations of thermocouples from feed end.

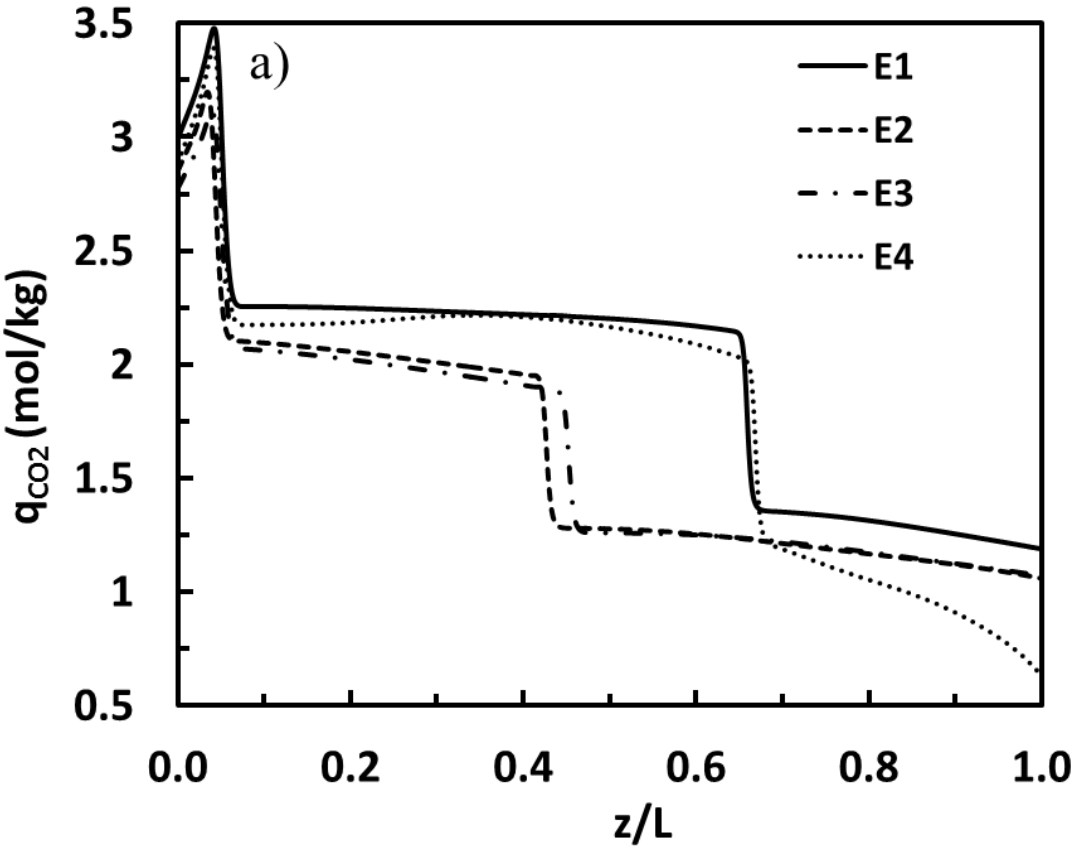


**Figure 4.11** Bed profiles at end of HR step of modelling results for E1-4.

# CHAPTER 5

# TWO-STAGE PSA SYSTEM FOR $CO_2$ REMOVAL DURING CLOSED-LOOP HUMAN SPACE EXPLORATION MISSIONS

## 5.1 Summary

A novel two-stage pressure swing adsorption (PSA) system has been developed to remove metabolic $CO_2$ removal from the spacecraft cabin air of the International Space Station (ISS). This PSA system enriches and recovers the $CO_2$ to make it suitable for use in a Sabatier reactor ($CO_2$ reduction). This two-stage PSA process utilizes Stage 1 to concentrate metabolic $CO_2$ from about 0.2667 vol% to about 40 to 60 vol% and Stage 2 to further enrich the $CO_2$ product from Stage 1 up to > 97 vol% $CO_2$, while recovering at least 95% of it, which corresponds to removing 4.0 kg/day of $CO_2$. Each stage of this PSA system utilizes a combination of equalization, cocurrent depressurization, heavy and light reflux cycle steps to facilitate significant heavy component enrichment and recovery (i.e., $CO_2$) from a dilute feed stream. The first generation of this two-stage PSA process utilizes beaded commercial adsorbent, i.e., 13X zeolite, in both stages. These two PSA systems were designed via simulation using the Dynamic Adsorption Process Simulator (DAPS). The DAPS results were validated using an experimental multi-bed PSA system. DAPS was then used to scale up Stage 1 and scale down stage 2 to size the full scale two-stage PSA system that might someday be used on the ISS. The modeling results from

Stage 1 revealed that longer heavy and light reflux step times played an important role in concentrating the $CO_2$ in the heavy product and modeling results from Stage 2 showed that a heavy reflux step was essential to achieving the desired performance. Implications from these modeling and experimental results began to hint at the possibility of significantly concentrating $CO_2$ from ambient air up to around 10 to 15 vol% at relatively high recovery using a simple PSA cycle.

The objectives of Stage 1 PSA system are to demonstrate a novel Stage 1 PSA process that utilizes with aforementioned objectives via DAPS and to do a parametric study to reach the desired performances with minimal loss on $N_2$ and utilizing less power for vacuum. In addition to Stage 1 PSA system objectives, the objectives of Stage 2 PSA system are to determine PSA cycle schedules that satisfactorily meet desired requirements for Stage 2 (aforementioned above) with minimal losses of $N_2$, via simulations, and to demonstrate experimentally a selected PSA from preliminary study using 4 bed PSA system, and to validate the model against the experimental results from the 4 bed system with no adjustable parameters.

## 5.2. 1st Stage PSA System for $CO_2$ Removal During Closed-Loop Human Space Exploration Missions

The main objective of the sub chapter is to demonstrate a novel Stage 1 PSA process that utilizes with modified objectives, the complete recovery of $CO_2$ with more modest enrichments (60-80%) from 0.2667 vol. % $CO_2$ concentration in feed stream, via DAPS, and do parametric study to reach the desired performances with minimal loss on $N_2$ and utilizing less power for vacuum. Since the new goal is to have better recoveries with modest

purities, the PSA schedule coming from Chapter 3 has been adjusted to recover more $CO_2$ with less purities by adding production light reflux step.

### 5.2.1 1st Stage PSA Cycle Description

A typical PSA process involves a cyclic process where a number of interconnected vessels containing adsorbent/adsorbents undergo successive pressurization and depressurization steps in order to produce a continuous stream of purified product.

The steps of the 1st stage PSA cycle include feed (F), idle (I), heavy reflux (HR), equalization down (E), co-current depressurization (CoD), counter-current depressurization (CnD), light reflux (LR), equalization up (E*) and light reflux pressurization (LPP). The operation of 3-bed 10-step PSA cycle is described in Figure 5.1 along with the cycle sequence. Each row in the cycle sequence represents all the different cycle steps a given bed undergoes over the entire cycle, whereas each column represents which cycle step is being run by which bed at a particular $t_s$. The sequence of operation is developed by following a simple methodology called graphical approach (Mehrotra et al., 2011). The unit block shown in the Figure 5.1 by a shaded area consists of five ($t_{s,1}$, $t_{s,2}$, $t_{s,3}$, $t_{s,4}$ and $t_{s,5}$) unit step times where all steps are being run by one of the three beds and the total cycle time is composed of multiple consecutive unit blocks where the operations are repeated again and again. Therefore, the cycle shown in Figure 5.1 with the unit block is used to perform the parametric study for stage one.

The operation of first unit block, bed 1 is fed from bottom at atmospheric pressure for a period equivalent to the sum of all unit step times ($t_{s,1}$, $t_{s,2}$, $t_{s,3}$, $t_{s,4}$ and $t_{s,5}$). The reason of covering all the unit step times by feed (F) step during the operation of bed 1 is to

maintain a continuous feed flow throughout the cycle. During this operation, the preferentially adsorbed species (in this case $CO_2$) is captured by the adsorbent in the bed and a product stream is collected from the top of bed 1.

Next, bed 2 undergoes an idle (I) step for a period of $t_{s,1}$ and $t_{s,2}$ where valves at both ends of the bed is physically closed so that no gas can come in or go out of the bed. The reason of having an idle step in a cycle sequence is to maintain the alignment of coupled steps. During $t_{s,3}$, the bed undergoes a heavy reflux (HR) step which is ringed with heavy gas providing from another bed undergoing light reflux (LR2) step. Heavy reflux (HR) step is operated in this case at atmospheric pressure like feed step. The purpose of having HR step in the sequence is to enhance the loading of heavy component in the column. It is important to mention that a compressor is necessary to provide feed to HR step by pulling gas from LR2 step. During $t_{s,4}$, bed 2 undergoes a co-current equalization depressurization (E) step where it is co-currently blown down to another intermediate pressure to provide gas from its light end to another bed undergoing equalization pressurization (E*) step. Finally, bed 2 is co-currently blown down (CoD) to another intermediate pressure for a period of $t_{s,5}$. The rate of CoD is controlled by a valve coefficient ($Cv_{CoD}$) in order to reduce the loss of adsorbent material due to attrition.

Finally, bed 3 is in counter-current blow down (CnD) step during $t_{s,1}$, which bed 3 is depressurized counter-currently to a low pressure and the pressure at the end of this step is controlled by a valve coefficient ($Cv_{CnD}$). During CnD, heavy gas is collected as product from the bottom of bed. Next during $t_{s,2}$, the bed undergoes light reflux (LR1) step. In this step, the bed is fed from light end with a portion of the light gas (LRR1) coming from another bed undergoing feed (F) step. The pressure at the end of this step is controlled by

a valve coefficient ($Cv_{LR}$) associated with the step. During LR1, heavy gas is collected as product from the bottom of bed. Another light reflux (LR2) step fed from light end with a portion of the light gas (LRR2) is occurring during $t_{s,3}$. The entire heavy product collected during LR2 step is sent back to HR step. The purpose of having LR step in the sequence is to regenerate the bed. Then during $t_{s,4}$, the bed is equalized with another bed from the light end to bring the pressure up to an intermediate level. This equalization pressurization (E*) step helps to reduce operating cost as well to improve PSA performance. Finally during $t_{s,5}$, the bed is re-pressurized to atmospheric pressure using the light gas from the light end of the bed undergoing feed step. After this phase same operation is repeated to complete the overall cycle.

Simulations for 1st stage, which is 3-bed 10-step PSA cycle, were carried out using a FORTRAN based in house dynamic adsorption process simulator (DAPS).

Finally, the performance of a PSA process is calculated in terms of purity, recovery (or kg produced $CO_2$/day). In this study, these are defined are follows:

$$Throughput\left[\frac{L(STP)}{kg.h}\right] = \frac{Fresh\ total\ Feed(SLPM)\ in\ Feed\ step*60}{Mass\ of\ adsorbent(kg) in\ all\ beds} \quad (5\text{-}1)$$

$$Purity[\%] = \frac{CO_2(mol) obtained\ as\ product\ during\ CnD\ and\ LR1 steps}{total\ Product(mol) obtained\ during\ CnD\ and\ LR1\ steps} * 100 \quad (5\text{-}2)$$

$$Recovery[\%] = \frac{CO_2(mol) obtained\ as\ product\ during\ CnD\ step}{Fresh\ CO_2(mol) fed\ in\ Feed\ step} \times 100 \quad (5\text{-}3)$$

$$CO_2\ removal\left[\frac{kg}{day}\right] = CO_2\ fed\left[\frac{kg}{day}\right] * Re_{CO_2} \quad (5\text{-}4)$$

In addition to recovery and purity, energy which is an indicator of the operation cost of the process was calculated by following equations for a given step:

$$E[J] = \sum_i^s \int_{t=0}^{t_{step}} \left(\frac{\gamma}{\gamma-1}\right) RT \left[\left(\frac{P_H}{P(t)}\right)^{\frac{\gamma-1}{\gamma}} - 1\right] \frac{1}{\eta} m_{step}(t)dt \quad (5\text{-}5)$$

$$m_{step}(t)\left[mol/_s\right] = \frac{P_{step}(t)\ 1000\ v_{step}(t)\ A\ \varepsilon_b}{R\ T(t)} \quad (5\text{-}6)$$

$$P[W] = \frac{E[J]}{t_{cycle}/_{number\ of\ bed}} \quad (5\text{-}7)$$

In the cycles studied for Stage 1, the energy consuming steps are CnD, production light reflux step (LR1), and light reflux step (LR2), and CoD steps and the value of $P_H$ is 101.325 kPa.

Cumulative $CO_2$ gas phase concentration equation, given in below, has been used to explain the $CO_2$ breaking through during the particular step.

$$\overline{y_{CO_2,cum}} = \frac{\int_0^{t_{step}} y_{CO_2}(t).v(t).C_T(t)dt}{\int_0^{t_{step}} v(t).C_T(t).dt}, C_T(t) = \frac{P_{step}(t)*1000}{RT_{step}(t)} \quad (5\text{-}8)$$

### 5.2.2. Bed and Adsorbent Characteristics for Stage 1

An overview of the bed and adsorbent characteristics for stage 1, feed gas concentrations used as input parameters in the simulations and process characteristics are summarized in Table 5.1. The feed stream for stage 1 contains 0.2667vol % $CO_2$ with 79.0 vol % $N_2$, balance with $O_2$. Commercial 13X zeolite beads were used as the adsorbent. Equilibrium adsorption isotherm parameters for $CO_2$ and $N_2$ and $O_2$ were obtained by fitting Triple Process Langmuir (TPL) isotherm to experimental data obtained and the fitted equilibrium parameters are summarized in Chapter 2 with heat of adsorption values for all gases used in this study. The mass transfer coefficients for $CO_2$, $N_2$ and $O_2$ were obtained

experimentally from the single bed rapid PSA apparatus and macropore mass transfer parameters are summarized in Chapter 2.

### 5.2.3. Parametric Study

A detailed parametric study for Stage 2 via running simulations is conducted in order to investigate the effects of various process parameters on process performance indicators such as purity and recovery. The parameters studied include HR/LR/F step time, thus cycle time, light reflux ratio (LRR) or light reflux flows for LR1 and LR2 steps, counter-current depressurization pressure ($P_{CnD}$), light reflux pressure ($P_{LR1\&2}$), and production light reflux step (LR1) time ($t_{s,2}$). The ranges of all the parameters during the parametric study are summarized in Table 5.2.

### 5.2.4 Result and Discussion for Stage 1 PSA System

A parametric study was conducted to evaluate the effects of various parameters on the cyclic steady state PSA performance. The conditions of 1$^{st}$ stage simulations, S1-15, have been run in this study were given in Table 5.2 with cycle sequence. In the 1$^{st}$ stage simulations, base case in the Table 5.2 comes from the previous Chapter. The varied conditions of 1$^{st}$ stage simulations include HR/LR/F step time (thus cycle time), different light reflux ratios (LRR), thus LR flows, counter-current depressurization pressure ($P_{CnD}$), light reflux pressure ($P_{LR\&2}$), and production light reflux (LR1) step time, while keeping counter-current depressurization step time ($t_{s,\ 1}$ = $t_{CnD}$ = 200s) and co-current depressurization pressurization pressure ($P_{CoD}$ = 10kPa) constant in the parametric study as can be seen from Table 5.2. Stage 1 PSA process performance with required power results from DAPS was given in Table 5.3. Three Pfeiffer vacuum pumps have been used

in the Stage 1. The performance curve for Pfeiffer vacuum pump model ACP 40 has been shown in Figure 5.2. The LR operating pressures for Stage 1 are 4 and 5 kPa for parametric study, can be seen from Table 5.2. This particular pump can handle maximum 65slpm and 55slpm at 4kPa and 5kPa respectively, calculated from the vacuum pump performance figure.

The overall process performance was judged in terms of the purity and recovery of $CO_2$ in the heavy product and the required energies. The $CO_2$ purity was defined as the average mole fraction of $CO_2$ in the heavy product, Equation 5-2. $CO_2$ recovery was defined as the moles of $CO_2$ in the heavy product divided by the moles of $CO_2$ fed to the process cumulatively during the feed, Equation 5-3, with $CO_2$ removal equation, Equation 5-4. Another process performance, required energy which is an indicator of the operation cost of the process was calculated by Equations from 5-5 to 5-7.

#### 5.2.4.1 Effect of HR/LR/F step time, (thus cycle time)

To study this effect the parameters that being held constant are production light reflux (LR1) flow rate (15.5slpm), light reflux (LR2) flow rate (55.0slpm), counter-current blow down pressure (0.5kPa), light reflux (LR1&2) pressures (5kPa), and co-current blow down pressure (10kPa), production light reflux time (50s), and counter-current depressurization step time (200s) as shown in Table 5.2. The values for $t_{s,3}$ are given in Table 5.2; 1475s, 1575s, 1675s, 1975s, 2475s, and 3475s. The pressures for other steps are 101.325kPa at the end of feed, heavy reflux and light product pressurization steps, between 43 and 45kPa at the end of equalizations steps as shown in Table 7.

In a typical PSA process, cycle time determines the length of operation of a particular step in a fixed cycle schedule. As increasing the cycle time increases proportionally the length of associated cycle steps for a fixed cycle schedule; HR/LR steps as well as feed step in this paper. Results shown in Figure 5.3-a) indicate that the purity of heavy product increases with increasing $t_{s,3}$. Longer cycle time helps to increase the length of corresponding step proportionally, the longer duration forces more $CO_2$ to adsorb by the adsorbent at a certain temperature and pressure. In other words, the bed gets saturated higher with $CO_2$ at the end of HR step as shown in Figure 5.4, which shows bed profiles at the end of HR step for each run at periodic steady state. From Figure 5.4, it can be easily seen that the front is moving through the end of bed by increasing $t_{s,3}$. Hence, the purity shows an increasing trend with increasing $t_{s,3}$.

On the other hand, recovery of $CO_2$ increases up to $t_{s,3}$ = 1975s then stays almost constant for $t_{s,3}$ = 2475s, and then decreases by increasing $t_{s,3}$ as shown in Figure 5.3-a). In a typical PSA cycle, recovery of heavy product decreases by increasing cycle time. It is important to notice that feed step time, heavy reflux step time and light reflux step time, thus cycle time have been changed at the same time by changing $t_{s,3}$ value in Table 5.2. A likely explanation for the observed trend is that the depth of penetration of mass transfer zone of $CO_2$ into the bed increases with the increase of cycle time which in turn enhances the loss of $CO_2$ in the light end. To understand which particular step is causing an increase in heavy product recovery, $CO_2$ losses from light end for each step (Feed, HR, CoD, LR, and LPP) can be seen from Figure 5.5, which shows relative $CO_2$ losses versus $t_{s,3}$ for aforementioned steps. In Figure 5.5, a relative loss of $CO_2$ in HR step is increasing by increasing $t_{s,3}$. A basic explanation for this increase is that the bed is saturated with more

$CO_2$, which can be seen from (Figure 5.4) that causes $CO_2$ to break through from light end. Therefore, $CO_2$ loss increases by increasing $t_{s,\,3}$. $CO_2$ loss during CoD step decreases slightly by increasing $t_{s,\,3}$ (Figure 5.5). CoD step time for these runs is not changing so the amount of $CO_2$ leaving the bed at the end of CoD step does not have a big change, but the amount of $CO_2$ into the bed during feed step is increasing by increasing $t_{s,\,3}$. Therefore, $CO_2$ loss during CoD decreases by increasing $t_{s,\,3}$. These two steps do not have the same trend that $CO_2$ recovery has, so these steps are not the main reason of the king in $CO_2$ recovery. The other steps that cause the loss of $CO_2$ from light end are feed, LR, and LPP. Since some portion of light product from feed end goes to light reflux and light product pressurization steps, the combination of these steps needs to be count to investigate $CO_2$ losses in light end as shown in Figure 5.5. In this combination step, $CO_2$ losses decrease at the beginning of increased $t_{s,\,3}$, then increase as well as $CO_2$ recovery increases first then decreases by increased $t_{s,\,3}$, so it can be said that the main reason for the trend that $CO_2$ recovery has is feed steps. To better understanding, cumulative $CO_2$ gas phase concentration ($\bar{y}CO_{2,\,cum}$), given in Equation (5-8), from the beginning to the end of feed step needs to be investigated deeply for the runs base and S1-5 as shown in Figure 5.6. It can be seen from Figure 5.6 that $\bar{y}CO_{2,\,cum}$ at the end of feed step is decreasing when $t_{s,\,3}$ values are increasing up to 2475s, compare to $t_{s,\,3}$ is 1475s (base case), which causes an increase in $CO_2$ recovery that means that the bed gets better saturated with $CO_2$ in the feed step by increasing $t_{s,\,3}$. For $t_{s,\,3}$ = 2475s, $\bar{y}CO_{2,\,cum}$ is decreasing slightly or almost the same compare to base case, so $CO_2$ recovery stays almost constant. For $t_{s,\,3}$ = 3475s, $\bar{y}CO_{2,\,cum}$ starts increasing compare to $t_{s,\,3}$ = 2475s, 1975s, 1675s and 1575s, which causes a decrease in $CO_2$ recovery that means that $CO_2$ starts breaking through during the feed steps and the

bed loses some of the $CO_2$ from light end during that specific run, which is S5. It is important to notice that $\bar{y}CO_{2,\,cum}$ for $t_{s,\,3}$ = 3475s is still lower that the value for base case, so the $CO_2$ recovery for $t_{s,\,3}$ = 3475s is still higher than the one $t_{s,\,3}$ = 1475s. Therefore, the recovery of $CO_2$ increases up tu run number S3, and stays almost constant for S4, then it decreases for further increased $t_{s,\,3}$ (S5). To explain the main reason that $CO_2$ starts breaking through for further increased $t_{s,\,3}$, during the feed step the time ratios of feed step and light reflux step for all four $t_{s,\,3}$ values have an essential role. The time ratios of these two steps are increasing by increasing $t_{s,\,3}$, 0.82, 0.83, 0.84, 0.86, 0.88 and 0.91 for base and S1 through 5, respectively. It can be said that during the light reflux step, the bed is regenerated as much as like a clean bed for particular $t_{s,\,3}$, S4, but further increase of $t_{s,\,3}$, run number 5, the bed has the maximum regeneration level that already achieved at the previous $t_{s,\,3}$ value while still increasing time for both light reflux and feed steps. That situation leads $CO_2$ to breaking through during feed step.

The total energy for run numbers base and S1-5 is increasing by increasing $t_{s,\,3}$ as can be seen from Figure 5.3-b). This figure shows the effect of $t_{s,\,3}$ in total required energy, which is summation of required energies of CnD, CoD, and LR1&2 in this work. The main time portion of the cycle from energy consumption steps is light reflux 2 step, LR2. Time fractions of LR2 to total cycle are increasing by increased $t_{s,\,3}$. Since the pump pulls gases which are coming from LR in 5kPa to HR in 101.325kPa for longer time, more energy is needed with the increasing time fraction of LR. Therefore, total required energy increases by increasing $t_{s,\,3}$.

### 5.2.4.2. Effect of production Light Reflux (LR1) step flow rate

Figure 5.7 summarizes the net results for $CO_2$ recovery and purity in heavy product and energies as a function of production light reflux step flow rate ($F_{LR1}$). The parameters that are held constant during the simulation include $t_{s,3}$ (1475s), counter-current blow down pressure (0.5kPa), light reflux (LR1&2) pressures (5kPa), feed flow rate (627 slpm), and co-current blow down pressure (10kPa), production light reflux time (50s), light reflux step flow rate (55slpm) and counter-current depressurization step time (200s) as shown in Table 5.2. The pressures for those runs are 101.325kPa at the end of feed, heavy reflux and light reflux pressurization steps, around 45kPa at the end of equalizations steps. The production light reflux step flow rate values for this parametric study are 15.5, 17.5, and 20slpm; corresponding runs are base, S6, and S7 in Table 5.2.

Figure 5.7-a) shows that purity of $CO_2$ decreases while recovery of $CO_2$ stays almost constant with increasing production light reflux step flow rate. The $CO_2$ front at the end of the heavy reflux step is the same for all three runs (base, S6, S7) as can be seen from Figure 5.8; that means that the bed is having same adsorbed amount of $CO_2$ for all cases. However, production light reflux step flow rate is increasing from base case to S7. That means that the pump is pulling more light-product gases to reach the same lower pressure for all cases during this production step. These light products dilute the heavy product. Therefore, purity of heavy product decreases by increasing production light reflux step flow rate. On the other hand, the main reason that heavy product recovery stays almost constant is because of heaving the same $CO_2$ front at the end of the heavy reflux step. In other words, the bed has the same amount of $CO_2$ for all three runs, so the same amount of

$CO_2$ is coming out of the bed in this production step; which causes having similar heavy product recoveries for these runs.

Figure 5.7-b) shows the effect of production light reflux step flow rate ($F_{LR1}$) in total required energy. The total energy for the corresponding runs (base, 6, 7) is increasing only around 1 watt (almost constant) by increasing production light reflux step flow rate. Total energy means in this work is required energies for CoD, CnD, and LR1&2 to increase the stream pressure from the pressure at the end of these steps to atmospheric pressure. The amount of gases leaving the bed during the LR1 step is increasing by increasing production light reflux step flow rate. That causes the pump to pull more gases, which need more energy. However, the time portion of this particular step to total cycle is too small, total required energy stays almost constant by increasing production light reflux step flow rate.

#### 5.2.4.3. Effect of LR2 step flow rate

Figure 5.9 summarizes the net results for $CO_2$ recovery and purity in heavy product and energies as a function of light reflux 2 step flow rate ($F_{LR2}$). The parameters that are held constant during the simulation include $t_{s,\ 3}$ (1475s), counter-current blow down pressure (0.5kPa), light reflux (LR1&2) pressures (5kPa), feed flow rate (627 slpm), and co-current blow down pressure (10kPa), production light reflux time (50s) and flow rate (15.5slpm), and counter-current depressurization step time (200s) as shown in Table 5.2. The pressures for those runs are 101.325kPa at the end of feed, heavy reflux and light reflux pressurization steps, around 45kPa at the end of equalizations steps. The light reflux 2 step flow rate values for this parametric study are 55, 58, 62, and 65slpm; corresponding runs are base, S8-10 in Table 5.2.

Figure 5.9-a) shows that purity of $CO_2$ increases slight while recovery of $CO_2$ increases dramatically (compare to purity) by increasing light reflux 2 step flow rate ($F_{LR2}$). As HR and LR steps are coupled together, any increase in the number of moles produced from LR step will increase the partial pressure of $CO_2$ during the constant total pressure operation of HR step. This increased partial pressure of $CO_2$ causes the higher saturated bed with $CO_2$ in HR step, so the front is moving to the end of bed during HR step, as can be seen from Figure 5.10, by increasing light reflux 2 step flow rate. Operating the light reflux step with higher flow rate of light product regenerated the adsorbent better but might be diluted the heavy product. That might be the reason of having a slight increase in purity of heavy product compare to recovery. The other reason of increasing recovery of heavy product by increasing light reflux ratio is having more regenerated bed during HR step; less $CO_2$ is leaving the bed at the end of HR step by increasing light reflux 2 step flow rate. The capacity of the bed has been used more with increasing light reflux ratio. Therefore, recovery of $CO_2$ increases by increasing light reflux 2 step flow rate.

Figure 5.9-b) shows the effect of light reflux 2 step flow rate in total required energy. The total energy for the corresponding runs (base, S8-10) is increasing by increasing light reflux 2 step flow rate. Total energy means in this work is required energies for CoD, CnD, and LRR to increase the stream pressure from the pressure at the end of these steps to atmospheric pressure. The amount of gases leaving the bed during the LR step is increasing by increasing light reflux ratio, because the bed is going to end up at the same lower pressures for all cases. That causes the pump to pull more gases to reach the same lower pressures for all cases by increasing light reflux 2 step flow rate, which need more energy. Therefore, total energy increases by increasing light reflux 2 step flow rate.

### 5.2.4.4. Effect of production LR step time ($t_{s,2}$)

Figure 5.11 summarizes the net results for $CO_2$ recovery and purity in heavy product and energies as a function of production light reflux step time ($t_{s,2}$). The parameters that are held constant during the simulation include $t_{s,3}$ (1475s), counter-current blow down pressure (0.5kPa), light reflux (LR1&2) pressures (5kPa), feed flow rate (627 slpm), and co-current blow down pressure (10kPa), light reflux step flow rate (55slpm) and counter-current depressurization step time (200s) as shown in Table 5.2. The pressures for those runs are 101.325kPa at the end of feed, heavy reflux and light reflux pressurization steps, around 45kPa at the end of equalizations steps. The production light reflux step time values for this parametric study are 50, 75, and 100s; corresponding runs are base, S11, and S12 in Table 5.2.

Figure 5.7-a) shows that purity of $CO_2$ decreases while recovery of $CO_2$ stays almost constant with increasing production light reflux step time ($t_{s,2}$). The $CO_2$ front at the end of the heavy reflux step is the same for all three runs (base, S11, S12) as can be seen from Figure 5.12; that means that the bed is having same adsorbed amount of $CO_2$ for all cases. However, production light reflux step time is increasing from base case to S12. That means that the pump is pulling light-product gases for longer time to reach the same lower pressure for all cases during this production step. These light products dilute the heavy product. Therefore, purity of heavy product decreases by increasing production light reflux step flow rate. On the other hand, the main reason that heavy product recovery stays almost constant is because of heaving the same $CO_2$ front at the end of the heavy reflux step. In other words, the bed has the same amount of $CO_2$ for all three runs, so the same

amount of $CO_2$ is coming out of the bed in this production step; which causes having similar heavy product recoveries for these runs.

Figure 5.11-b) shows the effect of production light reflux step time ($t_{s,\,2}$) in total required energy. The total energy for the corresponding runs (base, 11, 12) is increasing only around 4 watt by increasing production light reflux step time. Total energy indicates required energies for CoD, CnD, and LR1&2 to increase the stream pressure from the pressure at the end of these steps to atmospheric pressure. The pump needs to pull gases for longer time during production light reflux step; this situation causes an increase of required energy. However, the time portion of this particular step to total cycle is too small even if it increases for those runs, total required energy increases slightly by increasing production light reflux step time ($t_{s,\,2}$).

#### 5.2.4.5. Effect of Counter-Current Depressurization Pressure ($P_{CnD}$)

Figure 5.13 shows the effect of counter-current desorption pressure ($P_{CnD}$) on cyclic steady state performance for the PSA cycle. To study the effect of $P_{CnD}$, the simulations were performed at a constant HR/LR sime, $t_{s,\,3}$ (1475s), light reflux (LR1&2) pressures (5kPa), feed flow rate (627 slpm), and co-current blow down pressure (10kPa), light reflux step flow rate (55slpm) and counter-current depressurization step time (200s), and production light reflux time (50s) as shown in Table 5.2. The only parameter that is changed was $P_{CnD}$ (0.5, 0.2, 0.1kPa); corresponding runs are base, S13, and S14, respectively. The other pressures for those runs are 101.325kPa at the end of feed, heavy reflux and light reflux pressurization steps, around 45kPa at the end of equalizations steps.

In general, the desorption pressure enhances the working capacity of the bed for a fixed high pressure. The valve coefficient during CnD step in adjusted in such a way that the final pressure at the end of step reaches a desired low pressure. It can be seen from Figure 5.13-a) purity of $CO_2$ stays constant with the decrease of desorption pressure for a particular cycle time. The observed behavior in Figure 5.13-a) for $CO_2$ purity can be described with the help of Figure 5.14, which shows the bed profiles at the end of heavy reflux step. In the figure, the $CO_2$ front is moving backward by decreasing low pressure, which causes decrease in purity of $CO_2$. The pump is pulling more light-product gases to reach the lower pressure at the end of the CnD step; that dilutes the heavy product stream with light products. On the other hand, recovery of $CO_2$ increases by decreasing CnD final pressure. To decrease the low pressure, more $CO_2$ is leaving the bed as a heavy product, which leads an increase on heavy product ($CO_2$) recovery.

The total energy for runs (base, S13, and S14) increases by decreasing CnD final pressure as can be seen from Figure 5.13-b). This figure shows the effect of $P_{CoD}$ in total required energy, which is the summation of required energies for CnD, CoD, and LR1&2 steps in this work. Required energy for CnD step is increasing by decreasing CnD final pressure because the pumps needs to pull more gases to get the lower pressures at the end of CnD step. Therefore, total required energy increases by decreasing counter-current desorption pressure ($P_{CnD}$).

#### 5.2.4.6. Effect of Light Reflux Pressures ($P_{LR1\&2}$)

Figure 5.15 summarizes the net results for $CO_2$ recovery and purity in heavy product and energies as a function of light reflux pressures ($P_{LR1\&2}$). The parameters that

are held constant during the simulation include HR/LR sime, $t_{s,3}$ (1475s), counter-current blow down pressure (0.5kPa), feed flow rate (627 slpm), co-current blow down pressure (10kPa), light reflux step flow rate (55slpm) and counter-current depressurization step time (200s), and production light reflux time (50s) as shown in Table 5.2. The only parameter that is changed was $P_{LR}$ (5, 4kPa); corresponding simulations are base and S15, respectively. The other pressures for those runs are 101.325kPa at the end of feed, heavy reflux and light reflux pressurization steps, around 45kPa at the end of equalizations steps.

From Figure 5.15-a), purity of heavy product ($CO_2$) increases slightly (almost constant) while recovery of heavy product ($CO_2$) increases dramatically by decreasing the pressure at the end of the light reflux steps (LR1&2). Low pressure for light reflux step means more regenerated bed with light product gases. Since heavy reflux step is being fed from light reflux-2 step product stream that causes moving the $CO_2$ front to the end of bed during heavy reflux step (Figure 5.16). That means that the bed is being used more than with high $P_{LR}$ case which causes an increase in purity and recovery of $CO_2$. The reason of having a slight increase in purity of heavy product might be diluted the heavy product stream with light products ($N_2$, $O_2$) to reach lower pressures.

Figure 5.15-b) shows the effect of $P_{LR}$ in total required energy. The total energy for the corresponding runs is increasing by decreasing LR pressure. The pump is pulling more gases to reach the low LR pressures during this step, so energy needed for LR increases by decreasing LR final pressure. Therefore, total energy increases by decreasing $P_{LR}$.

## 5.3. 2nd Stage PSA System for $CO_2$ Removal during Closed-Loop Human Space Exploration Missions

The main objectives of the sub chapter are to develop a Stage 2 PSA process that utilizes more than 4kg $CO_2$ removal / day (recoveries >95%) with purities are more than 97 vol. % and with minimal losses of $N_2$ from 40-60 vol. % $CO_2$ concentration in feed stream, and to demonstrate experimentally a selected PSA using 4 bed PSA system, and to validate the model against the experimental results from the 4 bed system with no adjustable parameters. As a starting point to develop a new PSA cycle for Stage 2, the available Sequal PSA cycle, which was used for air separation before by the author with smaller pellets and with micropore limited diffusion LDF approach, has been modified by adding heavy reflux (HR) step and converted to 4-bed system in order to experimentally demonstrate modified Sequal PSA process by using 4-bed PSA apparatus, which has bigger pellets with macropore limited diffusion LDF approach, to reach the desired performance, via simulations. A new 4-bed PSA cycle step sequence and schedule has been thus conceived and studied using DAPS. The preliminary DAPS results have been then used to determine the 4-bed experimental conditions. Three 4-bed experiments were carried out by using 4-bed PSA apparatus.

### 5.3.1 2nd Stage PSA Cycle Description

The steps of the 2nd stage PSA cycle include feed (F), equalization down (E1), heavy reflux (HR), equalization down (E2), counter-current depressurization (CnD), light reflux (LR), equalization up (E2*), equalization up (E1*) and light product pressurization (LPP). The operation of 4-bed 9-step PSA cycle is described in Figure 5.17 along with the

cycle sequence. The unit block shown in the Figure 5.17 by a shaded area consists of three ($t_{s,1}$, $t_{s,2}$, and $t_{s,3}$) unit step times. Therefore, the cycle shown in Figure 5.17 with the unit block is used to perform the parametric study for stage two.

The operation of first unit block, bed 1 is fed from bottom at atmospheric pressure for a period equivalent to the sum of all unit step times ($t_{s,1}$, $t_{s,2}$, and $t_{s,3}$). During feed step $CO_2$ is captured by the adsorbent in the bed and a product stream is collected from the top of bed 1. Next, bed 2 undergoes a co-current equalization depressurization (E) step for a period of $t_{s,1}$ where it is co-currently blown down to an intermediate pressure to provide gas from its light end. During $t_{s,2}$, the bed undergoes a heavy reflux (HR) step which is ringed with heavy gas providing from another bed undergoing light reflux (LR) step. Heavy reflux (HR) step is operated in this case at an intermediate pressure. During $t_{s,3}$, bed 2 undergoes a second co-current equalization depressurization (E) step where it is co-currently blown down to another intermediate pressure to provide gas from its light end. Bed 3 is in counter-current blow down (CnD) step during $t_{s,1}$, which bed 3 is depressurized counter-currently. During CnD, heavy gas is collected as product from the bottom of bed. Next during $t_{s,2}$, the bed undergoes light reflux (LR) step with a portion of the light gas (LRR). The entire heavy product collected during LR step is sent back to HR step. Then during $t_{s,3}$, the bed is equalized with another bed from the light end to bring the pressure up to an intermediate level (E2*). Finally, bed 4 is having equalization up step (E1*). Then during $t_{s,2}$ and $t_{s,3}$, the bed is re-pressurized to atmospheric pressure using the light gas from the light end of the bed undergoing feed step. After this phase same operation is repeated to complete the overall cycle.

In the current PSA cycle, the desired product is $CO_2$ which is the preferentially adsorbed species. Therefore, the performance of the process is evaluated on the basis of $CO_2$ recovery and $CO_2$ purity in the heavy product. Recovery of $CO_2$ is defined as the number of moles of $CO_2$ withdrawn as product during production step (CnD) divided by the number of moles of $CO_2$ fed to the PSA process during the feed step. On the other hand, $CO_2$ purity is defined as the mole fraction of $CO_2$ leaving the bed during the CnD step.

Simulations for 2$^{nd}$ stage (4-bed 9-step PSA cycles) were carried out using a FORTRAN based in house dynamic adsorption process simulator (DAPS).

Finally, the performance of a PSA process is again calculated in terms of purity, recovery (or kg produced $CO_2$/day) by using Equations 5-2 through 5-4 given in section 5.2.1.

In addition to recovery and purity, energy which is an indicator of the operation cost of the process was calculated by following equations 5-5 through 5-7 given in section 5.2.1. In the cycles studied for Stage 2, the energy consuming steps are CnD, LR, and HR steps (HR pressure in at intermediate pressure in that particular PSA cycle) the value of $P_H$ is 101.325 kPa.

### 5.3.2. Bed and Adsorbent Characteristics

An overview of the bed and adsorbent characteristics for stage 2 preliminary DAPS simulations, feed gas concentrations, and kinetic properties used as input parameters in the simulations and process characteristics are summarized in Table 5.4. The bed radius and length as well as the cycle time for stage 2 preliminary DAPS simulations have been chosen in such a way that $CO_2$ not breaking through. The feed flows and light reflux ratios (LRR)

for stage 2 preliminary DAPS simulations have been chosen with the idea that the $CO_2$ net flow into the feed step and the $N_2$ net flow into LR step were maintained the same. In addition to Stage 2 preliminary DAPS simulation the bed and adsorbent characteristics, an overview of the bed and adsorbent characteristics for stage 2 scale-up simulations, experiments and model validation, feed gas concentrations, equilibrium and kinetic properties used as input parameters in the simulations and process characteristics are summarized in Table 5.5. The feed stream for stage 2 consists of 40.0vol % $CO_2$ with 60.0 vol % $N_2$. Commercial 13X zeolite beads were used as the adsorbent. Equilibrium adsorption isotherm parameters for $CO_2$ and $N_2$ and $O_2$ were obtained by fitting Triple Process Langmuir (TPL) isotherm to experimental data obtained and the fitted equilibrium parameters are summarized in Chapter 2 with heat of adsorption values for all gases used in this study. The mass transfer coefficients for $CO_2$, $N_2$ and $O_2$ were obtained experimentally from the single bed rapid PSA apparatus and macropore mass transfer parameters are summarized in Chapter 2.

### 5.3.3. Experimental Section

A typical schematic diagram of the PSA experimental system used in this study is shown in Figure 4.4. The system is equipped with four adsorption beds (1, 2, 3 and 4), seven mass flow controllers (FC), F21, F22, F23, F24, F25, F31, F32 in Figure 4.4, three mass flow meters (FM), F11, F12, F13 in Figure 4.4, one light product tank, two heavy product tanks, eighteen thermocouples (nine connected with first three beds and seven with last bed, one with light product tank and one with large heavy product tank), seven pressure transducers (four of them are coupled with four beds and the remaining two are with light product tank and large heavy product tank, and one with vacuum pumps), vacuum pumps

and valves (1 to 50). In lower part of the columns, the line connected with the valves 6, 12, 18 and 24 is used to provide feed to the adsorption columns whereas the lines coupled with valves 5, 11, 17, 23 and valves 4, 10, 16, 22 are used as counter-current blow down/light reflux (CnD/LR) and heavy reflux (HR) lines, respectively. Similarly in the upper trend of the columns, the line incorporated with the valves 1, 7, 13 and 19 is used as the product line during feed step, the one coupled with the valves 38, 39, 40, 41, and 25 is for the product line during heavy reflux (HR) step and the line connected with the valves 3, 9, 15, 21 and 28 is used for light product pressurization (LPP) as well as light reflux (LR) steps. In addition, the current system has the facility to operate the PSA cycle by incorporating equalization (EQ) step which is accomplished by using the line connected with the valves 2, 8, 14 and 20, and finally the line with valve 49 in addition to the valves 2, 8, 14, 20 is used for co-current blow down (CoD).

The thermocouples used in the experimental set-up shown in Figure 4.4 are K-type thermocouples which are used to measure the centerline temperatures of the beds as well as the temperatures of the light and heavy product tanks. In each bed, a series of three thermocouples are distributed axially throughout the bed which shows the bed temperature profiles at one quarter, half way and three quarters into the bed from the feed end. In addition, a fifteenth thermocouple which is not shown in the schematic diagram is used to measure the ambient temperature. Also, a total of three heaters coupled with each adsorption bed provided the facility of heating the bed uniformly. The power input to all the heaters is controlled by using twelve variable autotransformers (range 0 to 120/140V, type 3PN1O1O). The signals from all the thermocouples are sent to the signal conditioner

as input to the computer which displays real time temperature as the system is running (Bhadra 2012).

The mass flow controllers and mass flow meters used in the system are supplied by Tylan General/Brooks/MKS which have the ability to measure and/or control the mass flow rates of the gas accurately and reliably. All the meters and controllers are digitally controlled by two DX-5 Digital Power Supply instruments from UNIT instruments, Inc and one Hasting Power Supply-Model 200. Each unit of this instrument from UNIT instruments, Inc has five individual channels (eight of them have been using) and Hasting Power Supply unit has two. Each mass flow controller channel controls and displays the set point and actual flow for the channel as a percentage of full scale units. All the seven pressure transducers used as pressure sensors are supplied by Omega Dyne Inc. The outputs from all the pressure transducers are converted to absolute pressures which are displayed on the screen of the computer. The valves used for the system are all from Swagelok which are opened or closed depending on the duration of each step of a cycle. Valves 1 through 26 are Swagelok® U series bellows-sealed valves which provide enhanced reliability, versatility, and safety with a secondary containment system that prevents leaks to atmosphere even if the primary seal fails. These valves have a very high operating temperature and pressure (343 0C and 2500 psig) and are operated on double actuation mode (opened and closed by air). On the other hand, the rest of the valves are operated on single actuation mode (opened by air but closed by spring) except the valves with handle which are metering valves. The pressure and temperature ratings of these valves are about 3220 psig and 65 $^{o}$C, respectively. It is worthwhile to note that all the instruments and

devices are controlled by a single CPU which is used to save the outputs from all the devices, if necessary (Bhadra 2012).

The system is designed in such a way that provides the facility to measure the feed (F), light product (LP) during feed, light product (LP) during heavy reflux, mixed light product (LP), heavy product (HP) and heavy reflux (HR) concentrations using a 6-port valve manufactured by Swagelok. This valve is connected to a residual gas analyzer (RGA), a small and usually rugged mass spectrometer, which is basically a vacuum instrument that operates near $10^{-6}$ mbar pressure. At high or atmospheric pressure, the aperture assembly of RGA is insufficient to reduce the pressure while maintaining the response time. In order to facilitate the sampling at this pressure, a pressure reduction device which is actually a capillary is coupled with the RGA. The length of the capillary is selected on a trial and error basis in order to maintain fast response time (Bhadra 2012). Back and front views of 4-Bed PSA apparatus are shown in Figure 4.5.

LabVIEW program controls the valves and recording pressures, temperatures, and flowrates from different locations of the PSA experimental system. Front Panel of LabVIEW Program is shown in Figure 4.6. MS Excel file is being used for input file in which user can define PSA step properties by deciding flowrates, timing, and on/off position of each valve (Bhadra 2012).

### 5.3.4. Result and Discussion

#### 5.3.4.1. Preliminary Study to Develop a PSA System for Stage 2

Firstly, it is important to indicate that enormous simulations with again extensive parametric study to reach the desired performances had been run before deciding the

conditions as well as the bed dimensions and especially the PSA cycle. Those simulations are not given in this thesis. A new 4-bed PSA cycle step sequence and schedule with two different feed flow rates and light reflux ratios to maintain the same the $CO_2$ net flow into the feed step and the $N_2$ net flow into LR step for both cases were conceived and studied using DAPS. They are referred to as Feed I and II. These 4-bed preliminary DAPS simulations were carried out based on to reach desired performances, which are more than 97 vol% $CO_2$ enrichment while recovering at least 95% of it, which corresponds to removing 4.0 kg/day of $CO_2$. The process performances for both Feed I and II are given in Table 5.6. The results in the table show very clearly that Feed II simulation resulted with both better purities and recoveries. Feed II simulation has ended up with 98.1 vol% $CO_2$ purity, and 96.1 % $CO_2$ recovery, which means 4.07 kg $CO_2$ removal / day. The corresponding Stage 2 bed size for preliminary study was 3.0 inches long and 2.0 inches in diameter (ID). It utilized a modest vacuum pressure of 5.0 kPa and intermediate heavy reflux pressure of 55kPa. From the preliminary study with smaller pellets, which means by using micropore limited linear driving force (LDF) approach, Feed II conditions selected for model validation through the 4-bed PSA apparatus.

#### 5.3.4.2. Scale-up the Selected PSA Cycle to 4-bed PSA Apparatus

Before start running the experiments by using the dimensions and properties of available 4-bed PSA apparatus for model validation, the feed flow rate coming from the preliminary simulation was scaled up to 4-bed PSA experimental set-up. The dimensions and properties of the 4-bed PSA experimental apparatus were given in Table 5.5. So, the feed flow rate was scaled up based on the ratio of the total mass of adsorbent per bed in each system. This increased the feed flow rate from 3.75 SLPM to 24.5 SLPM for a feed

containing the same $CO_2$ concentration with the Feed II simulation in feed stream; 40 vol% $CO_2$ (given in Table 5.7). Effect of scaled up feed flow rate and step times used in DAPS simulations and corresponding performances were given in Table 5.8. Four preliminary DAPS results with the scale-up flows are shown in Table 5.8 from S-1 to S-4. Since S-1 did not meet the desired performance because preliminary simulations with micropore limited LDF approach were based on high mass transfer 0.3 mm beads, the feed flow rate was decreased as shown for S-2 to S-4 because of losing $CO_2$, which is heavy product, from light end. However, the desired performance was still not attained at the end of S-4. Then, the step times ($t_{s,1}$, $t_{s,2}$, $t_{s,3}$) were increased by decreasing the total feed flow with the same ratio in order to reach the desired performance. So, the cycle step times of equalization down 1, E1, ($t_{s,1}$), heavy reflux , HR, ($t_{s,2}$), and equalization down 2, E2, ($t_{s,3}$) were changed from 10-20-10 s to 15-30-15 s, and then to 20-40-20 s. This change also changed the total cycle time. The results of four simulations using 15-30-15 s for the E1, HR and E2 cycle step times, and using 20-40-20 s for the E1, HR and E2 cycle step times are shown in Table 5.8. Decreasing feed flow rate as well as increasing cycle time helped to avoid from $CO_2$ (heavy product) breaking though from light end, which causes an increase in the heavy product ($CO_2$) recovery. As can be seen from S-1 to S-4 in Table 5.8, recovery increases by decreasing the feed flow rates because high flow rates at the same working pressures might cause high $CO_2$ saturation in the bed, which leads $CO_2$ to break through from light end. $CO_2$ purities for those cases are decreasing by decreasing feed flow rates because the bed is fully saturated with $CO_2$ for the case with higher flows, it is even losing some from light end, and so more $CO_2$ pure stream can be obtained during the production step with higher feed flows. Same explanation is valid for S-5 through S-8,

which has longer step times ($t_{s,1}$, $t_{s,2}$, $t_{s,3}$: 15-30-15s) than S-1 thought S-4, with lower feed flow rates. The combination of increase in step times as well as a decrease in feed flow rate work fine until S-10 in Table 5.8, after S-10 recovery starts decreasing. The most likely explanation for this behavior is that the feed flow rates and unequally step times are not enough for $CO_2$ to adsorb on the solid surface. That means that the bed does not have enough $CO_2$ in solid phase that can obtain as a heavy product, thus purity is also decreasing for those cases. Among those simulations, Only S-6 met the desired performance. Therefore, The S-6 process conditions have been chosen as a starting point to run the experiments in 4-bed PSA apparatus, but restricted by conditions defined by the unit.

#### 5.3.4.3. Experiments

Three experiments for the 2nd stage were conducted on the 4-bed PSA experimental set-up to reach the overall process performance, more than 4kg $CO_2$ produced/day with over 97% $CO_2$ purity, for closed-loop human space exploration missions.

##### 5.3.4.3.1. PSA Cycle Description for Experiments

PSA cycle steps used in the experiments consist of feed (F), idle (I), heavy reflux (HR), equalization down (E), co-current depressurization (CoD), counter-current depressurization (CnD), light reflux (LR), equalization up (E*) and light reflux pressurization (LPP). The operation of 4-bed 9-step PSA cycle is described in Figure 5.17 along with the cycle sequence. As shown in the figure, the cycle sequence is divided into 12 unequally unit step times of length. The flow schematic of the unit block depicted in gray in cyclic schedule is also described in the figure. The other four unit blocks are just the repetition of the same steps but with different sequence. Therefore, it is noteworthy to

describe the cyclic operation of the present cycle more specifically on the basis of the unit block. 4-bed 10-step PSA experiments have been done by using available in-house 4-bed PSA experimental set-up, shown in Figure 4.4.

The adsorption beds 1, 2, 3 and 4 are filled with Zeolite 13X adsorbent. Bed, adsorbent properties for the experiments and model validation were given in Table 5.5. The adsorbent was prepared for cycling by first regenerating with heating under continuous upward Helium flow (~ 0.1 SLPM) up to 350 $^{o}$C at 101.325kPa and the regenerated (i.e., dry) weight of the adsorbent was obtained from the regeneration data. The adsorbent beds were further regenerated in-situ, under vacuum and continuous Helium flow (~0.1 SLPM) by increasing the temperature around 350$^{o}$C via 8 band heaters connected around the beds prior to each experiment. At the end of regeneration period, the beds were cooled down to the room temperature. The feed gas mixture (0.4% $CO_2$ in $N_2$) has been obtained by using two mass flow controllers for $CO_2$ and $N_2$ separately. These feed stream gases are introduced to the upstream of bed 1 (z/L = 0) at high pressure ($P_H$) through opened valves 6 and 1 and is allowed to pass through for a duration of $t_{s,1}$ s (shown as $t_{CnD}$ in Figure 5.17) to have preferentially adsorbed species ($CO_2$) adsorbed and the high pressure product stream enriched with less strongly adsorbed species ($N_2$) leaves the column from the other end (z/L = 1.0) of the bed which is sent to the light product tank through needle valves N-9 and N-10. At this moment, with valves 10, 11, 12, 7, 39, 9, and 46 of bed 2, valves 22, 23, 24, 19, 41, 21, and 48 of bed 4 closed and the remaining valves 8 and 20 of beds 2 and 4 opened, the two beds are connected through their product ends to equalize pressure. In this case, beds 2 and 4 are at co-current equalization pressurization 1 (E1) and equalization depressurization 1 (E1*), respectively. This equalization pressurization step helps to save

energy because the gas, partially depleted of strongly adsorbed species from high pressure bed is used to pressurize the other bed at low pressure to an intermediate pressure. During this operation, $t_{s,1}$, beds 3 undergoes countercurrent blow down step. During this step, one end of the column is closed while the other is exposed to a vacuum pump. Valves 13, 14, 40, 15, 16 and 18 are kept closed and the bed is depressurized to a low pressure ($P_L$) through opened valve 17 and all the desorbed gas is sent to the heavy product tank. As a result of pressure decrease, $CO_2$ from the adsorbent gets desorbed and exits the bed. At the end of the operation in first unit step time of $t_{s,1}$ s, beds 1 undergoes feed step which is conducted according to the procedure described above for duration of next unit step time of $t_{s,2}$ s. During this operation time, $t_{s,2}$ s, bed 3 undergoes light reflux step (LR) by opening valve 17, 15, and 27 while valves 10, 12, 7, 8, 39, and 46 are kept closed. Bed 3, light reflux step operated at $P_{LR}$ to facilitate desorption of $CO_2$. This light reflux step helps to clean the bed from heavy product by sending light product gases; therefore, breaking through of heavy gases from light end can be prevented by the help of light reflux step. The $CO_2$ rich effluent from the light reflux purge step enters the heavy reflux step, which bed 2 undergoes to this HR step by opening valves 10, 8 and 49 (to use the vacuum pump to maintain the intermediate pressure that the bed has from equalization down 1 step). The intermediate pressure for HR step is adjusted by using manual needle valve. In heavy reflux (HR) step, the blow down gas emanating from this light reflux step is fed to the feed end of the column at intermediate pressure ($P_{HR}$) usually. The purpose of this step is to increase the loading of heavy component in the solid phase. Also, undesirable light gas present in the void space is flushed out of the bed as it is replaced with pure $CO_2$. These factors cumulatively help to increase the enrichment of heavy component during CnD step. During $t_{s,\ 2}$, bed 4

undergoes light product pressurization step by closing valves 22, 23, 24, 19, 20, 41 and 27 while opening valves 21 and 28. The purpose of incorporating light product pressurization (LPP) step is to push the concentration wave towards the feed end of the column thereby, enhancing the performance of the process. During the operation of the next unit step time of the unit block, $t_{s,3}$, bed 1 is at feed step and beds 2 and 3 are at second equalization step and bed 4 is again light product pressurization step. Continuous feed flow during entire PSA cycle has been achieved with this way. The operating procedure of feed step is the same to the procedure described above. With valves 10, 11, 12, 7, 39, 9, and 46 of bed 2, and valves 16, 17, 18, 13, 40, 15 of bed 3 closed and the remaining valves 8 and 14 of beds 2 and bed 3 opened, the two beds are connected through their product ends to equalize pressure. And bed 4 is at light product pressurization step with the same operating procedure for bed 4 shown above. In this case, beds 2 and 3 are at co-current equalization pressurization 2 (E2) and equalization depressurization 2 (E2*), respectively. This equalization pressurization step helps to save energy because the gas, partially depleted of strongly adsorbed species from high pressure bed is used to pressurize the other bed at low pressure to an intermediate pressure. Similarly, the consecutive operation in each bed of corresponding unit block for particular step is repeated until the periodic steady state is reached. With setting a 6-port valve, the transient as well as periodic steady state concentration profiles of light and heavy products can be monitored by using RGA. An in-house built LabView program and National Instruments data acquisition and control system were used to control valve operation, cycle sequencing, and mass flow controller and to monitor the temperature, pressure and flow rate profiles with time. The periodicity was verified by observing the steady temperature profiles of all thermocouples at different

locations of the bed as well as by monitoring the steady heavy and light product concentrations profiles by RGA.

#### 5.3.4.3.2. PSA Cycle Process Performance Indicators

Once the system was reached to periodic steady state for a particular set of operating conditions, all the temperature, pressure, flow rate, heavy product and light product profiles were captured to evaluate the periodic state performance indicators. The process performance indicators for the PSA process were evaluated on the basis of enrichment, recovery and throughput. The overall process performance was judged in terms of the purity and recovery of $CO_2$ in the heavy product and $N_2$ in the light product. The $CO_2$ purity was defined as the average mole fraction of $CO_2$ in the heavy product, and $CO_2$ recovery was defined as the moles of $CO_2$ in the heavy product divided by the moles of $CO_2$ fed to the process cumulatively during the feed (Eqn 5-2 and 5-3). The enrichment and recovery of both heavy and light components were calculated from the concentration profiles captured by RGA after the steady state situation was reached. After every set of experiment, the RGA was trained with running different $CO_2$-$N_2$ standards namely 0, 0.5, 1, and 2 % $CO_2$ and from 10% $CO_2$ to 100% $CO_2$ with increment of 10% by using two mass flow controllers for $CO_2$ and $N_2$.

A total of three runs were carried out to study the effect of some process parameters. A few experiments have been run before these three experiments. However, the process performance was not met because a 5 kPa vacuum pressure was not achieved experimentally under those conditions. To remedy this situation the feed flow rate was halved (6.67slpm) and the cycle time was doubled ($ts_{,1}$-$t_{s,2}$-$t_{s,3}$: 30-60-30s) compare to S-6 simulation conditions. Thereafter, CnD step time, which is $t_{s,\,1}$, was increased by decreasing

E2 step time, which is $t_{s,3}$, (to maintain same cycle time) in order to reach lower pressures with the 4-bed PSA experimental set-up. The parameters studied include the heavy reflux/light reflux, thus total cycle time and CnD step time, light reflux ratio, and $P_{CnD}$. The 4-bed Stage 2 experimental conditions and parameters for E1-3 are shown in Table 5.9. The process performance in terms of purities and recoveries of $CO_2$ in the heavy product and $N_2$ in the light product is shown in Table 5.10.

All three experimental runs in Table 5.10 gave respectable performances, as all of them achieved a vacuum pressure of 5 kPa during the LR step. However, only Experiment 3 met the desired criteria. This run resulted in a Stage 2 PSA process performance of 98.10 vol% $CO_2$ purity and 97.46% $CO_2$ recovery (4.13kg $CO_2$ removal/day) at a feed flow rate of 6.67 SLPM. The full scale Stage 2 PSA process only requires a feed flow rate of 3.75 SLPM when the feed concentration is 40 vol% $CO_2$ and 60 vol% $N_2$. Accordingly, when scaled by keeping the same experimental bed length and the feed velocity fixed, the new bed dimensions for the 4-bed Stage 2 PSA process were 0.5017 m long and 0.0381 m in diameter. From Table 5.10, after experiment 1, $CO_2$ breaking thorough has been observed, which causes losing heavy product from light end, thus less purities. That why HR/LR time, $t_{s,2}$ has been started to decrease for the case for experiment 2 and 3 in order to increase $CO_2$ recovery or in order to avoid losing $CO_2$ from light end. Therefore, this decrease helped to observe an increase in $CO_2$ recoveries as can be seen from Table 5.10.

Temperature and pressure histories of one of the experiments are shown in Figure 5.18 and Figure 5.19, respectively. From temperature history figure, Figure 5.18, it can be easily seen that major temperatures start rising during feed step and at the end of equalization down 2 step (E2) $CO_2$ front reaches the end of the bed. The temperature

increase, which is observing in T-5 trough T-7 thermocouples in Figure 5.18, is because $CO_2$ is adsorbing again the location at the end of the bed. During equalization down-2 step light end is opening, and so mostly light product is sending to another bed, which causes a decrease in the bed pressure but an increase in $CO_2$ partial pressure. That increase in $CO_2$ partial pressure causes $CO_2$ to re-adsorb again. As can be seen from the Figure 5.18, temperatures in the feed end are decreasing because of desorption of the gas species but temperatures in the light end are increasing because of the $CO_2$ adsorption. Pressure history of one bed for the E3 run during one entire cycle at steady state is shown in Figure 5.19. Small drops during feed in Figure 5.19 is because one of the other beds is starting to light product pressurization step (LPP). The reason to have a king during heavy reflux step is because the ends of the bed was closed during previous step, the equalization down 1 step (E1), and then during the heavy reflux step both ends opened, flows starts flowing. Thefore, that flow causes the instant increase in pressure.

After evaluating the recoveries and enrichments of all the components in both heavy and light ends, a material balance calculation was performed to calculate the error associated with the system. In each case, the resulting species errors were given in Table 5.10.

#### 5.3.4.4. Model Validation

The DAPS model was validated against experimental data obtained from Experiment 1-3. Figure 5.20 shows the experimental data and the model predictions for the pressure profiles at periodic state for the entire PSA cycle which encompasses 9 cycle steps namely feed step, equalization down 1 step, heavy reflux step, equalization down 2 step, counter-current blowdown step, light reflux purge step, equalization up 2 step, equalization

up 1 step and a light product pressurization step as can be seen from Figure 5.20. The solid line indicates the experimental data whereas the dashed line shows the model predictions. The Model was adjusted to match the experimental pressures by changing Cvs of valves of pressure changing steps. From the figure it can be easily seen that model and experimental pressure history overlaps for feed, heavy reflux, equalization down, CnD, and light reflux steps while having little bit difference in equalization steps. Figure 5.21 shows the temperature profiles at periodic state for seven different thermocouples in the bed for experiment 3. The solid line indicates the experimental data whereas the dashed line shows the model predictions. Results show good match between modeling and experiments especially the time that temperature starts rising up. As Figure 5.21 shows, the higher concentration wave front reaches thermocouple T-7 in experiment but T-6 in model validation. Thus, the front's location for experiment is 86.07% in the bed and for model is anywhere between 73.41% and 86.07% in the bed. The main reason having higher maximum temperature in the model than the experiment is having only one lumped heat transfer coefficient with only one energy balance equation for all gas and solid phases, and the wall. And the other reasons might be having small heat transfer coefficient and assuming no wall thickness in the model. These the differences in the model cause less heat to escape from the bed, which causes having higher temperatures in the model. Thus, the model was able to mostly predict the temperature profiles and position for the entire PSA cycle of experiments without any fitting parameters such as kinetic and thermodynamic. The $CO_2$ purity and $CO_2$ recovery in the heavy component and $N_2$ recovery in the light component calculated by DAPS is compared to the experimental results in Table 5.11.

The results show a close agreement between experiment and model without any fitting parameters (kinetic and thermodynamic) and for a wide range of concentrations (0.4-90.0% $CO_2$). Therefore, the model behind DAPS was validated and will now be used to simulate a variety of PSA cycles and process conditions for removal and concentrating $CO_2$ during closed-loop human space exploration missions.

## 5.4. Conclusion

### 5.4.1. Conclusion of 1st Stage PSA Cycle Simulations

The practical feasibility of carbon dioxide separation and recovery from air-$CO_2$ mixtures was demonstrated by means of a new Stage 1 PSA cycle by using an in-house process simulator. A 3-bed 10-step Stage 1 PSA system was configured and utilized to study concentration and separation of $CO_2$ from air (0.2667% $CO_2$, 79.0% $N_2$, and balanced $O_2$) using Zeolite 13X as adsorbent. PSA Cycle included feed (F), idle (I), heavy reflux (HR), co-current equalization depressurization (Eq), co-current depressurization (CoD), counter-current depressurization (CnD), production light reflux (LR1), light reflux-2 (LR2), counter-current equalization pressurization (Eq*) and Light Product Pressurization (LPP) steps. The best run (S15) ended up with producing a heavy product stream containing 67.3 vol% $CO_2$, 91.7% $CO_2$ recovery (4.34 kg/day of $CO_2$ being removed) and with only 0.13% $N_2$ loss to the heavy product. The vacuum utilized during regeneration step was within the specified level and flow rate. The main objectives of Stage 1 PSA system are fully recovery $CO_2$, at least more than 4 kg $CO_2$ removal/day) with more modest $CO_2$ enrichments. Therefore, the objectives could be reached with 3-bed 10-step Stage 1 PSA system and with the specific vacuum pumps.

### 5.4.2. Conclusion of 2nd stage PSA System

The practical feasibility of carbon dioxide separation and recovery from $N_2$-$CO_2$ mixtures was demonstrated by means of a new PSA cycle for Stage 2 by using an in-house process simulator and experimentally by using 4-bed PSA experimental set-up. Thereafter, model validation has been done with DAPS, in house simulator. A 4-bed 9-step Stage 2 PSA process was configured and utilized to study concentration and separation of $CO_2$ from $N_2$ (40% $CO_2$, 60% $N_2$) using Zeolite 13X as adsorbent. PSA Cycle included feed (F), co-current equalization depressurization 1 (E1), heavy reflux (HR), co-current equalization depressurization 2 (E2), counter-current depressurization (CnD), light reflux (LR), counter-current equalization pressurization 2 (E2*), counter-current equalization pressurization 1 (E1*), and Light Product Pressurization (LPP) steps. Preliminary study to develop a PSA process for Stage 2 has been done via simulation. Experiments (E1-3) for Stage 2 with 4-bed PSA apparatus have been done with achievable experimental conditions at scale. Model validation that required no adjustment of kinetic or thermodynamic parameters has been done for 2nd stage.

Overall, target process performance for NASA has been achieved with two-stage PSA system. Overall two-stage PSA process is shown in Figure 5.22. Two-stage PSA performances are 98.10% $CO_2$ purity with 97.46% $CO_2$ recovery, (4.13kg $CO_2$ removal / day) from 0.2667 vol. % $CO_2$ concentration in feed stream. Stage 1bed dimensions are I.D: 10.62 in with L: 19.75 in, while Stage 2 bed dimensions are I.D: 1.5 in with L: 19.75 in.

**Table 5.1** Stage 1 PSA bed, adsorbent, and process characteristics.

| **Bed characteristics** | |
|---|---|
| Bed radius ($r_i$), m | 0.13484 |
| Bed length (L), m | 0.50165 |
| Bed porosity ($\varepsilon_b$) | 0.425 |
| Wall density, kg/m$^3$ | 8000 |
| Wall thickness, m | 0.0 |
| Heat transfer coefficient ($h_w$), kW/m$^2$.K | 0.0024 |
| Heat of adsorption of $CO_2$, $N_2$, $O_2$ ($\Delta H_i$), kJ/mol | 39.57, 19.54, 15.33 |
| **Adsorbent characteristics** | |
| Adsorbent | 13X Zeolite |
| Pellet radius ($r_p$), m | 0.0015 |
| Pellet density ($\rho_p$), kg/m$^3$ | 1100 |
| Pellet porosity ($\varepsilon_p$) | 0.54 |
| Mass of adsorbent per bed, kg/bed | 18.13 |
| **Process characteristics** | |
| Feed mole fraction for $CO_2$, $N_2$, $O_2$ ($yi^F$) | 0.0002667, 0.79, 0.207333 |
| Feed temperature ($T^F$), K | 292.0 |
| Outside wall temperature ($T_o$), K | 292.0 |
| High pressure ($P_H$), kPa | 101.325 |
| Feed Flow ($F^F$), SLPM | 627 (24.35SCFM) |
| Throughput (L(STP)/kg/h) | 691.6 |
| Cycle time ($t_{cycle}$), s | See Table 5.2 |
| Low pressure ($P_L$), kPa | See Table 5.2 |
| Light Reflux Ratio (LRR) | See Table 5.2 |
| CoD pressure ($P_{CoD}$), kPa | See Table 5.2 |
| Light Reflux Pressures ($P_{LR1\&2}$), kPa | See Table 5.2 |

**Table 5.2** Input parameters of 3-Bed 9-Step PSA process for parametric study via running simulations using the cycle depicted below.

| Bed 1 | FEED | | | | |
|---|---|---|---|---|---|
| Bed 2 | I | | HR | Eq | CoD |
| Bed 3 | CnD | LR1 | LR2 | Eq* | LPP |
| Step time | $t_{s,1}$=200s | $t_{s,2}$ | $t_{s,3}$ | $t_{s,4}$=25s | $t_{s,5}$=50s |

| **Run#** | **$P_{CnD}$** | **$P_{LR1\&LR2}$** | **$t_{s,3}$** | **$t_{s,2}$** | **$t_{cycle}$** | **$F_{LR1}$** | **$F_{LR2}$** |
|---|---|---|---|---|---|---|---|
| *Effect of HR/LR (thus scycle time)* | | | | | | | |
| **Base** | 0.5 | 5 | 1475 | 50 | 5400 | 15.5 | 55 |
| **S1** | 0.5 | 5 | **1575** | 50 | **5700** | 15.5 | 55 |
| **S2** | 0.5 | 5 | **1675** | 50 | **6000** | 15.5 | 55 |
| **S3** | 0.5 | 5 | **1975** | 50 | **6900** | 15.5 | 55 |
| **S4** | 0.5 | 5 | **2475** | 50 | **8400** | 15.5 | 55 |
| **S5** | 0.5 | 5 | **3475** | 50 | **11400** | 15.5 | 55 |
| *Effect of production LR step flow rate* | | | | | | | |
| **Base** | 0.5 | 5 | 1475 | 50 | 5400 | 15.5 | 55 |
| **S6** | 0.5 | 5 | 1475 | 50 | 5400 | **17.5** | 55 |
| **S7** | 0.5 | 5 | 1475 | 50 | 5400 | **20** | 55 |
| *Effect of LR2 step flow rate* | | | | | | | |
| **Base** | 0.5 | 5 | 1475 | 50 | 5400 | 15.5 | 55 |
| **S8** | 0.5 | 5 | 1475 | 50 | 5400 | 15.5 | **58** |
| **S9** | 0.5 | 5 | 1475 | 50 | 5400 | 15.5 | **62** |
| **S10** | 0.5 | 5 | 1475 | 50 | 5400 | 15.5 | **65** |
| *Effect of production LR step time* | | | | | | | |
| **Base** | 0.5 | 5 | 1475 | 50 | 5400 | 15.5 | 55 |
| **S11** | 0.5 | 5 | 1475 | **75** | 5475 | 15.5 | 55 |
| **S12** | 0.5 | 5 | 1475 | **100** | 5550 | 15.5 | 55 |
| *Effect of $P_{CnD}$* | | | | | | | |
| **Base** | 0.5 | 5 | 1475 | 50 | 5400 | 15.5 | 55 |
| **S13** | **0.3** | 5 | 1475 | 50 | 5400 | 15.5 | 55 |
| **S14** | **0.1** | 5 | 1475 | 50 | 5400 | 15.5 | 55 |
| *Effect of $P_{LR}$* | | | | | | | |
| **Base** | 0.5 | 5 | 1475 | 50 | 5400 | 15.5 | 55 |
| **S15** | 0.5 | **4** | 1475 | 50 | 5400 | 15.5 | 55 |

*: Values in bold correspond to the parameters changed in the parametric study, with all other parameters fixed.

**Table 5.3** Stage 1 PSA process performance results from parametric study via DAPS.

| Run# | $CO_2$ **Purity (%)** | $CO_2$ **Recovery (%)** | $CO_2$ **removed daily (kg)** | $N_2$ **losses (%)** | **Power (watt) (80% eff )** |
|---|---|---|---|---|---|
| **Base** | 66.72 | 83.44 | 3.95 | 0.13 | 469.9 |
| **S1** | 68.12 | 83.78 | 3.96 | 0.12 | 500.2 |
| **S2** | 69.42 | 84.06 | 3.98 | 0.11 | 530.5 |
| **S3** | 72.82 | 84.50 | 3.99 | 0.09 | 621.5 |
| **S4** | 77.25 | 84.44 | 3.99 | 0.07 | 773.0 |
| **S5** | 82.87 | 82.98 | 3.92 | 0.05 | 1076.3 |
| **Base** | 66.72 | 83.44 | 3.95 | 0.13 | 469.9 |
| **S6** | 65.00 | 83.52 | 3.95 | 0.13 | 470.4 |
| **S7** | 63.07 | 83.58 | 3.95 | 0.15 | 470.9 |
| **Base** | 66.72 | 83.44 | 3.95 | 0.13 | 469.9 |
| **S8** | 67.36 | 85.72 | 4.05 | 0.13 | 493.8 |
| **S9** | 68.07 | 88.35 | 4.18 | 0.12 | 525.5 |
| **S10** | 67.36 | 85.72 | 4.05 | 0.13 | 493.8 |
| **Base** | 66.72 | 83.44 | 3.95 | 0.13 | 469.9 |
| **S11** | 60.69 | 82.98 | 3.93 | 0.16 | 471.8 |
| **S12** | 55.74 | 82.53 | 3.90 | 0.19 | 473.7 |
| **Base** | 66.72 | 83.44 | 3.95 | 0.13 | 469.9 |
| **S13** | 66.66 | 83.87 | 3.97 | 0.13 | 474.9 |
| **S14** | 66.76 | 84.23 | 3.98 | 0.13 | 486.9 |
| **Base** | 66.72 | 83.44 | 3.95 | 0.13 | 469.9 |
| **S15*** | **67.32** | **91.74** | **4.34** | **0.13** | **521.7** |

* The run in bold corresponds to the best run and thus the run chosen to supply feed to the Stage 2 PSA process.

**Table 5.4** Stage 2 preliminary DAPS simulations bed, adsorbent, and process characteristics.

| | |
|---|---|
| **Bed characteristics** | |
| Bed radius ($r_i$), m | 0.0254 |
| Bed length (L), m | 0.0762 |
| Bed porosity ($\varepsilon_b$) | 0.425 |
| Wall density, kg/m$^3$ | 8000 |
| Wall thickness, m | 0.0 |
| Heat transfer coefficient ($h_w$), kW/m$^2$.K | 0.0024 |
| **Adsorbent characteristics** | |
| Adsorbent | 13X Zeolite |
| Pellet radius ($r_p$), m | 0.0015 |
| Pellet density ($\rho_p$), kg/m$^3$ | 1100 |
| Pellet porosity ($\varepsilon_p$) | 0.54 |
| Mass of adsorbent per bed, g/bed | 97.7 |
| **Process characteristics** | |
| Feed mole fraction for $CO_2$, $N_2$ ($yi^F$) | 0.4 / 0.6, 0.6 / 0.4 |
| Feed temperature ($T^F$), K | 292.0 |
| Outside wall temperature ($T_o$), K | 292.0 |
| High pressure ($P_H$), kPa | 101.325 |
| Feed Flow ($F^F$), SLPM | 2.5, 3.75 |
| Throughput (L(STP)/kg/h) | 383.7, 575.5 |
| Cycle time ($t_{cycle}$), s | 160 |
| Low pressure ($P_L$), kPa | 5 |
| Light Reflux Ratio (LRR) | 2.22, 5 |
| HR pressure ($P_{HR}$), kPa | ~ 55 |
| **Kinetic Properties** | |
| Micropore mass transfer coefficients for $CO_2$, $N_2$ , $k_{m,i}$, s$^{-1}$ | 1.0 |

**Table 5.5** Stage 2 scale-up simulations, experiments and model validation bed, adsorbent, and process characteristics.

| | |
|---|---|
| **Bed characteristics** | |
| Bed radius ($r_i$), m | 0.0254 |
| Bed length (L), m | 0.50165 |
| Bed porosity ($\varepsilon_b$) | 0.425 |
| Wall density, kg/m$^3$ | 8000 |
| Wall thickness, m | 0.0 |
| Heat transfer coefficient ($h_w$), kW/m$^2$.K | 0.0024 |
| **Adsorbent characteristics** | |
| Adsorbent | 13X Zeolite |
| Pellet radius ($r_p$), m | 0.0015 |
| Pellet density ($\rho_p$), kg/m$^3$ | 1100 |
| Pellet porosity ($\varepsilon_p$) | 0.54 |
| Mass of adsorbent per bed, g/bed | 97.7 |
| **Process characteristics** | |
| Feed mole fraction for $CO_2$, $N_2$ ($yi^F$) | 0.4 / 0.6, 0.6 / 0.4 |
| See Tables 5- through 5- | |
| **Kinetic Properties** | |
| Macropore mass transfer coefficients for $CO_2$, $N_2$ , $k_{M,i}$, s$^{-1}$ | 47, 70 |

**Table 5.6** Stage 2 preliminary PSA process performance results from DAPS.

| | **Feed I** | **Feed II** |
|---|---|---|
| **Feed (SLPM)** | 2.50 | 3.75 |
| **y**$CO_2$ | 0.60 | 0.40 |
| $CO_2$ **fed daily (kg)** | 4.24 | 4.24 |
| $\mathbf{L_b}$ **(in)** | 3.00 | 3.00 |
| $\mathbf{t_{cycle}}$ **(s)** | 160 | 160 |
| **LRR (%)** | 5.0 | 2.22 |
| $CO_2$ **purity in HP** | 94.0 | 98.1 |
| $CO_2$ **recovery in HP** | 95.1 | 96.1 |
| $CO_2$ **removed daily in HP (kg)** | 4.03 | 4.07 |

**Table 5.7** Scale-up conditions from the selected Feed II to 4-bed PSA apparatus.

| | **4-bed micropore model conditions** | **4-bed experimental set-up conditions** |
|---|---|---|
| **Feed (SLPM)** | *3.75* | *24.5* |
| **y**$CO_2$ | 0.40 | 0.40 |
| **y**$N_2$ | Balance | Balance |
| **$L_b$ (in)** | *3.0* | *19.75* |
| **$D_{b,i}$ (in)** | 2.0 | 2.0 |
| **LRR (%)** | 2.22 | 2.22 |
| **$P_{Feed}$ (kPa)** | 101.4 | 101.4 |
| **$P_L$ (kPa)** | 5.0 | 5.0 |
| **$P_{HR}$ (kPa)** | ~55 | ~55 |
| **$t_{cycle}$ (s)** | 200 | 200 |
| **$m_{ads}$ per bed (g)** | *97.7* | *639.6* |
| **$k_m$ for** $CO_2$, $N_2$ **($s^{-1}$)** | *1.0* | - |
| **$k_M$ for** $CO_2$, $N_2$ **($s^{-1}$)** | - | *47.0, 70.0* |
| **LDF approach** | $\frac{\partial \bar{\bar{q}}}{\partial t} = k_m(q^*(\bar{P},T) - \bar{\bar{q}})$ | $\frac{\partial \bar{\bar{q}}}{\partial t} = k^*{}_M(q^*(P,T) - \bar{\bar{q}})$ with $k^*{}_{M,i} = \frac{1}{1 + \frac{RT\rho_p}{\varepsilon_p}\frac{\partial q}{\partial P}\Big\|^*_{T,\bar{P}}} k_{M,i}$ |

*: the areas in Italic corresponds the changing conditions from preliminary simulations to 4-bed PSA apparatus.

**Table 5.8** Effect of scaled up feed flow rate and step times used in DAPS simulations and corresponding performances.

| | **Feed [SLPM]** | **HP $CO_2$ Recovery %** | **HP $CO_2$ Purity %** |
|---|---|---|---|
| **$t_{s,1}$-$t_{s,2}$-$t_{s,3}$ : 10-20-10s** | | | |
| **S-1** | 24.5 | 89.63 | 99.89 |
| **S-2** | 20 | 92.10 | 99.73 |
| **S-3** | 18 | 94.98 | 97.80 |
| **S-4** | 16 | 96.76 | 94.87 |
| **$t_{s,1}$-$t_{s,2}$-$t_{s,3}$ : 15-30-15s** | | | |
| **S-5** | 16.36 | 91.40 | 99.95 |
| **S-6** | **13.33** | **96.34** | **97.13** |
| **S-7** | 12.00 | 96.59 | 94.25 |
| **S-8** | 10.66 | 97.10 | 92.31 |
| **$t_{s,1}$-$t_{s,2}$-$t_{s,3}$ : 20-40-20s** | | | |
| **S-9** | 12.27 | 94.52 | 99.60 |
| **S-10** | 10.00 | 96.85 | 95.77 |
| **S-11** | 9.00 | 92.60 | 91.24 |
| **S-12** | 8.00 | 94.13 | 88.30 |

**Table 5.9** 4-bed Stage 2 experimental conditions and parameters

| Parameter | Exp-1 | Exp-2 | Exp-3 |
|---|---|---|---|
| **$F_{Feed}$ (SLPM)** | 6.67 | 6.67 | 6.67 |
| **Feed Pressure** | 102.68 | 102.65 | 102.66 |
| **$T_{Feed}$ ($^oC$)** | 23.60 | 23.77 | 22.10 |
| **$y_F$ ($CO_2$:$N_2$) (%)** | 40:60 | 40:60 | 40:60 |
| **$P_{CnD}$ (kPa)** | 8.28 | 8.52 | 7.53 |
| **$P_{LR}$ (kPa)** | 5.04 | 5.14 | 5.04 |
| **LRR (%)** | 2.09 | 2.08 | 2.27 |
| **$t_{cycle}$ (s)** | 480 | 460 | 440 |
| **$t_{s,1}$-$t_{s,2}$-$t_{s,3}$ (s)** | 45-60-15 | 45-55-15 | 45-50-15 |

**Table 5.10** 4-bed Stage 2 periodic state PSA process performance.

| Conditions | | | | | | | | Performance | | | | | |
|---|---|---|---|---|---|---|---|---|---|---|---|---|---|
| Exp | θ L(STP) $kg^{-1}h^{-1}$ | HR/LR Cycle Step Time [s] | $P_{max}$ [kPa] | $P_{min}$ [kPa] | $T_{max}$ [°C] | $T_{min}$ [°C] | LRR % | Gas | HP % Rec | HP % Pur | LP % Rec | LP % Pur | Mass Bal Error % |
| 1 | 155.7 | 60 | 102.7 | 5.04 | 38.1 | 14.7 | 2.09 | $CO_2$ | 92.04 | 99.33 | 6.29 | 3.98 | 1.67 |
| | | | | | | | | $N_2$ | 0.41 | 0.67 | 100.78 | 96.02 | 1.20 |
| 2 | 155.7 | 55 | 102.7 | 5.14 | 32.5 | 15.0 | 2.08 | $CO_2$ | 94.02 | 96.69 | 2.88 | 1.89 | 3.10 |
| | | | | | | | | $N_2$ | 2.14 | 3.31 | 99.30 | 98.11 | 1.44 |
| 3 | 155.7 | 50 | 102.7 | 5.04 | 34.5 | 13.5 | 2.27 | $CO_2$ | 97.46 | 98.10 | 2.43 | 1.58 | 0.11 |
| | | | | | | | | $N_2$ | 1.25 | 1.90 | 100.4 | 98.42 | 1.65 |

**Table 5.11** Comparison of experiment and model PSA process performances

| | Parameters | | | | HP | | | | LP | | |
|---|---|---|---|---|---|---|---|---|---|---|---|
| | $t_{cycle}$ (s) | $t_{s,2}$ (s) | $P_{min}$ (kPa) | LRR (%) | **Y**$CO_2$ [%] | | **Re**$CO_2$ [%] | | **Re**$N_2$ [%] | | Power [watt] |
| | | | | | Exp | Model | Exp | Model | Exp | Model | |
| **1** | 480 | 60 | 5.04 | 2.09 | **99.33** | **99.99** | **92.04** | **89.21** | **100.0** | **99.96** | **21.36** |
| **2** | 460 | 55 | 5.14 | 2.08 | **96.69** | **99.86** | **94.02** | **91.68** | **99.3** | **98.84** | **18.82** |
| **3** | 440 | 50 | 5.05 | 2.27 | **98.10** | **98.12** | **97.46** | **96.77** | **100.0** | **99.28** | **19.33** |

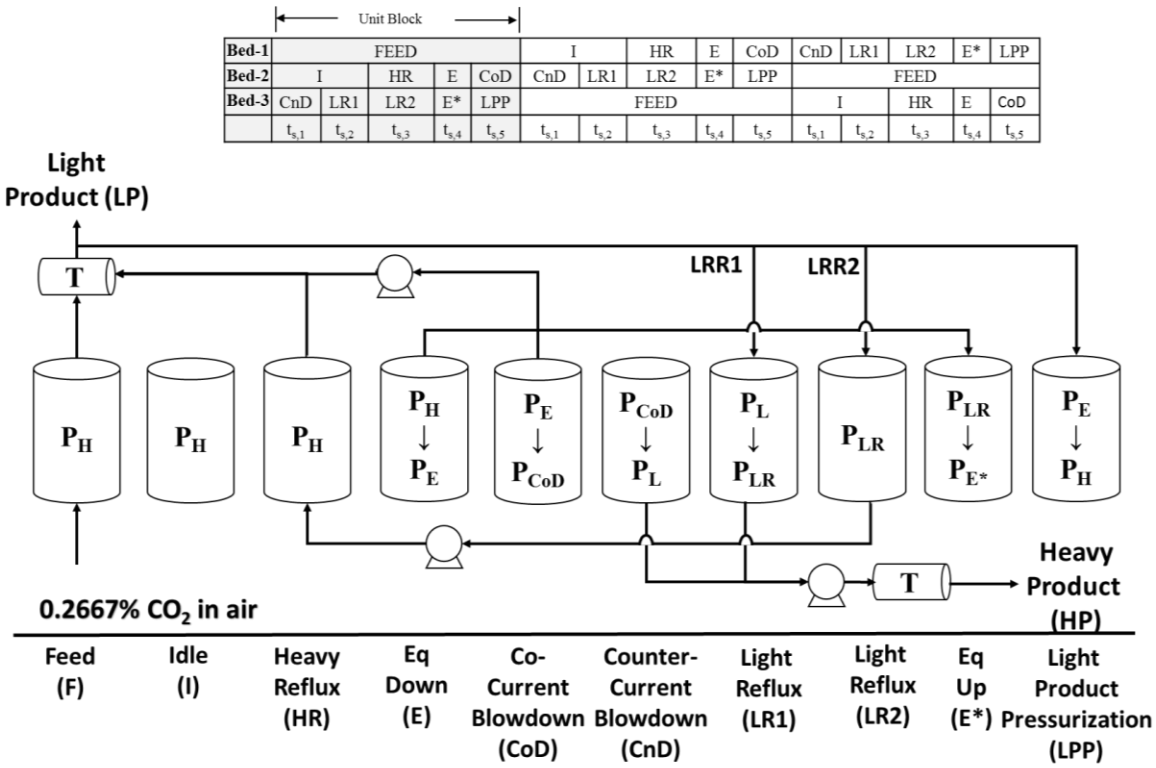


**Figure 5.1** Cycle sequence of 1st stage: 3-Bed 10-Step PSA Cycle

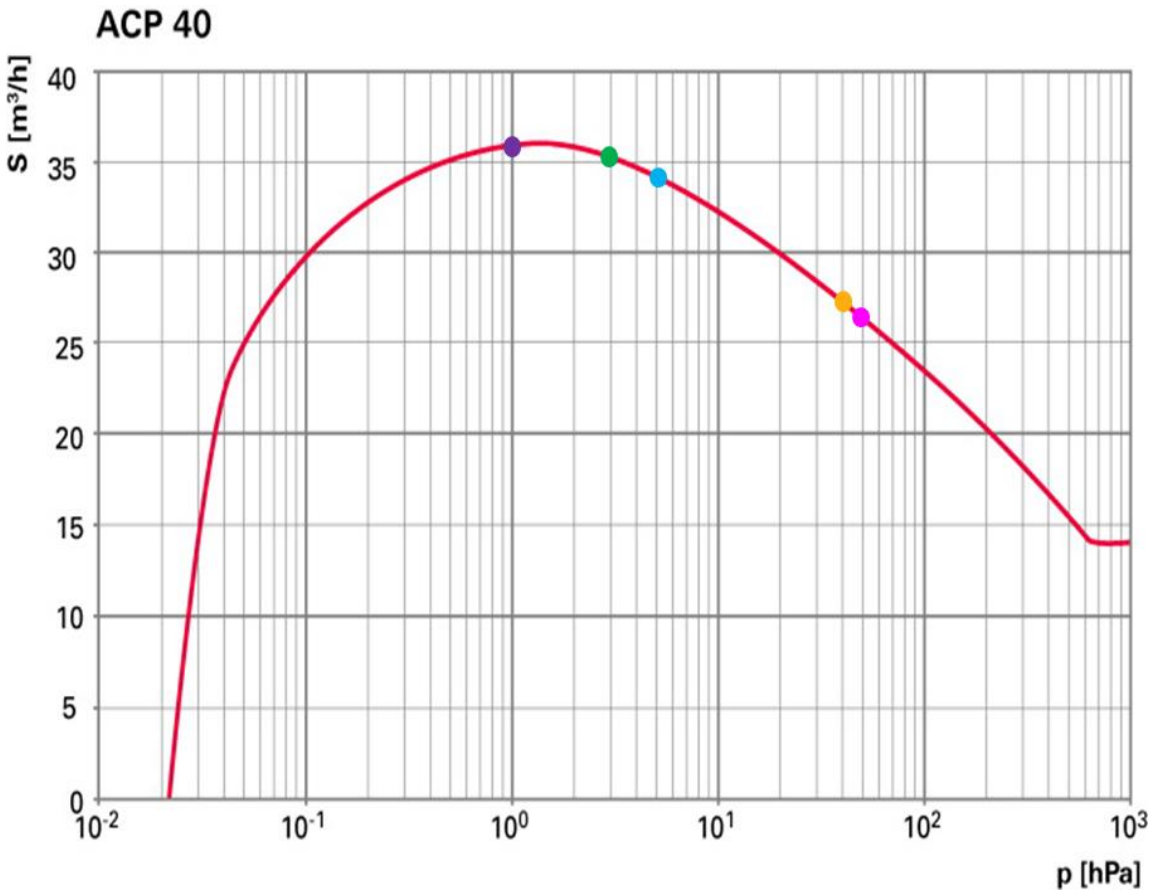


**Figure 5.2** Pfeiffer vacuum pump, model ACP 40 performance curve. The pressure and flow rate operating points during the CnD and LR steps for this Stage 1 PSA process operating at 0.1 kPa (purple), 0.3 kPa (green), 0.5 kPa (blue), 4kPa (orange) and 5kPa (pink) are indicated.

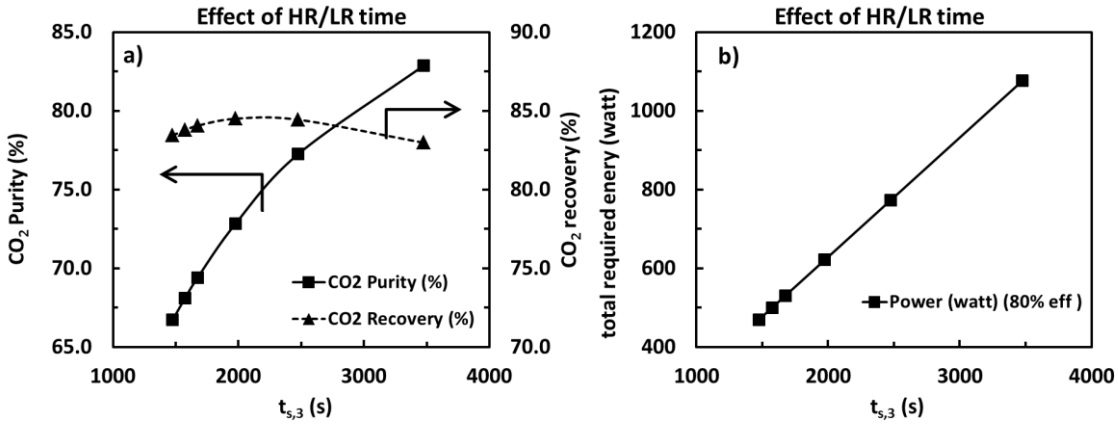


**Figure 5.3** Effect of HR/LR/F step time (thus cycle time) on cyclic steady state performance for the runs base and S1-5 in Table 5.2. a) $CO_2$ purity and recovery, b) Total Power.

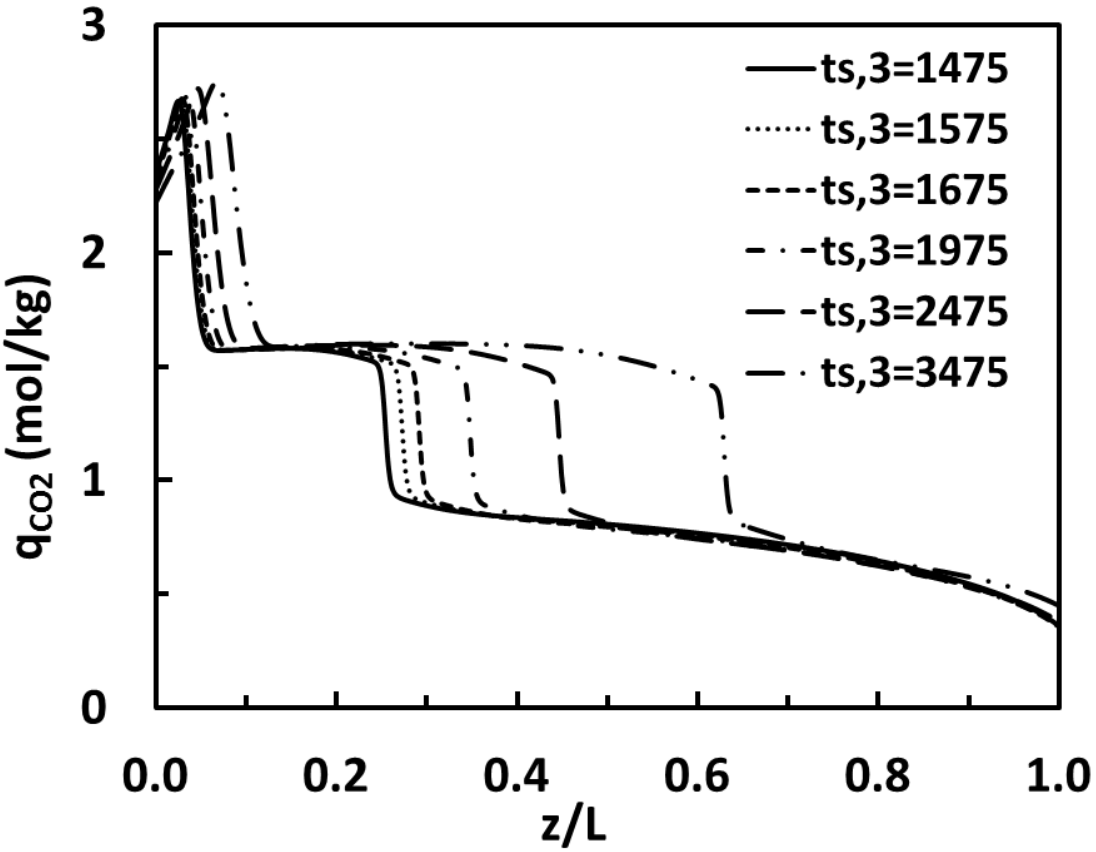


**Figure 5.4** Bed profiles at the end of HR step for each run (base and S1-5 in Table 5.2) at periodic steady state.

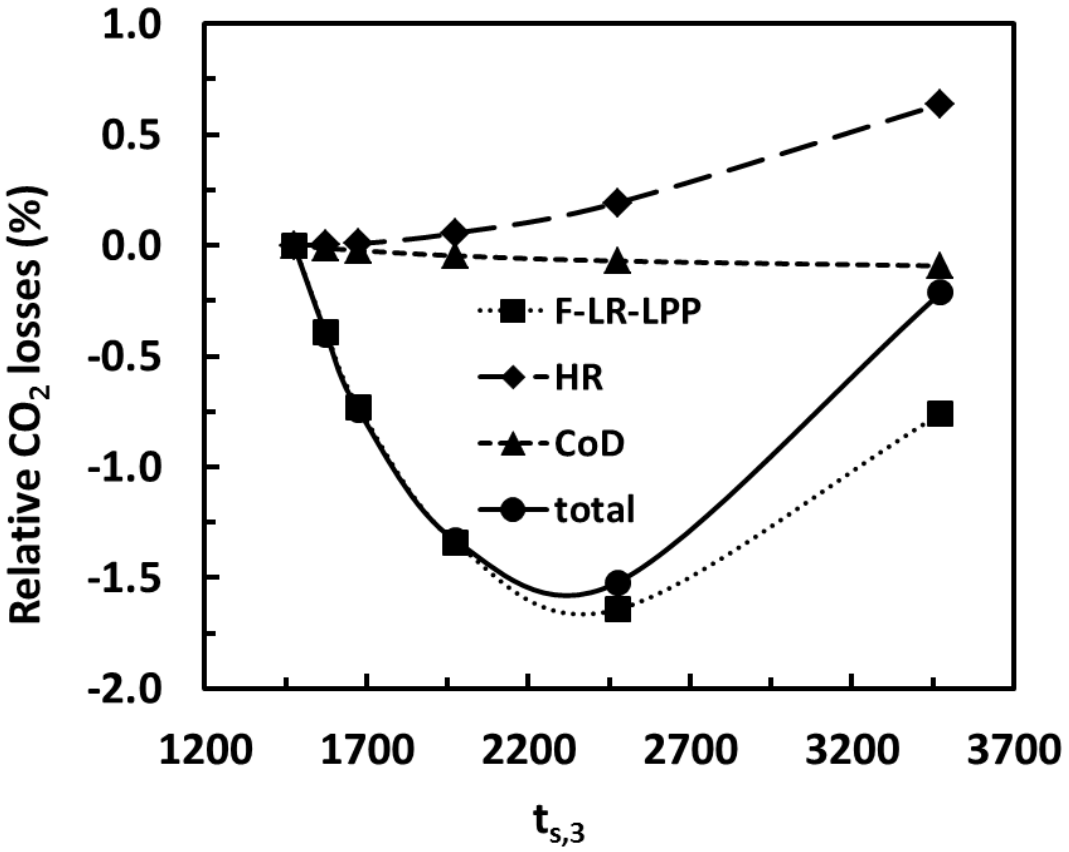


**Figure 5.5** Relative losses of $CO_2$ from light end (minus: decrease in $CO_2$ loss, +: increase in $CO_2$ loss relative to base case). Run numbers base and S1-5 in Table 5.2.

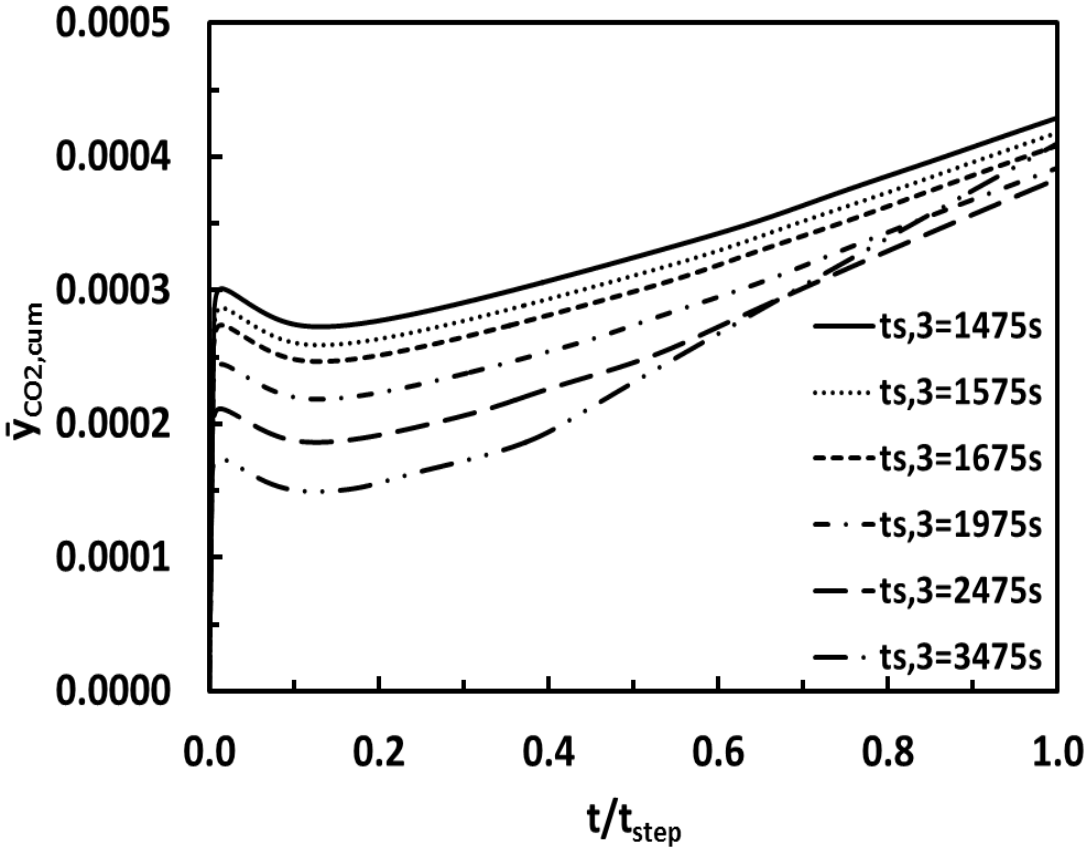


**Figure 5.6** Cumulative $CO_2$ gas phase concentration ($\bar{y}CO_{2,}$ cum) from the beginning to the end of feed step. Run numbers base and S1-5 in Table 5.2.

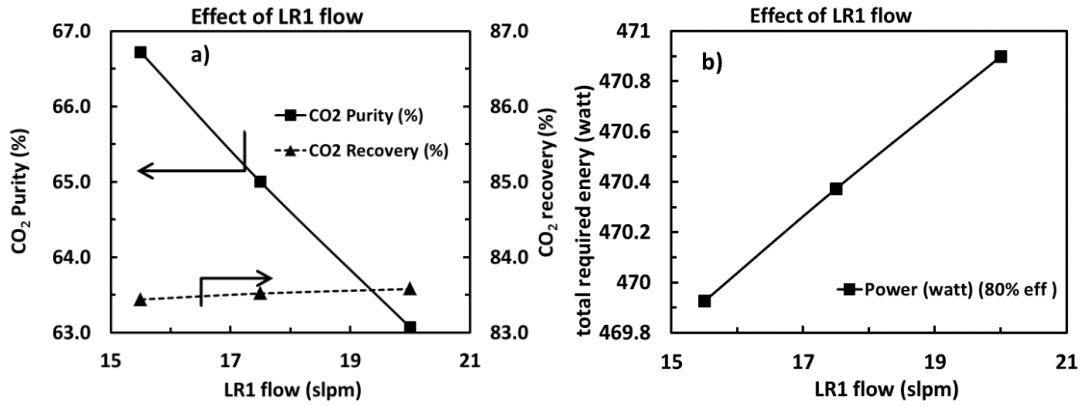


**Figure 5.7** Effect of production LR step flow rate ($F_{LR1}$) on cyclic steady state performance for the PSA cycle. Run numbers base and S6-7 in Table 5.2. a) $CO_2$ purity and recovery, b) Total Power.

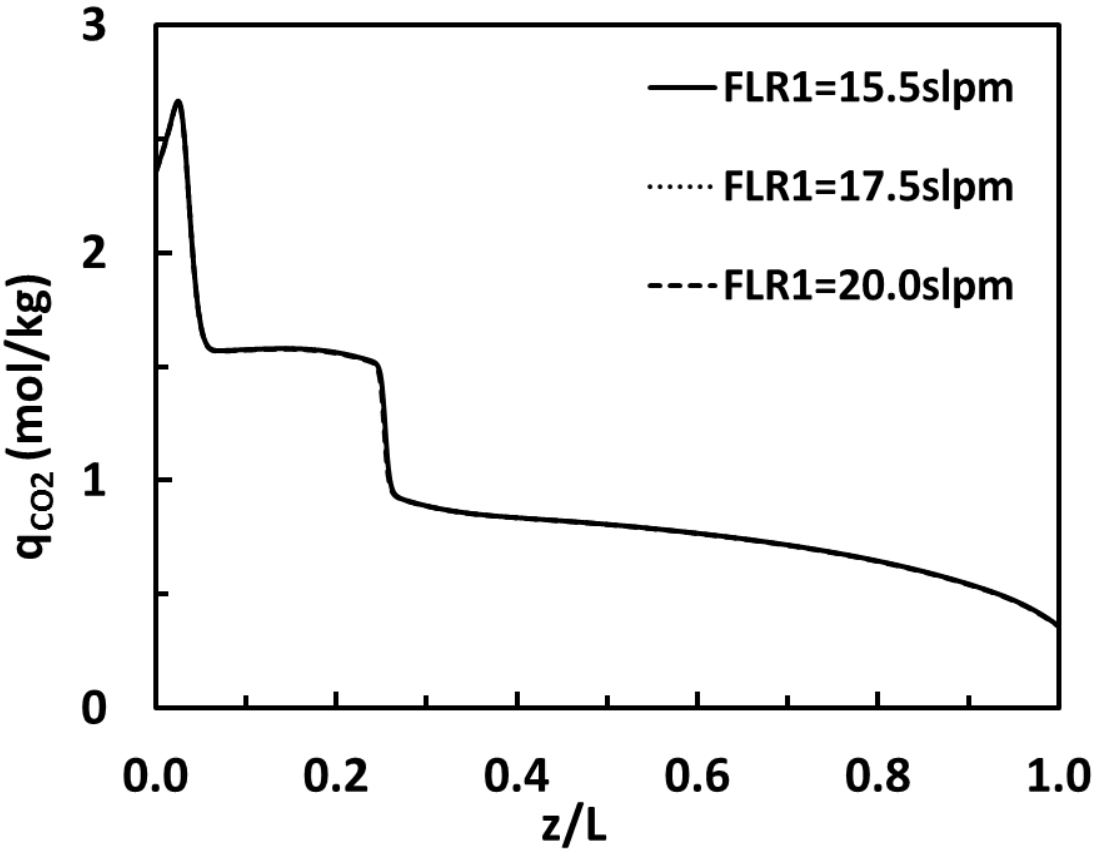


**Figure 5.8** Bed profiles at the end of HR step for the parametric study of production LR step flow rate ($F_{LR1}$), corresponding runs are base and S6-7 in Table 5.2 at periodic steady state.

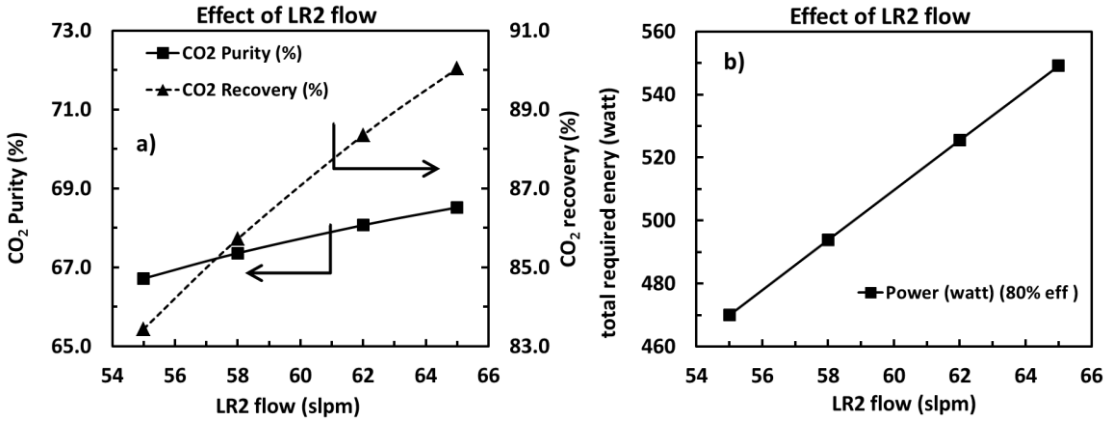


**Figure 5.9** Effect of light reflux 2 step flow rate ($F_{LR2}$) on cyclic steady state performance for the PSA cycle. Run numbers base and S8-10 in Table 5.2. a) $CO_2$ purity and recovery, b) Total Power.

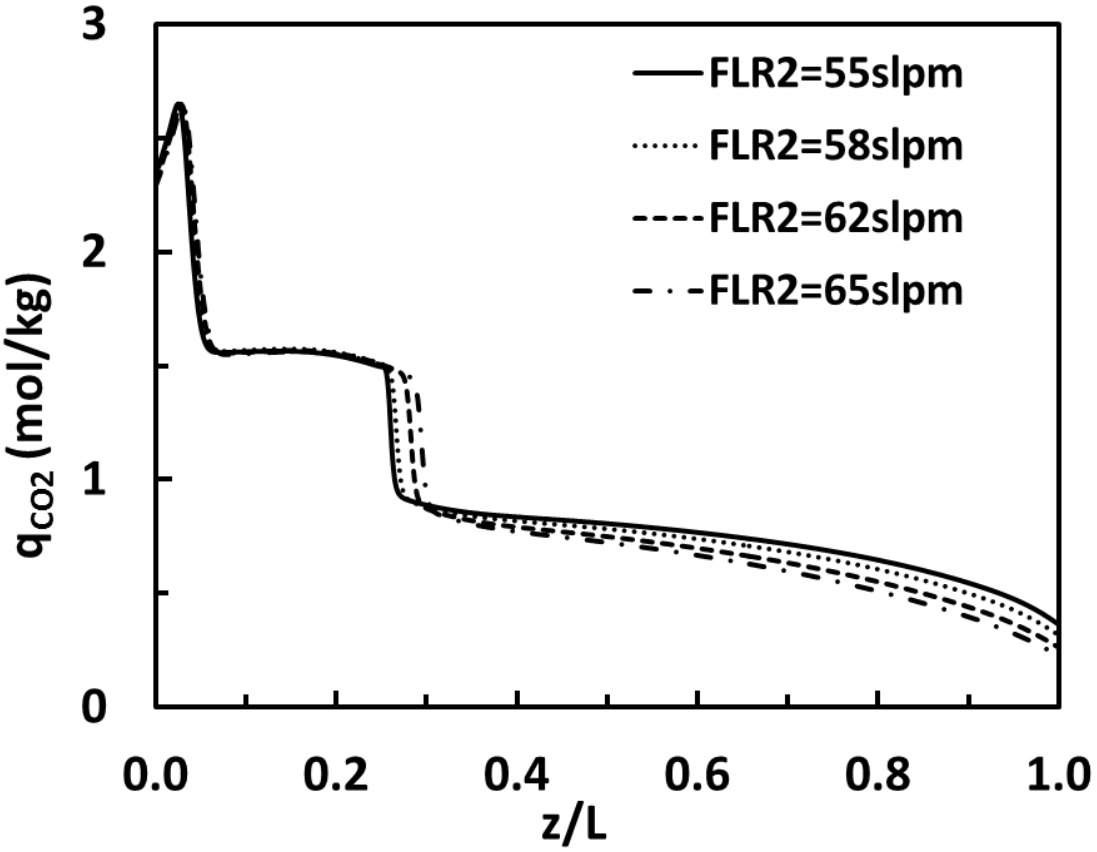


**Figure 5.10** Bed profiles at the end of HR step for the parametric study of light reflux 2 step flow rate ($F_{LR2}$), corresponding runs are base and S8-10 in Table 5.2 at periodic steady state.

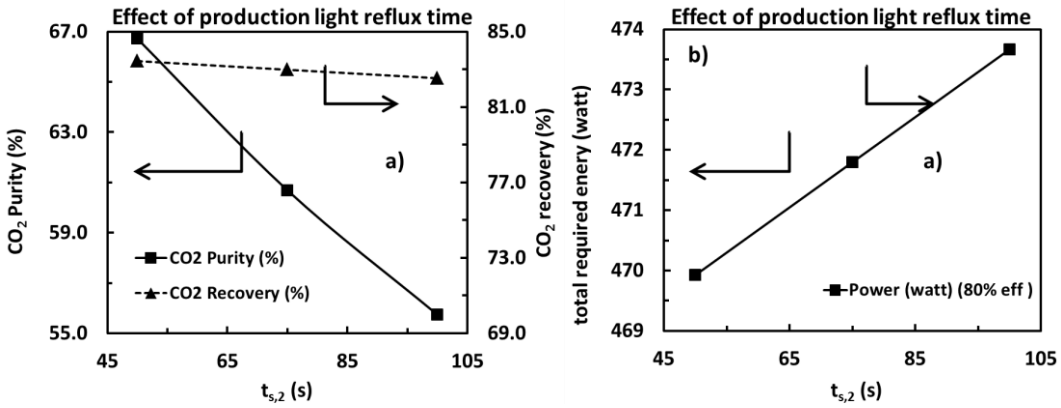


**Figure 5.11** Effect of production LR step time ($t_{s,2}$) on cyclic steady state performance for the PSA cycle. Run numbers base and S11-12in Table 5.2. a) $CO_2$ purity and recovery, b) Total Power.

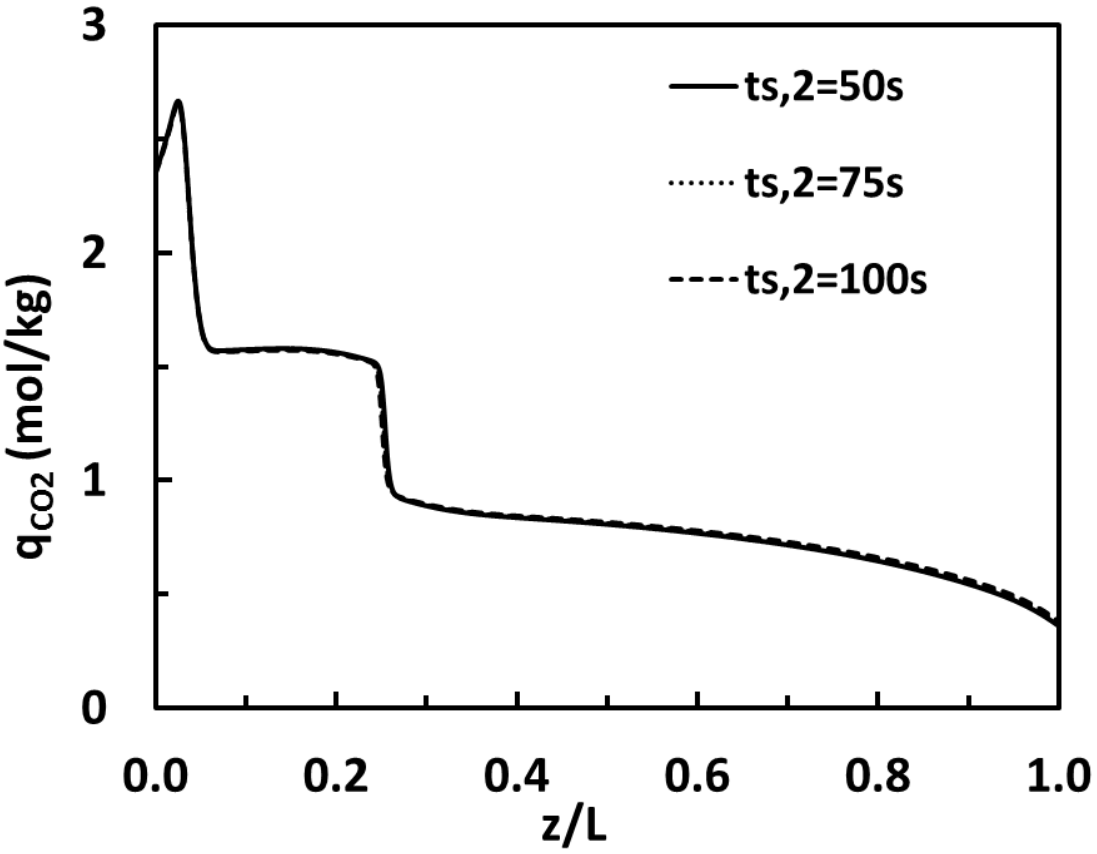


**Figure 5.12** Bed profiles at the end of HR step for the parametric study of production LR step time ($t_{s,2}$) effect at periodic steady state, corresponding runs are base and S11-12 in Table 5.2.

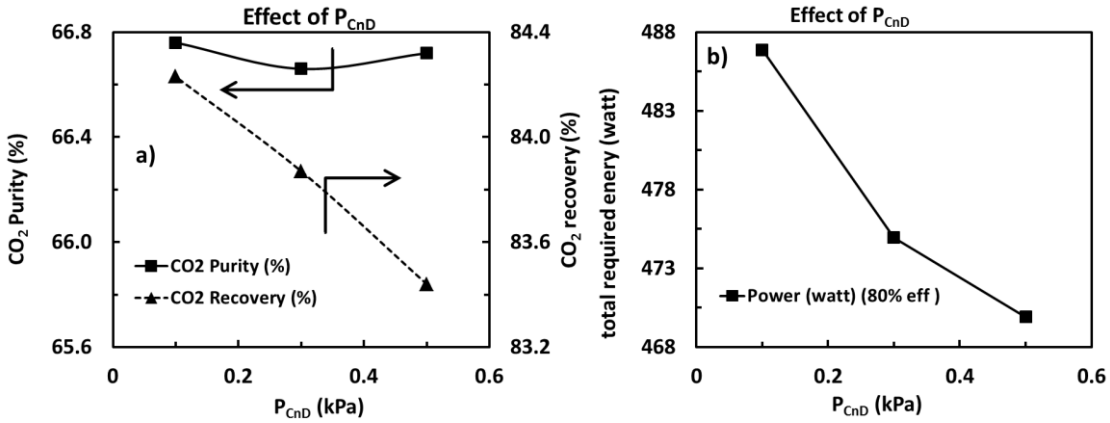


**Figure 5.13** Effect of counter-current depressurization pressure ($P_{CnD}$) on cyclic steady state performance for the PSA cycle. Corresponding runs are base, S13, and S14 in Table 5.2. a) $CO_2$ purity and recovery, b) Total Power.

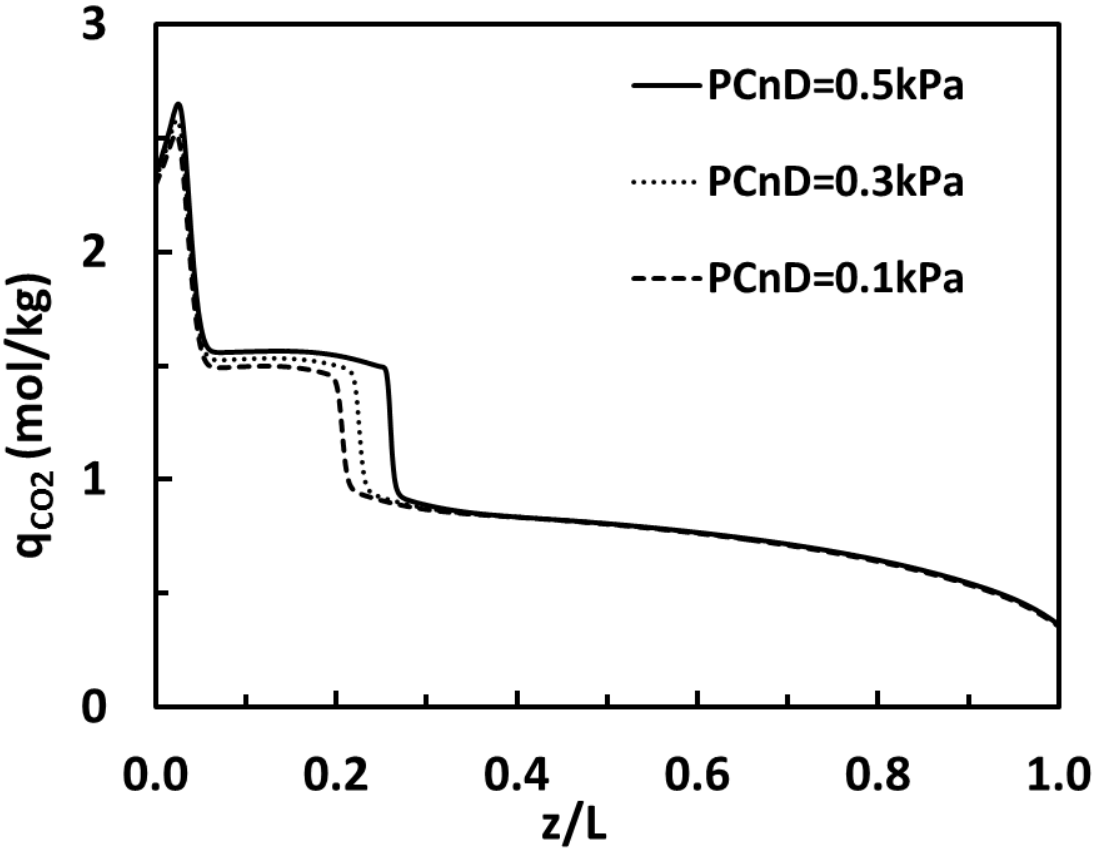


**Figure 5.14** Bed profiles at the end of HR step for the parametric study of counter-current depressurization pressure ($P_{CnD}$) effect, corresponding runs are base and S13-14 in Table 5.2 at periodic steady state.

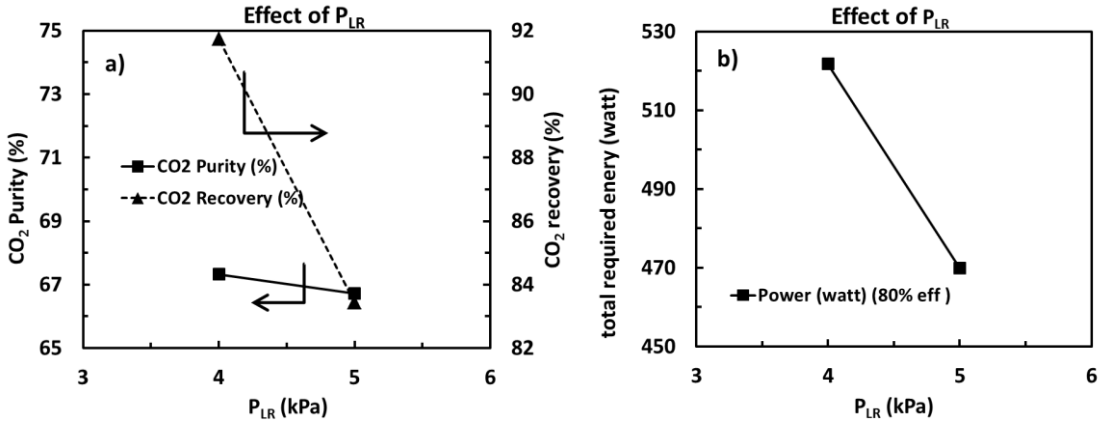


**Figure 5.15** Effect of light reflux pressures ($P_{LR1\&2}$) on cyclic steady state performance for the PSA cycle. Corresponding runs are base, and S15 in Table 5.2. a) $CO_2$ purity and recovery, b) Total Power.

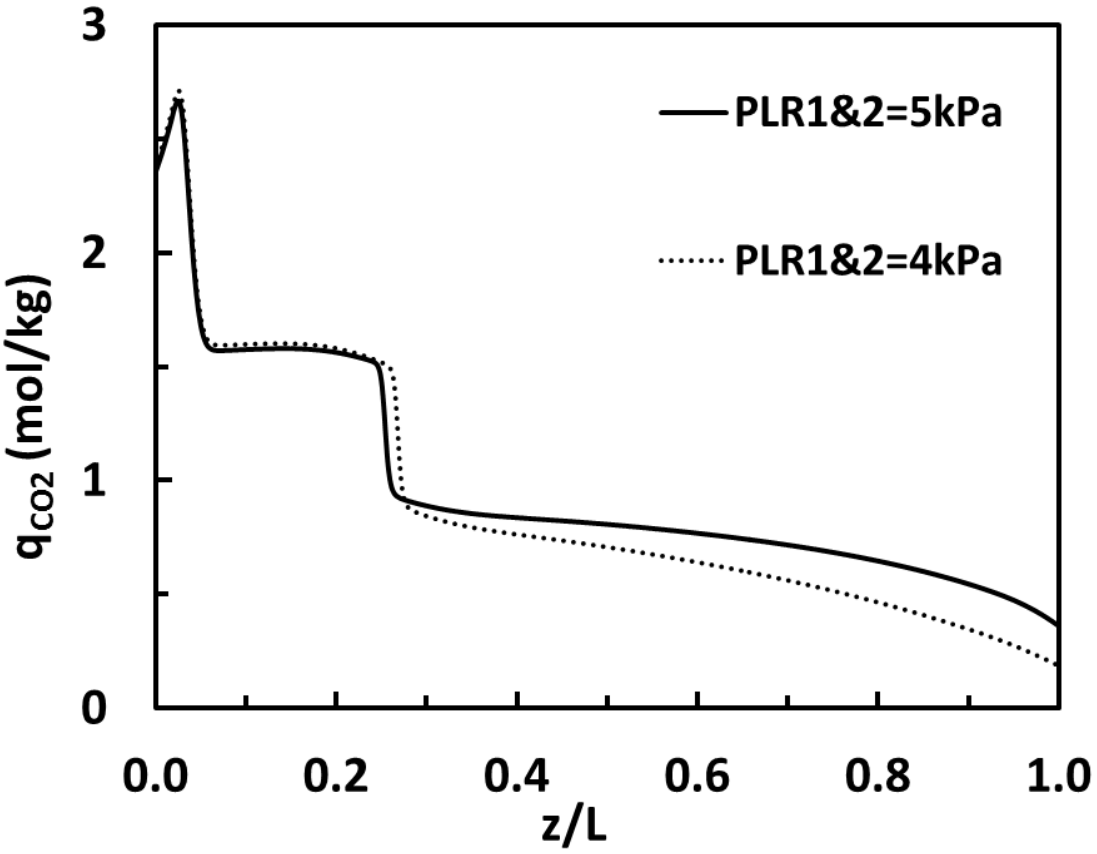


**Figure 5.16** Bed profiles at the end of HR step for the parametric study of light reflux pressures ($P_{LR1\&2}$) effect, corresponding runs are base and S15in Table 5.2 at periodic steady state.

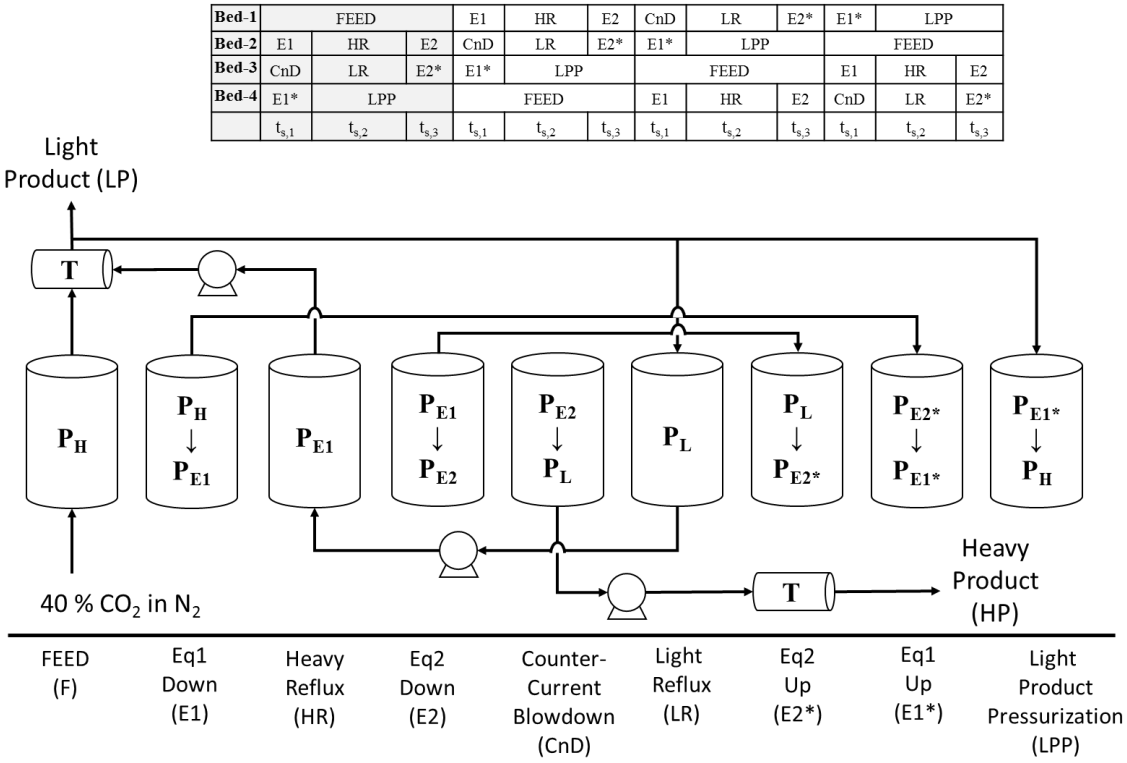


**Figure 5.17** New 4-bed 9-step Stage 2 PSA process cycle schedule and cycle step sequence with a heavy reflux (HR) step at an intermediate pressure between the two equalization (Eq) steps that uses the heavy product produced during the LR step as its feed source**.**

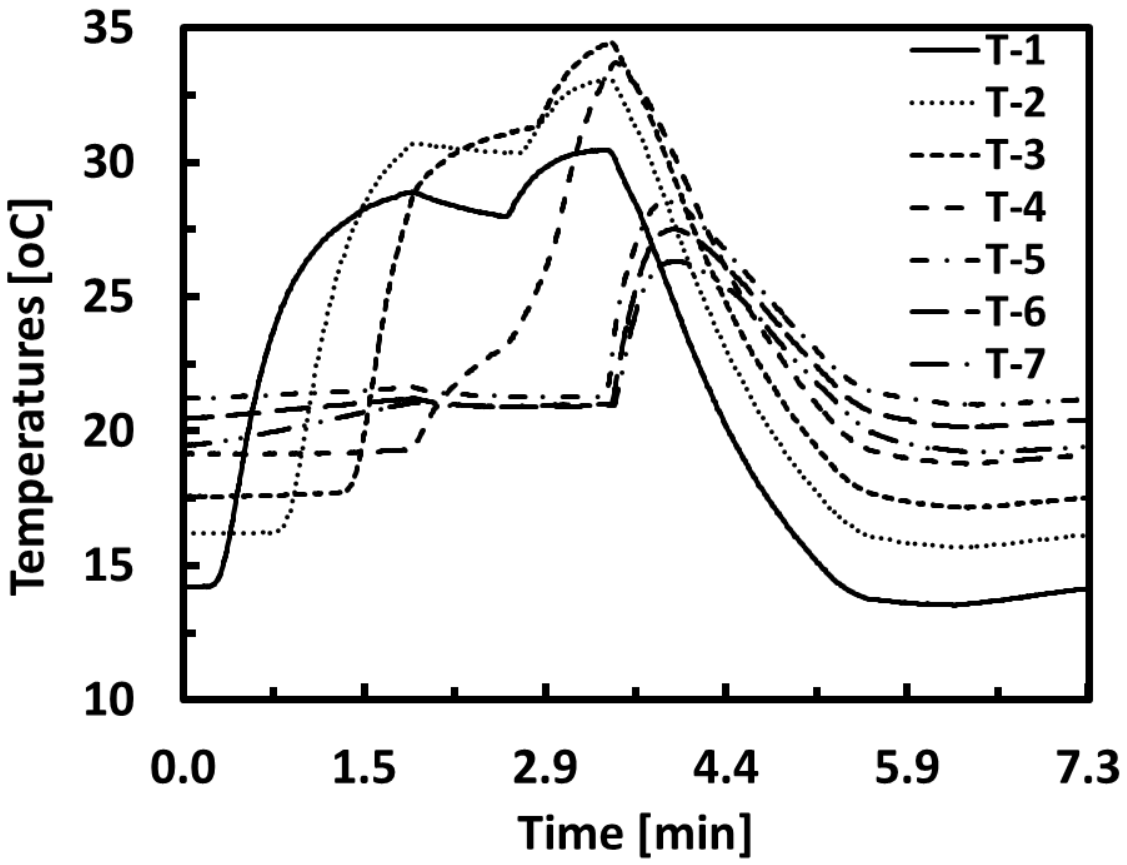


**Figure 5.18** Temperature history of one bed for the E3 during one entire cycle at steady state. 1-7 are locations of thermocouples from feed end. T1-7 (10.12%, 22.78%, 35.44%, 48.10%, 60.75%, 73.41%, 86.07%) are locations of thermocouples from feed end.

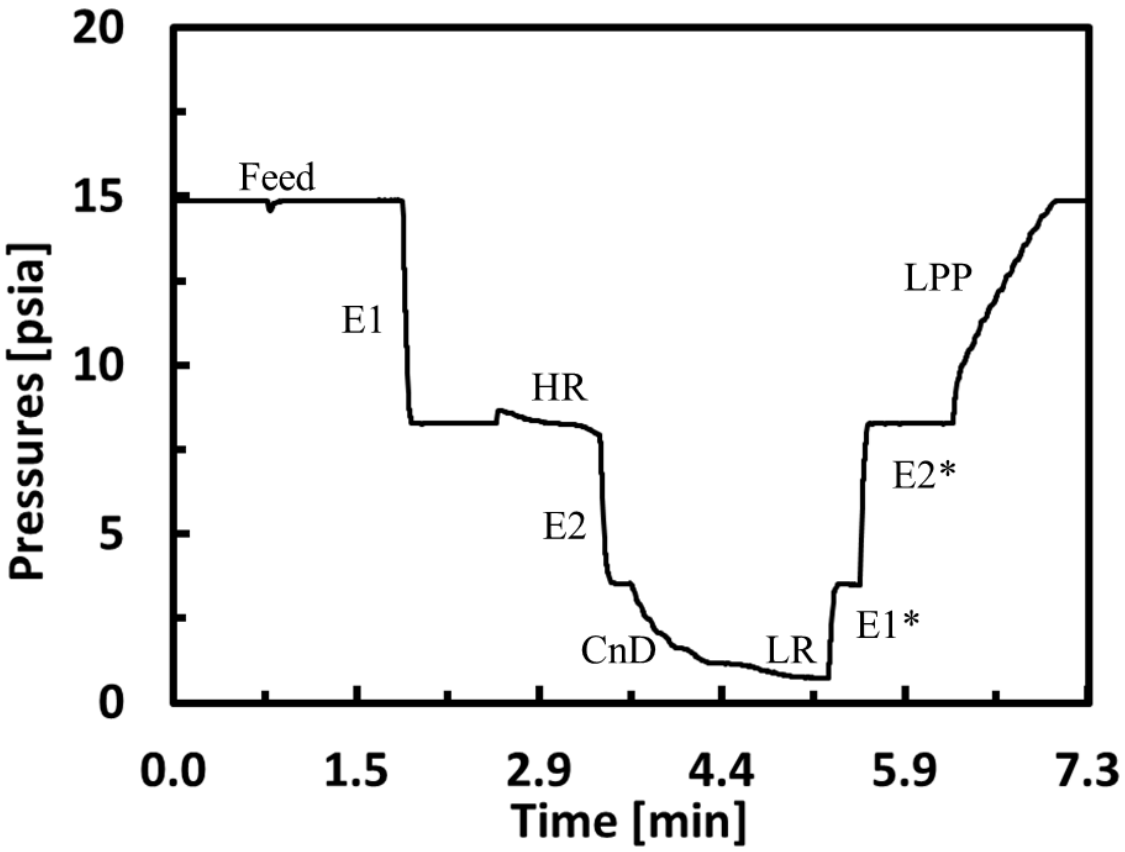


**Figure 5.19** Pressure history of one bed for the E3 run during one entire cycle at steady state.

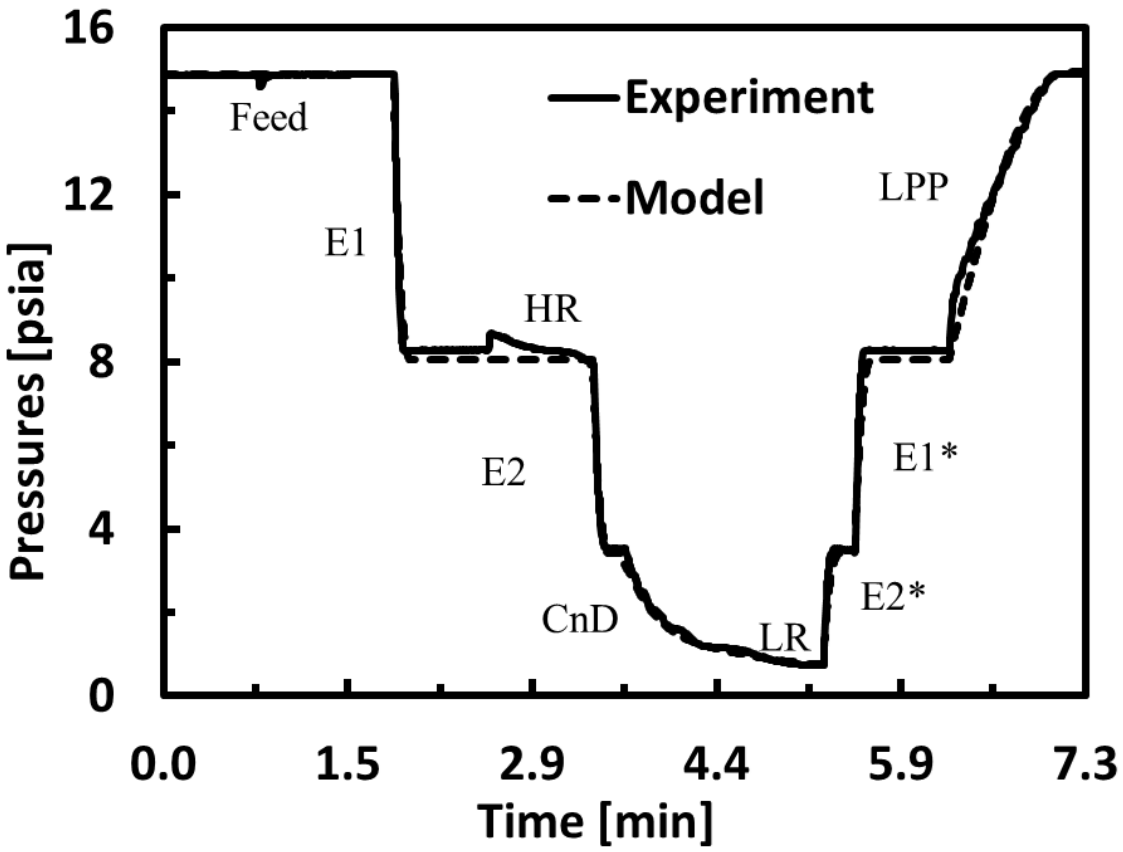


**Figure 5.20** Comparison of pressure history of one bed for the experiment 3, E (solid line) and model 3, M (dashed line) run during one entire cycle at steady state.

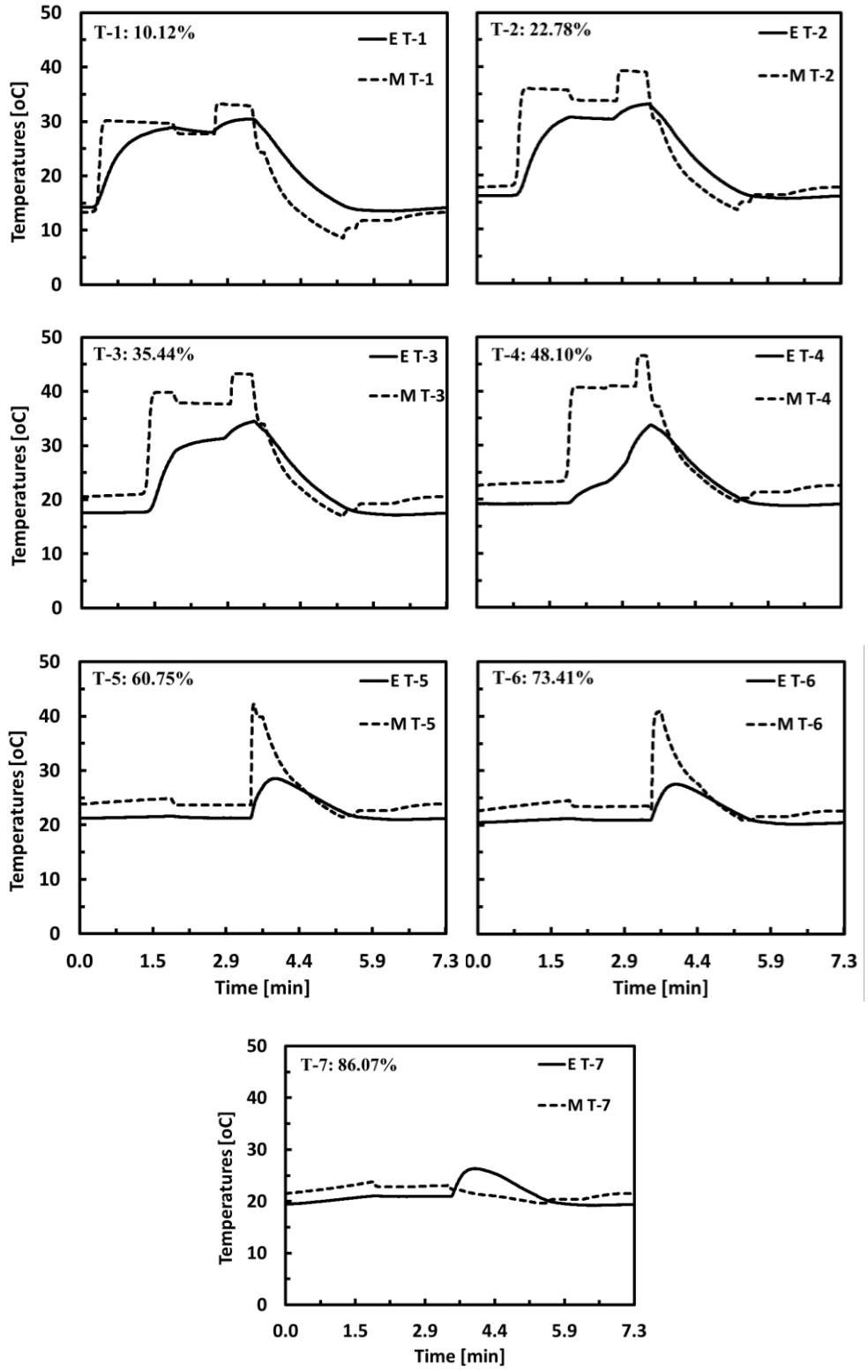


**Figure 5.21** Comparison of temperature histories of experiment 3, E, (solid) and model 3, M (dashed). T1-7 (10.12%, 22.78%, 35.44%, 48.10%, 60.75%, 73.41%, and 86.07% from T1 through T-7, respectively) are locations of thermocouples from feed end.

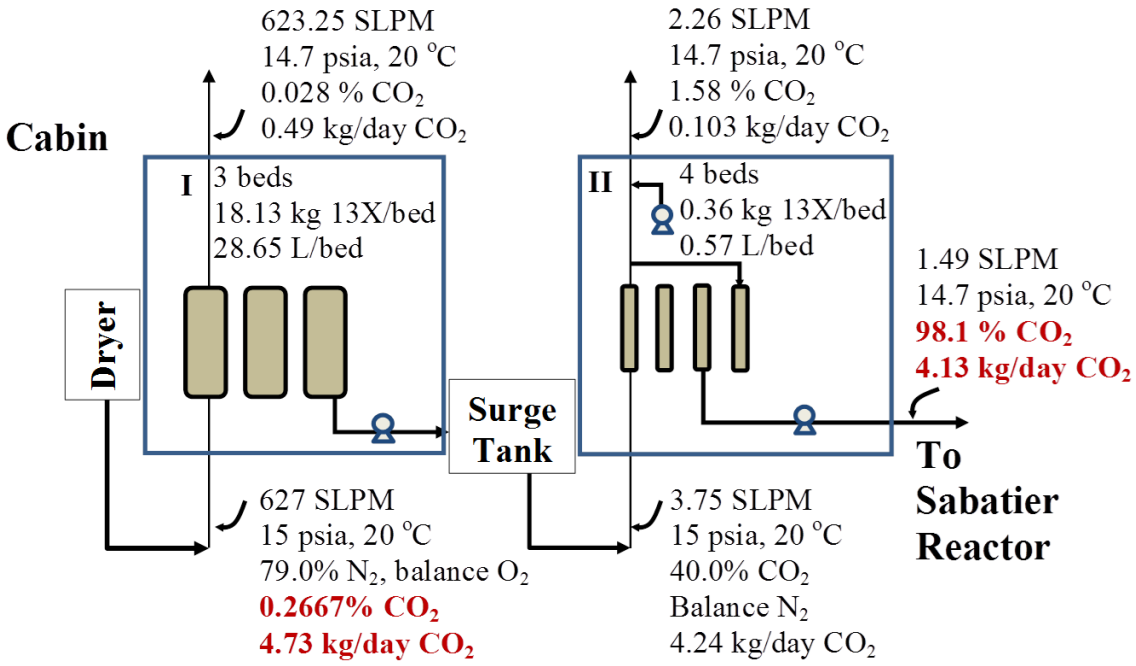


**Figure 5.22** Schematic of the two-stage PSA system designed to remove 4.0 kg/day of metabolic $CO_2$ from cabin air. Stage 1 is a 3-bed 10-step PSA process with the dimensions of I.D: 10.62 in, L: 19.75 in and Stage 2 is a 4-bed 9-step PSA process the dimensions of I.D: 1.5 in, L: 19.75in.

# REFERENCES


Baciocchi, Renato, Giuseppe Storti, and Marco Mazzotti. 2006. “Process Design and Energy Requirements for the Capture of Carbon Dioxide from Air.” *Chemical Engineering and Processing: Process Intensification* 45 (12): 1047–58. doi:10.1016/j.cep.2006.03.015.

Belmabkhout, Youssef, Rodrigo Serna-Guerrero, and Abdelhamid Sayari. 2010. “Amine-Bearing Mesoporous Silica for CO2 Removal from Dry and Humid Air.” *Chemical Engineering Science* 65 (11). Elsevier: 3695–98. doi:10.1016/j.ces.2010.02.044.

Bhadra, Shubhra Jyoti. 2012. “Purification of Ammonia by Pressure Swing Adsorption.”

Bowman, W. H., and R. M. Lawrence. 1971. “Life-Support Systems for Manned Space Flights.” *Space Resources for Teachers* 1: 526–28.

Brown, Peter n., Alan c. Hindmarsh, and r. Petzold Linda. 1994. “Using Krylov Methods in the Solution of Large-Scale Differential Algebraic Systems.”

Carey, R., A. Gomezplata, and A. Sarich. 1983. “An Overview into Submarine CO2 Scrubber Development.” *Ocean Engineering* 10 (4): 227–33. doi:10.1016/0029-8018(83)90010-0.

Carrasquillo, Robyn. 2013. “ISS Environmental Control and Life Support System (ECLSS) Future Development for Exploration.” In *2nd Annual ISS Research and Development Conference*.

Carrasquillo, Robyn L. 2008. “ISS ECLSS Technology Evolution for Exploration.” *American Institute of Aeronautics and Astronautics*.

Casaburri, Angelo A., Cathy A. Gardner, and Jane A. George. 1999. “Space Food and Nutrition: An Educator’s Guide with Activities in Science and Mathematics.”

Choi, SD, JH Drese, PM Eisenberger, and CW Jones. 2009. “A New Paradigm of Anthropogenic CO2 Reduction: Adsorptive Fixation of CO2 from the Ambient Air as a Carbon Negative Technology.” In *Presented at AIChE Annu. Meet.*

Council, National Research. 1997. *Advanced Technology for Human Support in Space*. The National Academies Press.

DallBauman, L A, and J E Finn. 1999. “Adsorption Processes in Spacecraft Environmental Control and Life Support Systems.” *Stud Surf Sci Catal* 120: 455–71. http://www.ncbi.nlm.nih.gov/entrez/query.fcgi?cmd=Retrieve&db=PubMed&dopt=Citation&list_uids=12741388.

Daues, K. 2006. “A History of Spacecraft Environmental Control and Life Support Systems.” *NASA Johnson Space Center*.

Diagne, Doudou, Motonobu Goto, and Tsutomu Hirose. 1995. “Parametric Studies on CO2 Separation and Recovery by a Dual Reflux PSA Process Consisting of Both Rectifying and Stripping Sections.” *Industrial Engineering and Chemical Research* 34 (9): 3083–89. doi:10.1021/ie00048a020.

Do, Duong D. 1998. *Adsorption Analysis: Equilibria and Kinetics*.

Dosch, M.P. 2006. “The Anesthesia Gas Machine.”

Ebner, Armin D, M L Gray, N G Chisholm, Q T Black, D D Mumford, M A Nicholson, and J A Ritter. 2011. “Suitability of a Solid Amine Sorbent for CO2 Capture by Pressure Swing Adsorption.” *Industrial & Engineering Chemistry Research* 50: 5634–41.

Ebner, Armin D, and James A Ritter. 2009. “State-of-the-Art Adsorption and Membrane Separation Processes for Carbon Dioxide Production from Carbon Dioxide Emitting Industries.” *Separation Science and Technology* 44 (6): 1273–1421. doi:10.1080/01496390902733314.

Ernsting, J. 1999. “Breathing Systems in Aerospace.” In *Institute of Electrical Engineers (IEE) Colloquium*, 24–27.

Ewert, Michael K, Daniel J Barta, and Jeff Mcquillan. 2009. “Exploration Life Support Technology Development for Lunar Missions.” *Space*.

Filburn, T., W.C. Dean, and G. Thomas. 1998. “Development of a Pressure Swing CO2/H2O Removal System for an Advanced Sapcesuit.” *SAE Paper No. 981673*.

Gatens, Robyn, and Gary A. Ruff. 2013. “Environmental Control & Life Support / Fire Safety Systems Maturation Team Status.”

Hodgson, E., D. Converse, M. Duggan, and G. Gentry. 2012. “Flexible Path Environmental Control and Life Support Technology—Possible First Steps to Move Beyond LEO.” In *AIAA 42nd International Conference on Environmental Systems*.

Howard, D., Perry, J., and Roman, M. 2014. “Lessons Learned from the Development and Implementation of the Atmosphere Re-Source Recovery and Environmental Monitoring Project.” In *AIAA Space 2014 Conference and Exposition*.

Hwang, Hyun Tae, Aadesh Harale, Paul K T Liu, Muhammad Sahimi, and Theodore T. Tsotsis. 2008. “A Membrane-Based Reactive Separation System for CO2 Removal in a Life Support System.” *Journal of Membrane Science* 315 (1–2): 116–24. doi:10.1016/j.memsci.2008.02.018.

Johnson, S. R. 1992. “Regenerative Trace Contaminant Control: New Test Method for Effects on Solid Amine.” *ICES Paper 921349*.

Johnson, scott R., george g. Garrad, and shirley m. Mitchell. 1993. “Multifunction Air Revitalization Systems: Combined CO2-Trace Contaminant Removal Using Solid Amines.” In *30th Space Congress Proceedings*.

Jones, Christopher W. 2011. “CO(2) Capture from Dilute Gases as a Component of Modern Global Carbon Management.” *Annual Review of Chemical and Biomolecular Engineering* 2: 31–52. doi:10.1146/annurev-chembioeng-061010-114252.

Kawai, T. 1986. “Monograph of PSA Technology.”

Keith, David, Minh Ha-duong, and Joshua Stolaroff. 2006. “Climate Strategy with CO2 Capture from the Air To Cite This Version : Climate Strategy with CO 2 Capture from the Air.” *Climatic Change* 74 (1–3): 17–45.

Knox, J.C. and Howard, D. 2007. “New Methods for the Adsorption of Carbon Dioxide and Water Vapor from Manned Spacecraft Atmospheres: Applications and Modeling.” In *Comsol Conference*.

Knox, J. C. 2000. “International Space Station Carbon Dioxide Removal Assembly TestingNo Title.” *Society of Automotive Engineers*.

Knox, J. C., R. Booth, H. Gauto, D. Trinh, R. Gostowski, R. Bush, C. Stanley, D. Watson, J. Thomas, and L. A. Miller. 2014. “Development of Carbon Dioxide Removal Systems for Advanced Exploration Systems 2012-2013.” In *International Conference on Environmental Systems*.

Knox, J. C., R. Gostowski, D. Watson, J. A. Hogan, E. King, and J Thomas. 2012. “Development of Carbon Dioxide Removal Systems for Advanced Exploration Systems.” In *International Conference on Environmental Systems*.

Knox, J. C., L. A. Knox, J. C., Gauto, H., Trinh, D., Winard, D., Gostowski, R., Watson, D., Kittredge, K., King, E., Thomas, J., and Miller, H. Gauto, D. Trinh, D. Winard, R. Gostowski, D. Watson, et al. 2013. “Development of Carbon Dioxide Removal Systems for Advanced Exploration Systems 2012-2013.” In *International Conference on Environmental Systems*.

Knox, James C., Robert Coker, Timothy L. Huff, Robyn Gatens, Lee A. Miller, and Christine Stanley. 2015. “Development of Carbon Dioxide Removal Systems for Advanced Exploration Systems 2014-2015.” In *45th International Conference on Environmental Systems*.

Knox, James C, Melissa Campbell, Karen Murdoch, Lee A Miller, and Frank Jeng. 2005. “Integrated Test and Evaluation of a 4-Bed Molecular Sieve (4BMS) Carbon Dioxide Removal System (CDRA), Mechanical Compressor Engineering Development Unit (EDU), and Sabatier Engineering Development Unit (EDU).” In *International Conference on Environmental Systems*.

L., Ingelfinger A., and Secord T. C. 1970. “Life Support for Large Space Stations.” *ASTRONAUTICS AND AERONAUTICS* 8: 56–64.

Lackner, K. S., S. Brennan, J. M. Matter, a.- H. a. Park, a. Wright, and B. van der Zwaan. 2012. “The Urgency of the Development of CO2 Capture from Ambient Air.” *Proceedings of the National Academy of Sciences* 109 (33): 13156–62. doi:10.1073/pnas.1108765109.

Lackner, K S. 2009. “Capture of Carbon Dioxide from Ambient Air” 106: 93–106. doi:10.1140/epjst/e2009-01150-3.

Lackner, Klaus, P Grimes, and H Ziock. 1999. “Capturing Carbon Dioxide from Air.” http://www.netl.doe.gov/publications/proceedings/01/carbon_seq/7b1.pdf.

Lackner, Klaus S, and Sarah Brennan. 2009. “Envisioning Carbon Capture and Storage : Expanded Possibilities due to Air Capture , Leakage Insurance , and C-14 Monitoring,” 357–78. doi:10.1007/s10584-009-9632-0.

Lackner, Klaus, Hans-Joachim Ziock, and Patrick Grimes. 1999. “Carbon Dioxide Extraction From Air: Is It An Option?” In *24th Annual Technical Conference on Coal Utilization & Fuel Systems*.

Mattox, E M, and D.M. Bardot. 2011. “Carbon Dioxide Removal System For Closed Loop Atmosphere Revitalization, Candidate Sorbents Screening And Test Results.” *62nd International Astronautical Congress, Cape Town, SA.*, 1–8.

Matty, Christopher M. 2010. “Overview of Carbon Dioxide Control Issues During International Space Station / Space Shuttle Joint Docked Operations.”

Mohammadi, Nima, Lutfi Erden, Armin D Ebner, and James A. Ritter. 2016. “Adsorption Equilibrium of Nitrogen, Oxygen, Argon, Carbon Dioxide, Carbon Monoxide, Methane, Ethane, Propane, Ethylene and Propylene on 13X Zeolite.” *To Be Submitted*.

Moore, P. 2007. “Miner Protection.” *Min. Mag.* 196.

Mulloth, Lila M, and John E Finn. 1998. “Carbon Dioxide Adsorption on a 5A Zeolite Designed for CO2 Removal in Spacecraft Cabins.” *Nasatm1998208752*, no. November: 1–12. http://www.scubaengineer.com/documents/carbon_dioxide_absorption_using_molecular_sieve.pdf.

Murdock, K. 2010. “Integrated Evaluation of Closed Loop Air Revitalization System Components.”

NASA. n.d. “Life Support Reference Guide: ECLS System Components, Oxygen, Carbon Dioxide.” *E-Mission Space Station Alpha*. http://www.e-missions.net/ssa/pdf/ReferenceGuide Life Support.pdf.

———. 2001. “Staying Cool on the ISS.”

NASA Facts. 2004. “International Space Station: Environmental Control and Life Support System.” *National Aeronautics and Space Administration*. http://www.nasa.gov/centers/marshall/pdf/104840main_eclss.pdf.

Nikulshina, V, N Ayesa, and A Steinfeld. 2008. “Feasibility of Na-Based Thermochemical Cycles for the Capture of CO 2 from Air — Thermodynamic and Thermogravimetric Analyses” 140: 62–70. doi:10.1016/j.cej.2007.09.007.

Pearson A.O., Jackson J.K. 1971. “Summary of a 90-Day Manned Test of a Regenerative Life Support SystemNo Title.” *Astronautical Research*, 149–62.

Perry, J., J. Knox, K. Parrish, M. Roman, D. Jan, and M. Abney. 2012. “Integrated Atmosphere Resource Recovery and Environmental Monitoring Technology Demonstration for Deep Space Exploration.” In *AIAA 42nd International Conf. on Env.Systems*.

Perry, Jay L, Morgan B Abney, Ruth E Conrad, Kenneth R Frederick, Zachary W Greenwood, Matthew J Kayatin, James C Knox, et al. 2015. “Evaluation of an Atmosphere Revitalization Subsystem for Deep Space Exploration Missions.” In *45th International Conference on Environmental Systems*.

Rahman, Md Atikur. 2016. “Development of a Pressure Swing Adsorption (PSA) Process for CO2 Capture from Flue Gas.” University of South Carolina.

Rudolph, H., G. Hebestreit, and D. Harzer. 2000. “Porous Foils Filled With Active Substances in Life Support Systems of Manned Space Flight.” *Journal of Plastic Film and Sheeting* 16 (4): 301–11. doi:10.1106/768H-PXC4-CHVC-3LRL.

Ruthven, D. M.; Farooq, S. 1994. *Pressure Swing Adsorption*.

Satyapal, Sunita, Thomas Filburn, H. Harvey Michels, and John Graf. 1999. “A Unique Solid Amine Sorbent Useful for Capturing Low Concentrations of Carbon Dioxide.” *Greenhouse Gas Control Technologies*, 113–18.

Satyapal, Sunita, Tom Filburn, John Trela, and Jeremy Strange. 2000. “NOVEL SOLID AMINE SORBENTS AND APPLICATIONS FOR CARBON Dioxide Removal,” 655–59.

———. 2001. “Performance and Properties of a Solid Amine Sorbent for Carbon Dioxide Removal in Space Life Support Applications.” *Energy and Fuels* 15 (2): 250–55. doi:10.1021/ef0002391.

Sherif, Dina El, James C Knox, Nasa Marshall, and Space Flight. 2005. “International Space Station Carbon Dioxide Removal Assembly ( ISS CDRA ) Concepts and Advancements.”

Stolaroff, Joshuah K, and David W Keith. 2008. “Carbon Dioxide Capture from Atmospheric Air Using Sodium Hydroxide Spray” 42 (8): 2728–35.

Suzuki, M. 1991. *Adsorption Engineering*. *Reactive Polymers*. Vol. 14. doi:10.1016/0923-1137(91)90043-N.

Tondeur, D.; Wankat, P. C. 1985. “Gas Purification by Pressure Swing Adsorption.” *Sep. Purif. Methods* 14 (2): 157.

Tsai, Chung-Yi A., Ipek Guray, Xia Tang, Tim Nalette, Catherine Thibaud-Erkey, C. Jeffrey Brinker, and George Xomerita. 2003. “Novel Amine-Functional Membrane for Metabolic CO2 Removal from Spacesuit Breathing Loop.” In *AIP Conference Proceedings*, 654:861–68. doi:10.1063/1.1541378.

Wieland, Paul. 1994. “Designing for Human Presence in Space : An Introduction to Environmental Control and Life.”

Yang, R. T. 1987. *Gas Separation by Adsorption Processes*.

Yoshida, Masayuki, James a. Ritter, Akio Kodama, Motonobu Goto, and Tsutomu Hirose. 2003. “Enriching Reflux and Parallel Equalization PSA Process for Concentrating Trace Components in Air.” *Industrial & Engineering Chemistry Research* 42 (8): 1795–1803. doi:10.1021/ie010114z.

Zeman, Frank S, and Klaus S Lackner. 2004. “Capturing Carbon Dioxide Directly from the Atmosphere.” *World Resource Review* 16 (2): 157–72. http://wordpress.ei.columbia.edu/lenfest/files/2012/11/ZEMAN_LACKNER_2004.pdf.